Mestrado Integrado em Engenharia Química

The Influence of the Orientation and Fit on Heat Transfer Properties of OCFS and CCFS Packings in Multi-Tubular Fixed-Bed Reactors

Tese de Mestrado

desenvolvida no âmbito da disciplina de

Projecto de Desenvolvimento em Instituição Estrangeira

Cláudia Cristina Reizinho Fortunato Cabral

Delft University of Technology

Universidade do Porto
Faculdade de Engenharia
FEUP

Departamento de Engenharia Química

Orientador na FEUP: **Prof. Dr. Alírio Rodrigues**

Orientador na empresa: **Ir. David Vervloet**
Ir. John Nijenhuis
Dr. Ruud van Ommen
Prof. Dr. Freek Kapteijn

Julho de 2008

Acknowledgments

On the development of this project many people have contributed to its success.

First of all, I would like to say that was a pleasure do Erasmus in Netherlands, especially making part of the Catalysis Engineering group. In a especial way I would like to thank to Prof. Dr. Freek Kapteijn for all the value that he has recognized in me. I also would like to thank to my daily supervisor David Vervloet for his help, advices and patience during the past 5 months.

I would like to thank to my office mates Koos, Michel, Anna, David Newsome, Malte and Bogdan for the good atmosphere. I really enjoy all the subjects that we have talked about. I also would like to thank to all Catalysis Engineering group, particularly to Joana, Rita, Nicla, Delphine, Marteijn and Ugur.

I really would like to thank in a particularly way to all the Professors in DEQ for making me the engineer that I am now.

Thanks to all my friends in Portugal that supported me during this 5 months, especially to Catarina, Rosângela, Mariana, Rui, Tiago, Ana, Joana Ângelo, Joana Oliveira, Filipa, André and Gil.

Many thanks to Bruno, my boyfriend, for all the patience and support during the last 5 months. I really enjoy all the moments that I pass with you in Netherlands, all the places that we went, our adventures and especially our life together.

Finally to my dear parents, José and Eva, for always support me during my life. Thanks for the education that you gave to me, the patience, constant support and all the important values that you have passed to me. Without you I would not be the woman that I am today.

Abstract

Structured packings are known for their excellent heat transfer properties in multi-tubular fixed-bed reactors. Previous research concluded that the open-cross flow structures (OCFS) and closed-cross flow structures (CCFS) have the best heat transfer performance compared to glass beads, foam and knitted wire.

The influence of the orientation on heat transfer properties of OCFS and CCFS packings in a single-tube fixed-bed reactor was studied. For both types of packings it was found that 90° alternating rotation of the packings is always better than 0° alternating rotation.

The influence of the fit on heat transfer properties of OCFS packings in a single-tube fixed-bed reactor was studied. It was concluded that the OCFS packings with a better heat transfer performance were the ones with a big gap between the edge of the packing and the reactor wall.

The heat transfer performance of the OCFS and CCFS packings are very similar. However, for high gas velocities the OCFS are clearly better than the CCFS packings.

It was concluded that the simplified 2-D pseudo-homogeneous plug flow model and the 2-D pseudo-homogeneous plug flow model are not good models to these types of packings.

Index

Page

Index of Appendices

Page

Index of Figures

Index of Figures in Appendices

Index of Tables

Index of Tables in Appendices

List of Symbols

a_v = surface area (m^{-1})

Cp_G = heat capacity of gas (J/(kg.K))

Cp_L = heat capacity of liquid (J/(kg.K))

D = diameter of the packings (m)

d_h = hydraulic diameter (m)

L = length (m)

$\dot{Q}$ = total amount of heat that is transferred (W)

r = radial position (m)

R = tube radius (m)

T = temperature (K)

$\overline{T}$ = average temperature (K)

$T_{m,in}$ = average of the inlet temperature profiles (K)

$T_{m,out}$ = average of the outlet temperature profiles (K)

T_w = temperature of the wall (K)

u_G = superficial gas velocity (m/s)

u_L = superficial liquid velocity (mm/s)

U_{ov} = overall heat transfer coefficient (W/(m^2.K))

U_{est} = estimated heat transfer coefficient (W/(m^2.K))

z = axial position (m)

Greek Letters

ε = porosity

α_w = wall heat transfer coefficient (W/(m^2.K))

$\lambda_{e,r}$ = effective radial thermal conductivity (W/(m.K))

λ_{static} = conductive component of the effective radial thermal conductivity (W/(m.K))

ρ_G = gas density (kg/m^3))

ρ_L = liquid density (kg/m^3))

θ = angle with horizontal for corrugation channel (deg)

1. Introduction

Oil, which is our most important source of energy today, is the owner of 40% of the world energy market and 90% of the transportation fuel (in the form of gasoline and diesel) market [1]. However, since the reserves of crude oil will vanish before the reserves of coal and natural gas, the employment of alternative sources of energy becomes very important. One of the alternative sources of energy which are likely to replace oil in the near future is synthetic fuel. Synthetic fuel is any liquid fuel obtained from coal, natural gas or biomass.

The conversion of coal (CTL) and natural gas (GTL) into hydrocarbons via Fischer-Tropsch synthesis has become attractive to many companies because the reserves of crude oil will vanish before the reserves of the coal and natural gas and the produced fuel is cleaner. Also the conversion of biomass (BTL) into hydrocarbons is an interesting alternative. The principal purpose of the Fischer-Tropsch process is to produce a synthetic petroleum substitute for use as synthetic fuel or as lubrication oil.

Fischer-Tropsch synthesis (FTS) is a highly exothermic reaction. Due to this, much attention has been paid to reactor selection, with emphasis on the ease of heat removal. A good heat removal decreases the temperature in the reactor and the selectivity of the reaction increases from C_1 to higher C_i products [2].

Many reactors have been suggested and even commercially applied since Fischer-Tropsch synthesis was discovered in the 1930's but each of them suffers from some kind of disadvantage [3]. There are three types of reactors for the FTS that are currently being used commercially: the multi-tubular fixed-bed reactor, the riser reactor and the slurry phase reactor [4].

Multi-tubular fixed-bed reactors suffer from a large radial temperature profile which consequently leads to a wider product distribution. Previous research [5] found that the performance of these reactors could be greatly improved with the use of structured packings. It was shown that the heat transfer properties of structured packings in these reactors vary strongly with the type of packing.

Structured packings typically consist of thin corrugated metal plates arranged in a way that they force fluids to take specific paths through the column, thereby creating a large surface area for contact between different phases. Apart from their advantages of reduced backmixing, improved radial heat transfer behaviour and low-pressure drop they also have the benefit of ease of scale-up.

The OCFS (open cross flow structures) and CCFS (closed cross flow structures) packings, see figure 1, have shown the best results thus far relating to the overall heat transfer coefficient,

comparing with glass beads, foams and knitted wire. For this reason the OCFS and the CCFS packings will be the focus for this continued research.

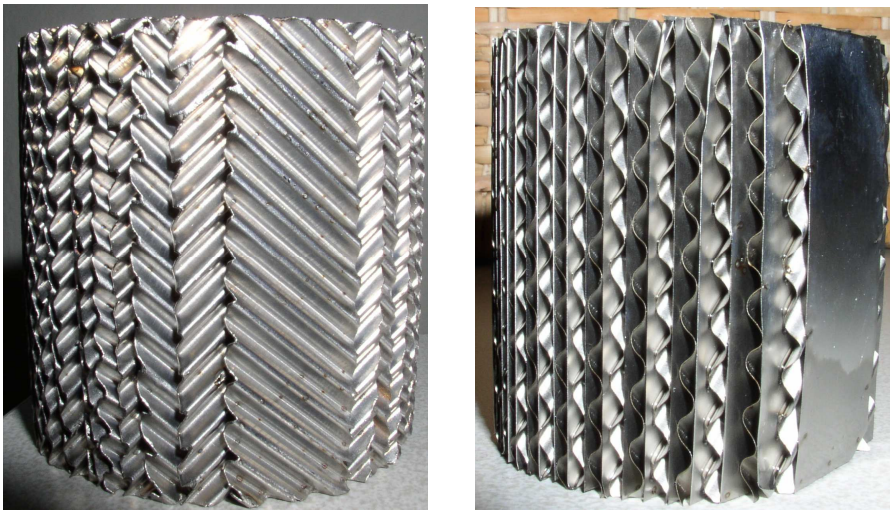

Figure 1 – CCFS (left) and OCFS (right) packings, with 5 cm of diameter.

The OCFS and CCFS belong to the same family of structured packings as they both consist of thin corrugated metal plates with the corrugations of the metal sheets inclined at an angle of 45^{o} with respect to the vertical axis. In the OCFS the channels are open to each other and hence the fluids from adjacent channels get remixed with each other thereby promoting radial mixing. In CCFS a flat sheet is inserted between two corrugated sheets thereby limiting the radial mixing to each channel.

Previous research [5] also concluded that the heat transfer properties of these packings depend on the orientation of the packing and the gap between the packing and the reactor wall. These packings do not have the same physical properties in all directions, they are anisotropic. This is the reason why these packings were not designed as single long cylindrical modules but rather as short cylindrical elements such that several of these elements turned by 90° at regular intervals could be used to fill the columns.

The heat transfer in tubes filled with catalytic random packings is usually calculated using the two-dimensional pseudo-homogeneous plug flow model with two parameters describing the overall heat transfer resistance: an effective radial thermal conductivity ($\lambda_{e,r}$) and a wall heat transfer coefficient (α_w). The $\lambda_{e,r}$ determines the heat transfer rate through the structured packing from the centre to the edge. The α_w determines the heat transfer rate from the edge of the packing to the wall [5].

In this thesis a single-tube fixed-bed reactor with structured packings (OCFS and CCFS) will be studied and consequently it will be tried to improve the heat removal and flatten the radial temperature profile on the reactor, so that the range of the final products of the Fischer-Tropsch reaction can be decreased.

1.1 Objectives

The objectives of this research project are (i) screening the influence of the orientation and the fit of the OCFS and CCFS packings in a single-tube fixed-bed reactor and (ii) suggest improvements on the packings to improve the heat transfer characteristics.

To fulfill the first objective of this research project experiments will be performed in a single-tube fixed-bed reactor with structured packings (OCFS and CCFS packings) with co-current down flow of gas (N_2) and liquid (ISOPAR-M). To determine the influence of the orientation of the packing in the heat transfer experiments will be performed with packings turned at 0° and 90° alternating. Both OCFS and CCFS packings will be studied. To determine the influence of the fit of the OCFS packings in the heat transfer experiments will be done with packings with different gaps (small, medium and big gap) between the edge of the packing and the reactor wall.

2. Literature Review

2.1 Gas-to-Liquid

Synthetic fuel or synfuel is any liquid fuel obtained from coal, natural gas or biomass. The process of producing synfuels is often referred to as Coal-to-Liquids (CTL), Gas-to-Liquids (GTL) or biomass-to-Liquids (BTL), depending on de initial feedstock.

The conversion of natural gas to hydrocarbons (GTL) is currently one of the most promising topics in the energy industry due to economic utilization of remote natural gas to environmentally clean fuels, specialty chemicals and waxes. Alternatively, coal or heavy residues can be used on sites where these are available at low costs [7]. As can be seen in table 2.1 the resources of coal and natural gas are very large compared to the ones of crude oil.

Table 2.1 – World fossil fuel reserves and consumption (EJ, 10^{18} J) [7].

	Reserves	**Consumption (1991)**
Coal	27,185	69.91
Natural Gas	4,512	79.44
Crude Oil	6,054	143.67

Since the reserves of crude oil will vanish before the reserves of the coal and natural gas, the liquefaction of those carbon sources via Fischer-Tropsch Synthesis has become attractive to many companies.

The principal purpose of Fischer-Tropsch process is to produce a synthetic petroleum substitute for use as synthetic fuel or as lubrication oil. Fischer-Tropsch (FT) technology can be briefly defined as the means used to convert synthesis gas containing hydrogen and carbon monoxide to hydrocarbons products. Interest in FT technology is increasing rapidly. This is due to recent improvements to the technology and the realization that it can be used to obtain value from stranded natural gas. In other words, remotely located natural gas will be converted to liquid hydrocarbon products (GTL) that can be sold in worldwide markets [8].

GTL fuel is colourless, odourless and free of sulphur and aromatics. It has a very high cetane number (75-80) - a measure of diesel combustion quality – compared to refinery diesel (45-55). The higher the cetane number, the more complete the combustion and the less waste is produced. It significantly reduces local emissions (particulate matter, NO_x, CO and hydrocarbons), either as a blend with diesel fuel, or 100% pure compared to refinery diesel fuel – even ultra low sulphur (50 ppm) diesel. GTL fuel is ideal for reducing pollution in major cities. Some other alternative fuels

require modifications to existing vehicles or the installation of a new fuel distribution infrastructure (filling stations). This may limit their initial usage to dedicated bus and truck fleets that only use a fixed refuelling location. However, the compatibility of GTL fuel with standard diesel infrastructure means it can be introduced into a market without the costs of modifying vehicles or installing new infrastructures [9].

2.2 Fischer-Tropsch Synthesis

Fischer-Tropsch synthesis (FTS) was discovered by Fischer and Tropsch, the German coal researchers, in 1923 and became first used in Germany in World War II. It is a process converting synthesis gas (a mixture of CO and H_2) into hydrocarbons.

The Fischer-Tropsch reaction forms hydrocarbons and water over a heterogeneous catalyst. The main hydrocarbon products are n-paraffins and α-olefins varying between methane and heavy waxes, but also other molecules like branched paraffins, alcohols, aldehydes and carbon acids are present in the product mixture [10]. The product molecular weight distribution depends on the catalyst, the temperature, the pressure and the H_2/CO ratio [4]. After separation and upgrading a part of FT derived products can be used as transportation fuels. Non-fuel (waxes) products can be hydrocracked to the desired transportation fuels or be recycled to the synthesis gas generation process step [10]. The major overall reactions of the FTS are summarized in table 2.2.

Table 2.2 – Major overall reactions of the Fischer-Tropsch synthesis [11].

Main reactions	
1. Paraffins	$(2n+1)\ H_2 + n\ CO \rightarrow C_nH_{2n+2} + n\ H_2O$
2. Olefins	$2n\ H_2 + n\ CO \rightarrow C_nH_{2n} + n\ H_2O$
3. Water gas shift reaction	$CO + H_2O \leftrightarrow CO_2 + H_2$
Side reactions	
4. Alcohols	$2n\ H_2 + n\ CO \rightarrow C_nH_{2n+2}O + (n\text{-}1)\ H_2O$
5. Boudouard reaction	$2\ CO \rightarrow C + CO_2$

The product of FTS, the so-called synthetic crude-oil, can be used directly in the refineries. It contains mainly linear hydrocarbons chains, and no S or N containing compounds. By hydrocracking of the synthetic oil, the heavy hydrocarbons (C_{19+}) are converted into diesel and kerosene. Isomerization, catalytic reforming, alkylation, and oligomerization, can further increase the octane number [12].

Typical conditions of FTS are pressures between 10-60 bar and temperatures in range of 200 - 350°C. An important aspect of FTS is the large heat of reaction, the formation for example of 1 mole of $–CH_2-$ is accompanied by a heat release of 165 kJ/mol, which imposes strong requirements on the process design of large-scale units [4].

Vannice et al [13] showed that the average molecular weight of hydrocarbons produced by FTS decreased in the following sequence: Ru > Fe > Co > Rh > Ni > Ir > Pt > Pd. However, only ruthenium, iron, cobalt and nickel have catalytic characteristics which allow considering them for commercial production. Nickel catalysts under practical conditions produce too much methane; ruthenium is too expensive and its worldwide reserves are insufficient for large-scale industry. So cobalt and iron-based catalysts are the most commonly catalysts used at industrial scale [14]. A brief comparison of cobalt and iron catalysts is given in Table 2.3.

Table 2.3 – Comparison of cobalt and iron FT catalysts [14].

Parameter	**Cobalt catalysts**	**Iron catalysts**
Cost	more expensive	less expensive
Lifetime	resistant to deactivation	less resistant to deactivation (coking, carbon deposit, iron carbide)
Activity at low conversion	comparable	
Productivity at high conversion	higher; less significant effect of water on the rate of CO conversion	lower; strong negative effect of water on the rate of CO conversion
Maximal chain growth probability	0.94	0.95
Water gas shift reaction	not very significant	significant
Maximal sulphur content	~ 0.1 ppm	~ 0.2 ppm
Flexibility (T and P)	less flexible; significant influence of T and P on hydrocarbon selectivity	flexible; methane selectivity is relatively low even at 613 K
H_2/CO ratio	~ 2	0.5 – 2.5
Attrition resistance	good	not very resistant

Although the reactor effluent contains a wide variety of components, the product distribution shows a strong regularity. Due to the polymerization-like growth mechanism, the selectivity to a certain product or product range will always be limited - Anderson-Schulz-Flory (ASF) distribution. According to Anderson, the product distribution of hydrocarbons can be described by the ASF equation:

$$m_n = (1-\alpha)\alpha^{n-1} \quad \textbf{(1)}$$

with m_n the mole fraction of a hydrocarbon with chain length n and the growth probability factor α independent of n. α determines the total carbon number distribution of the FT products. The range of α depends on the reaction conditions and catalyst type [15].

The next figure shows that the maximum primary selectivity towards products in the range of gasoline or diesel fuels is about 40% [16].

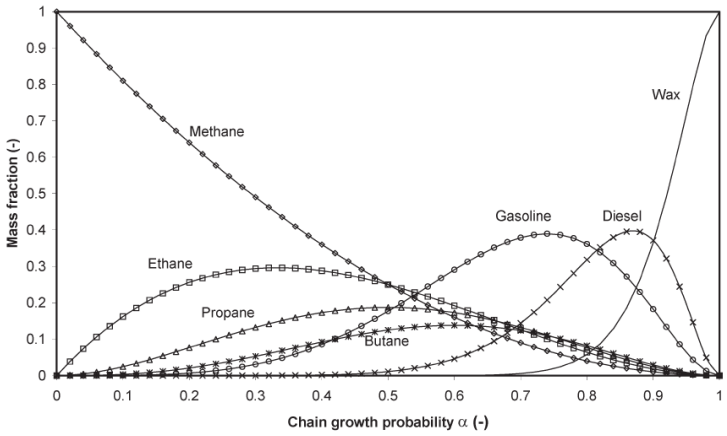

Figure 2 – Product selectivity as a function of ASF chain growth probability (α) [16].

Schulz [17] provides a qualitative overview of the influence of several process conditions on the selectivity of the FTS (see table 2.4).

Table 2.4 – Influence of certain process conditions on product selectivity characteristics: ↑ increase, ↓ decrease, * complex reaction.

	Chain growth probability	**Oleofin/Paraffin ratio**	**Carbon deposition**	**Methane selectivity**
Temperature ↑	↓	↓	↑	↑
Pressure ↑	↑	*	*	↓
H_2/CO ratio ↑	↓	↓	↓	↑
Conversion ↑	*	↓	↑	↑

The main challenge in FTS is maximizing the selectivity of the process to desired products or product ranges. However, the polymerization-like nature of FTS poses strong limitations on efforts to, for instance, selective production of valuable and high quality middle distillate range products. Moreover, the strong exothermal nature of FTS poses important limitations on the reactor design and operation of the FTS process. Also due to this, reactors suffer from unequal temperature distributions which consequently leads to a wider product distribution. The adiabatic temperature rise of FTS, 1600 K, makes heat removal a crucial issue, especially considering that temperature is an important

parameter in controlling process selectivity [10]. Therefore much attention has been paid to reactor selection, with emphasis on the ease of heat removal [18]. A good heat removal decreases the temperature in the reactor and the selectivity of the reaction increases from C_1 to higher C_i products. An increase in the temperature leads to a shift in the process selectivity towards methane formation and carbon deposition on the catalyst and, consequently, the catalyst deactivation [2].

The FTS is a process where several types of reactors have been proposed and even commercially applied since its discovery [3]. Different types of reactors have been used to overcome the various problems associated with the product selectivity, heat removal and uniform distribution of syngas. All of these reactors can be considered as nonoptimal compromises for reasons mentioned below.

Krishna and Sie [19] developed an effective strategy for multiphase reactor selection in which they analyze the process requirements in a systematic way. They distinguish three strategy levels: (i) catalyst design, (ii) injection and dispersion strategies and (iii) hydrodynamic flow regime. For each of these levels the ideal choice should be decided independently, considering the specific requirements of the process. The power of this approach is that independent of existing reactor configurations ideal configurations for various process aspects can be formulated [16].

From the catalyst design level, it follows that the optimal Fischer-Tropsch catalyst should have short diffusion lengths, a good accessibility and high activity. The injection and dispersion strategy level results in several needs and wishes. Plug flow behavior with respect to concentrations and mixed state of the temperature are strong needs. Staged injection of reactants and in situ removal of water vapor can be beneficial. The hydrodynamic regime imposes several preconditions. High productivity, good heat transfer and mass transfer are the most important preconditions [16].

Some of the requirements coming from the various strategies levels are difficult to combine in conventional reactors. Many reactors have been suggested but each of them suffers from some kind of disadvantage. There are three types of reactors for the FTS (see figure 3) that are currently being used commercially: the multi-tubular fixed-bed reactor, the riser reactor and the slurry reactor [4].

In the multi-tubular fixed-bed reactor (MTFBR) small-diameter tubes containing the catalyst are surrounded by circulating boiling water, which removes the heat of reaction. A high linear gas velocity is applied and unconverted synthesis gas is recycled to enhance heat removal. This reactor is suitable for operation at low temperature; there is an upper temperature limit of about 530 K, above which carbon deposition would become excessive, leading to blockage of the reactor. This reactor can be considered a trickle-flow reactor, since a large part of the products formed at relatively low operating temperatures are liquid (waxes: C_{19+}) [4]. The major disadvantage of this reactor is related to limited heat removal which leads to radial temperature profiles which consequently results in a wider product distribution.

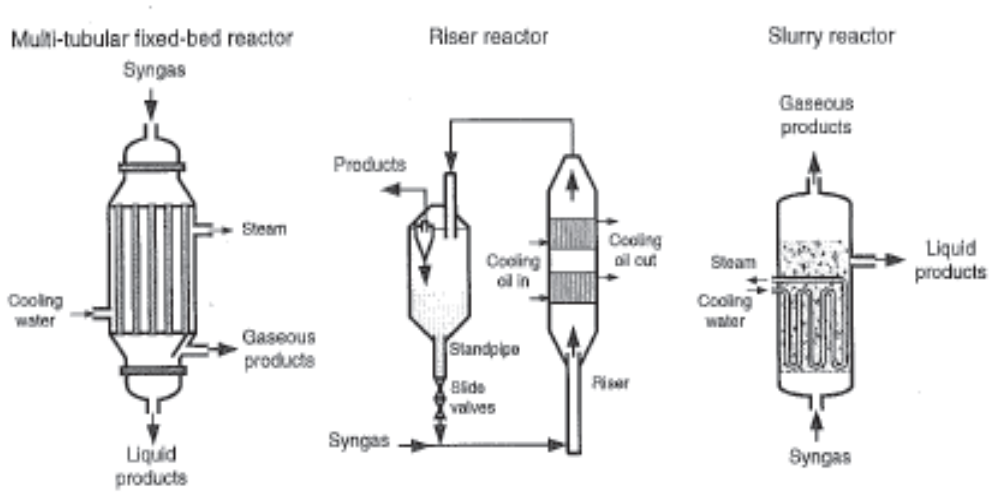

Figure 3 – Reactors used for Fischer-Tropsch synthesis [4].

In riser reactors for FTS two banks of the heat exchangers remove a significant part of the heat of the reaction, while the remainder is removed by the recycle and product gases, which are then separated from the catalyst by cyclones. The formation of heavy wax must be prevented, because this condenses on the catalyst particles causing agglomeration of the particles and thus defluidization. Therefore, this reactor is preferably used at temperatures of over 570 K. In the riser reactor gasoline is the major product however it produces a larger quantity of light products, such as methane, which are undesired.

In the slurry reactor, a finely divided catalyst is suspended in a liquid medium, usually the FT wax product, through which the synthesis gas is bubbled. This also provides agitation of the reactor contents. As the gas flows upwards through the slurry, it is converted into more wax by the FT reaction. The fine particle size of the catalyst reduces diffusional mass and heat transfer limitations. The heat generated by reaction is removed by internal cooling coils. The liquid medium surrounding the catalyst particles greatly improves heat transfer. The temperature in the slurry reactor must be not too low because then the liquid wax should become too viscous, while above about 570 K the wax hydrocracks, leading to a less favorable product spectrum. Separation of the product wax from the suspended catalyst has been a problem; a heavy product is produced so distillation and flashing are no options, while separation methods such as filtration and centrifugation are expensive [4].

As we can see in the table 2.5 the three reactors yield rather different product distributions.

Table 2.5 – Typical operations and selectivity data of the three reactors type used in FTS [4].

	Multi-tubular fixed-bed reactor	Riser reactor	Slurry reactor
Conditions			
Inlet *T* (K)	496	593	533
Outlet *T* (K)	509	598	538
Pressure (bar)	25	23	15
H_2/CO feed ratio	1.7	2.54	0.68[a]
Conversion (%)	60 - 66	85	87
Products (*wt%*)			
CH_4	2	10	6.8
C_2H_4	0.1	4	1.6
C_2H_6	1.8	4	2.8
C_3H_6	2.7	12	7.5
C_3H_8	1.7	2	1.8
C_4H_8	2.8	9	6.2
C_4H_{10}	1.7	2	1.8
$C_5 - C_{11}$ (gasoline)	18	40	18.6
$C_{12} - C_{18}$ (diesel)	14	7	14.3
C_{19}^+ (waxes)	52	4	37.6
Oxygenates	3.2	6	1

a – Higher ratio is also possible.

Currently, there are two operating modes: high- and low-temperature Fischer-Tropsch processes (Figure 4) [14].

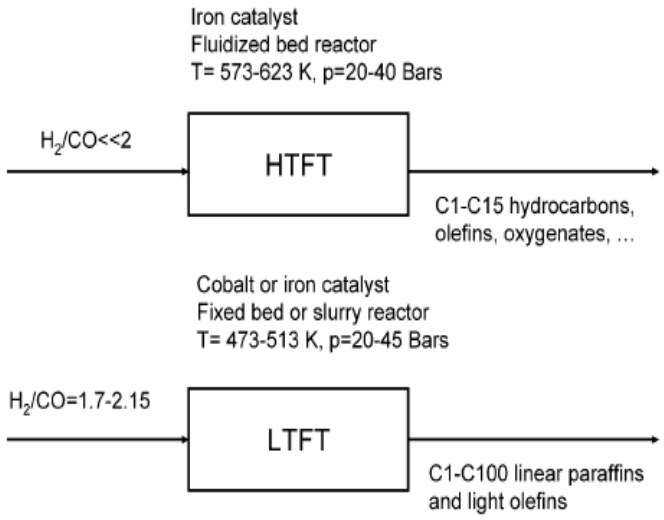

Figure 4 – High- and low-temperature Fischer-Tropsch processes [14].

In the high-temperature FT (HTFT) process syngas reacts in a fluidized bed reactor in the presence of iron-based catalysts to yield hydrocarbons in the $C_1 - C_{15}$ hydrocarbon range. This process is primarily used to produce liquid fuels, although number valuable chemicals, e.g., α-olefins, can be extracted from the crude synthetic oil. Oxygenates in the aqueous stream are separated and purified to produce alcohols, acetic acid, and ketones [14].

Both iron and cobalt catalysts can be used in the low-temperature FT process for synthesis of linear long-chain hydrocarbon waxes and paraffins. High-quality sulphur-free diesel fuels are produced in this process. Most of the FT technologies developed in the last two decades are based on the LTFT process. These new LTFT processes have involved syngas with a high H_2/CO ratio, which is generated by vapour-reforming, autothermal reforming, or partial oxidation using natural gas as a feedstock. Because of their stability, higher pass conversion, and high hydrocarbon productivity, cobalt catalysts represent the optimal choice for synthesis of long-chain hydrocarbons in the LTFT process [14].

Currently commercial operations of Fischer-Tropsch plants are in South Africa – Sasol (90% of the global production) and Malaysia – Shell (10% of the global production). Exxon, Rentech, Syntroleum, Energy International and others have developed pilot plants [12].

Previous research found that the performance of multi-tubular fixed-bed reactors could be greatly improved with the use of structured packings for the reasons mentioned in the next section.

2.3 Structured Packings

The term structured packing refers to a range of specially designed materials for use in absorption, distillation columns and chemical reactors. Structured packings typically consist of thin corrugated metal plates or gauzes arranged in a way that they force fluids to take specific paths through the column, thereby creating a large surface area for contact between different phases. Apart from their advantages of reduced backmixing, improved radial heat transfer behaviour and low-pressure drop, they also have the benefit of ease of scale-up.

Since the 1960s corrugated structures have been applied successfully in industrial distillation and absorption columns. The early packings were BX gauze packings and they were used for the separation of heat-sensitive products. In 1970s Mellapak structured packings opened up a large field of applications in chemistry, petroleum chemistry, and refinery and absorption processes [20]. It is estimated that today 25% of all refinery towers worldwide are fitted with structured packings. They are used to improve the heat transfer behavior and make process intensification possible. The next figure summarizes the history of corrugated structures since 1955.

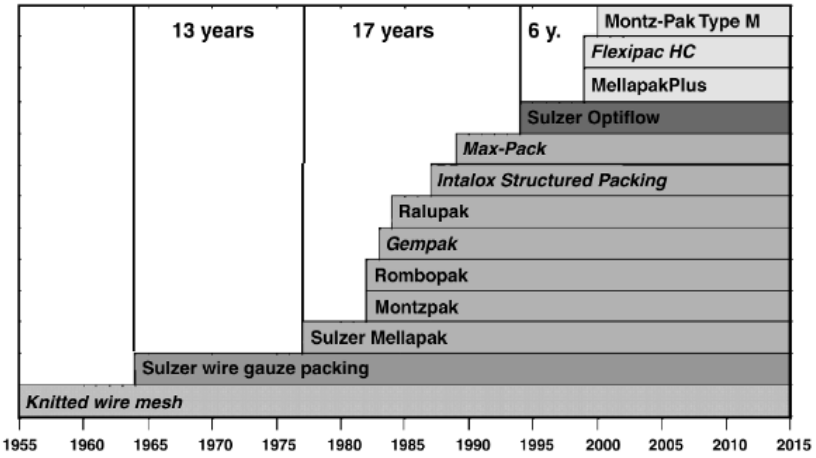

Figure 5 – History of structured packings [20].

In this thesis we are going to aboard the structured packings as potential catalytic structures to be applied for highly exothermic multiphase reactions operated in co-current mode. These packings can be classified in four categories:

1) Monolith, which are structures of parallel straight channels, with typical characteristics of low pressure drop, high porosity, high geometric surface areas, no radial exchange and heat transfer characteristics, which strongly depend on the monolith material;

2) Corrugated sheet/gauze packings which can be subdivided into:

   a. The Open Cross Flow Structure (OCFS), which consists of corrugated sheets stacked parallel to each other, and whose corrugation orientation is alternately inclined to the axis; typical characteristics are low pressure drop, high porosity, high geometric surface areas and efficient radial mixing.

   b. Closed Cross Flow Structure (CCFS) is a modification of OCFS, which consists of an additional flat plate between the corrugated sheets, forming closed channels inclined to the axis; typical characteristics are low pressure drop, high porosity, high geometric surface areas and mixing at the wall thus allowing efficient heat transfer from the packing to the coolant.

3) Multifilament Wire Mesh Packing, which consists of knitted multiple fine metallic filaments that are then crimped and spiral wound; typical characteristics are low pressure drop, high porosity, high geometric surface areas;

4) Open-celled foams, which are 3D cellular materials made of interconnected solid struts (pores), forming a sponge type tortuous path network; typical characteristics are low pressure drop, high porosity, high geometric surface areas, sufficient radial mixing and good heat transfer characteristics compared to glass beads [21].

Previous research [5] concluded that the OCFS and CCFS packings have shown the best results thus far to improve the heat removal on a multi-tubular fixed-bed reactor. See figure 6 where the overall heat transfer coefficient is represented for various packings with different type of conditions.

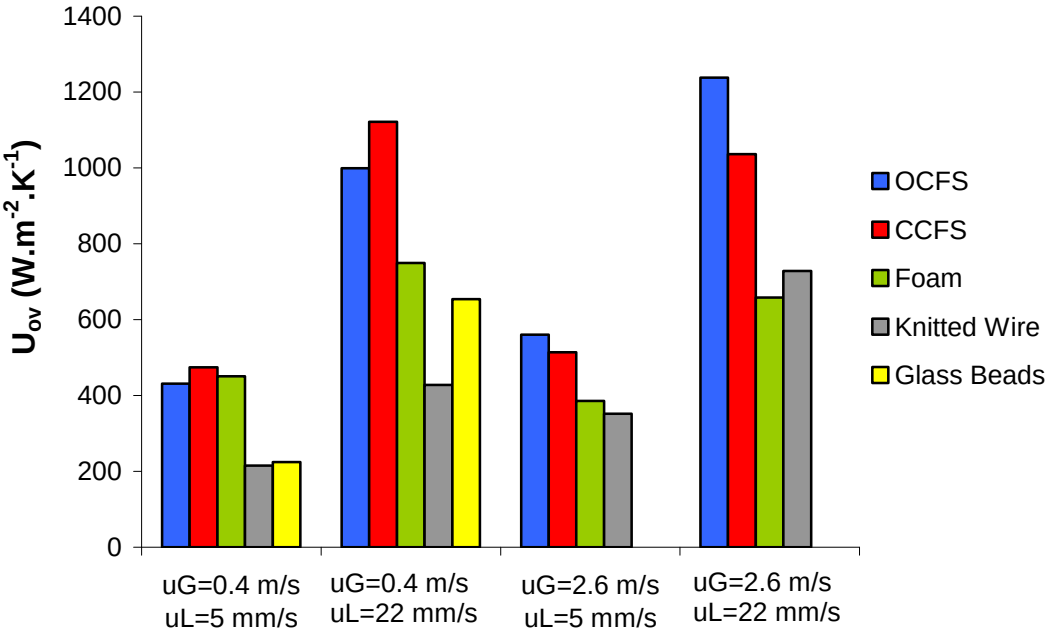

Figure 6 – Comparing U_{ov} for glass beads and structured packings for four different conditions [5].

It was also concluded that the heat transfer properties of these packings depend on the orientation of the packing and the gap between the packing and the reactor wall.

The OCFS and CCFS belong to the same family of structured packings as they both consist of thin corrugated metal plates with the corrugations of the metal sheets inclined at an angle of 45^{o} with respect to the vertical axis. The sheets are arranged vertically and parallel to each other, so that the corrugations of contiguous sheets are inclined alternately by $+\theta$ and $-\theta$. In the OCFS (see figure 7 (a) and (b)) the channels are open to each other and hence the fluids from adjacent channels get remixed with each other thereby promoting radial mixing. In CCFS (see figure 7 (c) and (d)) a flat sheet is inserted between two corrugated sheets thereby limiting the radial mixing to each channel. The open channel packing geometry is then transformed into a monolith-like structure with a multiplicity of closed inclined triangular channels [5].

These packings were not designed as single long cylindrical modules but rather as short cylindrical elements such that several of these elements turned by 90° at regular intervals could be used to fill the cold and hot section columns. This was necessary as the packings are anisotropic, i.e. the physical properties are not the same in all radial directions [5]. Therefore the heat distribution will not be the same thus obtaining different temperature profiles along different angular directions at the same axial position.

(a) (b) (c) (d)

Figure 7 – OCFS ((a) and (b)) and CCFS ((c) and (d)) packings rotated 0° and 90° into each other, with 5 cm of diameter, the value of θ is in these cases 45°.

Table 2.6 provides the geometric properties of the structured packings used in this study.

Table 2.6 – Geometric properties of the OCFS and CCFS packings [5].

Packing	Material	Porosity, ε	Surface Area, a_V (m^{-1})	Hydraulic radius, d_h (mm)	Diameter, D (cm)
OCFS	Stainless steel	0.84	1885	1.8	4.9
CCFS	Stainless steel	0.95	2400	1.6	4.9

Conventional open cross flow structures show three possible flow types within such structures, see figure 8.

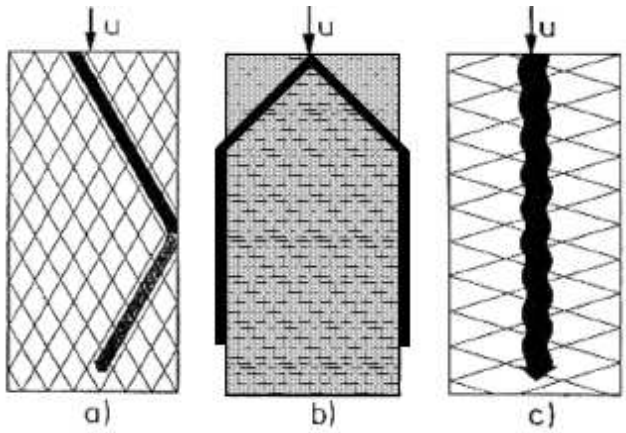

Figure 8 – Main fluid paths in open cross flow structures: a) flow following the valleys, b) bypassing flow, c) flow crossing the valleys [21].

In the first possible fluid path the liquid follows the orientation of the valleys in the corrugated sheets, is reflected at the side wall and returns through a valley of the opposite plate - see figure 8 a). This type of flow is very important for the heat transfer to and from the tube wall. For construction reasons there is a cleavage between the structures and the tube wall, thus creating a second flow type, a bypass flow in the gap between the structure and reactor wall - see figure 8 b). The flow type coming through the valleys is not directly reflected to the opposite plate, but tends to stay for a certain time in this bypass before leaving it again through another valley further downstream [22]. The third possible fluid path always stays inside the packing, winding itself around cross-points of the sheet's corrugations and ensuring the good mixing behaviour and the heat and mass transfer between fluid flow and structure surface - see figure 8 c). The relative amount of flow in each regime will depend on many factors, including the channel height, channel angle and channel width, flow regimes and size of the gap [6].

To increase the heat transfer to the reactor wall, in the CCFS the third main flow type - see Figure 8 c) - is closed by flat sheets between the corrugated layers. This forces the whole fluid flow to contact the reactor wall where the heat transfer takes place.

Initial flow distribution in CCFS packings is very important. Since there is no exchange of liquid between adjacent channels, radial mixing characteristics are poor. On the other hand, due to the fact that the liquid in adjacent channels do not mix, the mixing takes place at the wall [21].

The CCFS packings are characterized by almost no radial mixing within the structure. What makes this structure so special is that it is open at the wall and as the flow is directed from left to right and vice versa in the adjacent layers it directly hits the reactor tube wall causing optimal disturbances of the stagnant layers at the wall. If the channel size is sufficiently small, Taylor flow will be induced provided the ratio gas to liquid flow rate is in the right range. The pressure drop in these packings is lower than that of OCFS packings even though the closed channel has a higher surface area [23]. By inserting a flat sheet between two corrugated sheets the energy consuming gas–gas interaction at the channels crossing is removed. These type of packings are open at the wall and the flow directed from the structure to the wall, very efficiently helps in disturbing the laminar film present in the gap between the edge of the packing and the wall. This creates turbulence thus improving the heat transfer from the packing to the wall. These packings show a lower sensitivity to gap sizes between the skin of the packing and the wall [24].

2.3.1 Definition of the Heat Transfer Parameters

For reactions which are strongly exothermic or strongly endothermic a good heat transfer is important to guarantee a homogeneous radial temperature profile throughout the reactor. In

exothermic reactions, a poor heat transfer can induce hot spots, which favor side reactions, diminishing the selectivity of the desired product. Hot spots can also lead to fast deactivation or sintering of the active catalytic components and even to temperature runaway [22].

Strongly exothermic, like FTS, or endothermic processes are generally carried out in multitube reactors to permit heat removal, respectively heat supply, through a fluid medium that surrounds the tubes.

The heat transfer in tubes filled with catalytic random packings is usually calculated using the 2-D pseudo-homogeneous plug flow model with two parameters describing the overall heat transfer resistance: an effective radial thermal conductivity ($\lambda_{e,r}$) lumping together all heat transfer mechanisms within the fluid (conduction and convection) while neglecting temperature differences between the liquid and the solid phase, and a wall heat transfer coefficient (α_w) [4]. The $\lambda_{e,r}$ determines the heat transfer rate through the structured packing from the centre to the edge. The α_w determines the heat transfer rate from the edge of the packing to the wall [5]. In this model two main assumptions are made: (i) at any location of the reactor all three phases (gas, liquid, solid) are at the same temperature and (ii) plug flow conditions exist for the gas and liquid phases. This model also assumes that the packing is isotropic.

The 2-D model is given by the following equation [5]:

$$(u_L C_{p,L} \rho_L + u_G C_{p,G} \rho_G)\frac{\partial T}{\partial z} = \lambda_{e,r}\left[\frac{\partial^2 T}{\partial r^2} + \frac{1}{r}\frac{\partial T}{\partial r}\right] \tag{2}$$

with the following initial and boundary conditions:

$$z = 0\ ,\ T = T_{in} \tag{3}$$

$$r = 0\ ,\ \frac{\partial T}{\partial r} = 0 \tag{4}$$

$$r = R\ ,\ -\lambda_{e,r}\frac{\partial T}{\partial r} = \alpha_w (T_{r=R} - T_w) \tag{5}$$

The estimated overall heat transfer coefficient, U_{est}, is calculated from $\lambda_{e,r}$ and α_w using the following equation [22]:

$$\frac{1}{U_{est}} = \frac{1}{\alpha_w} + \frac{R}{4\lambda_{e,r}} \tag{6}$$

The previous equation is valid for a cylindrical coordinate system [22].

The overall heat transfer coefficient, U_{ov}, is calculated from the overall heat balance using the experimentally obtained temperature profiles. The total amount of heat transferred from the heat transfer column to the cooling water is:

$$\dot{Q} = U_{ov}\, 2\pi\, R\, L\, \Delta T_{LM} \tag{7}$$

where:

$$\Delta T_{LM} = \frac{\left(T_{m,in} - T_w\right) - \left(T_{m,out} - T_w\right)}{\ln \dfrac{\left(T_{m,in} - T_w\right)}{\left(T_{m,out} - T_w\right)}} \tag{8}$$

The total amount of heat that will be transferred from the column is:

$$\dot{Q} = \left(u_L \rho_L C_{p,L} + u_G \rho_G C_{p,G}\right)\left(T_{m,in} - T_{m,out}\right) \tag{9}$$

At steady state both heat fluxes are equal and U_{ov} can be calculated:

$$U_{ov} = \frac{\left(u_L \rho_L C_{p,L} + u_G \rho_G C_{p,G}\right)\left(T_{m,in} - T_{m,out}\right)}{2\pi R\, L\, \Delta T_{LM}} \tag{10}$$

The inlet and outlet temperatures are the average temperatures obtained from the mixing cup averages of the temperature profiles at the inlet and outlet of any section [5]. The mixing cup temperature is calculated using the following equation:

$$T_m = \frac{2\pi \int_0^R T_z(r)\, r\, dr}{2\pi \int_0^R r\, dr} = \frac{2}{R^2} \int_0^R T_z(r)\, r\, dr \tag{11}$$

For example, for the section A-B the inlet mixing cup temperature is calculated from ring A and the outlet of mixing cup temperature is calculated from ring B.

Is very difficult to fit the parameters $\lambda_{e,r}$ and α_w in equation (2) since the packings present a very flat radial temperature profile. Therefore the confidence intervals of those parameters will be very large. Since equation (6) uses those parameters to calculate the value of U_{est} this value is expected not to be reliable. To test this, the values of U_{est} and U_{ov} will be compared.

The total heat flux is dependent on both contributions, $\lambda_{e,r}$ and α_w. The next figure illustrates the effect of varying $\lambda_{e,r}$ and α_w on radial temperature profiles.

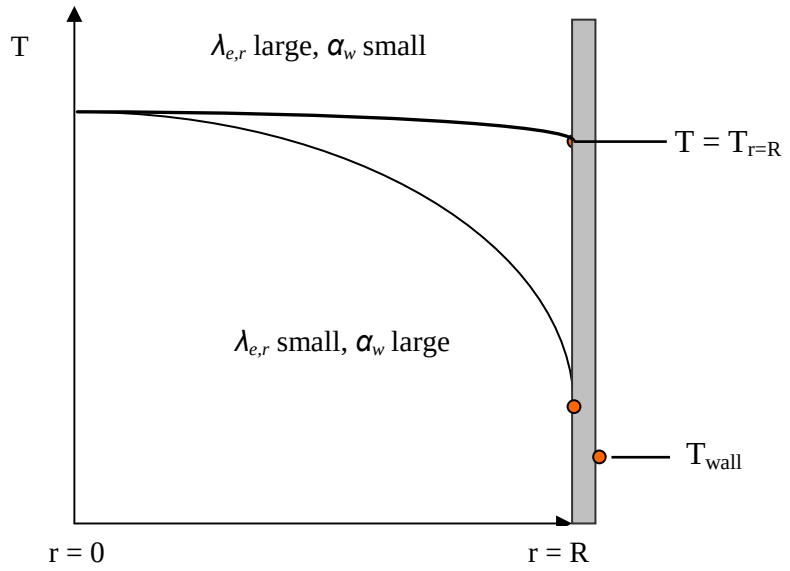

Figure 9 – Qualitative representation of the effect of varying heat transfer coefficients on radial temperature profiles.

Large values for $\lambda_{e,r}$ are given if the heat transport within the packing is good, resulting in almost uniform radial temperature profile. Small values of $\lambda_{e,r}$ lead to significant radial temperatures variations. Large values for α_w correspond to a good heat transfer between the wall and the packings resulting in a small temperature jump near the wall. Small α_w values allow only a poor heat transfer from the wall and lead to a large temperature difference between the wall and the fluid [22].

$\lambda_{e,r}$ for structured packings is typically larger than that for glass beads; this is due to the significant contribution of the radial convection component in addition to the improved static conductivity which depends mainly on the geometry of the matrix and the conductivity properties of the material. On the other hand, α_w is expected to be smaller in case of structured packings due to a defined gap present between the skin of the packing and the reactor wall [5].

There are two different ways of determine the heat transfer parameters mentioned above: (i) constant wall temperature approach and (ii) constant heat flux approach.

In the first approach the temperature at the wall of the heat transfer tube is maintained constant throughout the complete length of the column; this can be achieved by circulating heat transfer liquids in the jacket of the heat transfer column. Care has to be taken that the heat transfer area is sufficiently high to remove the heat from the heat transfer column; most importantly the circulation rates of the liquid in the jacket must be high enough to avoid any temperature variations in the wall along the length of the column.

In the second approach it is necessary that the column receives a constant heat flux along its entire length; this is commonly obtained by heating the column through its entire length by electrical

resistant wires such that provides a constant heat flux throughout and the heat flux is known. In this case the wall temperature will vary as the temperature profile is developing within the packing. The metal should be insulated at regular intervals in order to limit axial conduction in the wall; if is not done correctly it will result in large errors in measurement of wall temperatures and hence calculation of the wall heat transfer coefficient [5].

In this work the methodology of constant wall temperature was adopted for evaluating heat transfer rates in structured packings since the set-up was designed according to this methodology.

3. Experimental

3.1 Description of the Heat Transfer Set-Up

The heart of the set-up is a heat transfer column made of aluminum. Gas and liquid are first heated and fed co-currently to the top of the heat transfer column. The gas-liquid mixture is cooled by heat exchange with cooling water, thermostating the column externally. Temperature profiles are recorded radially and axially using several thermocouples. These profiles are then used to characterize the different packings based on their heat transfer rates through two parameters: the effective radial thermal conductivity ($\lambda_{e,r}$) and the wall heat transfer coefficient (α_w).

The heat transfer column is 1 m in length and has an internal diameter of 5.0 cm. The column consists of 6 modules, 4 of which are each 20 cm in length and 2 of which are each 10 cm in length. The smaller length columns are placed in the first part of the column where the driving force is the highest due to the biggest temperature difference between the gas-liquid mixture and the cooling water. This arrangement enables the measurement of the temperature profiles over shorter distances in the first part. The temperature sensors were mounted on rings which were placed at 4 axial positions each between 2 modules [5].

Previous measurements showed that the temperature of the gas-liquid mixture at the exit of the column, i.e. the temperature profile observed at 95 cm from ring D, got very close (within 1-2°C) to the temperature of the cooling water. Therefore to avoid this problem, the position of ring D was changed from 95 cm to 55 cm [5]. Thus the total length of the column became 60 cm with the ring D changed to 55 cm, see figure 10.

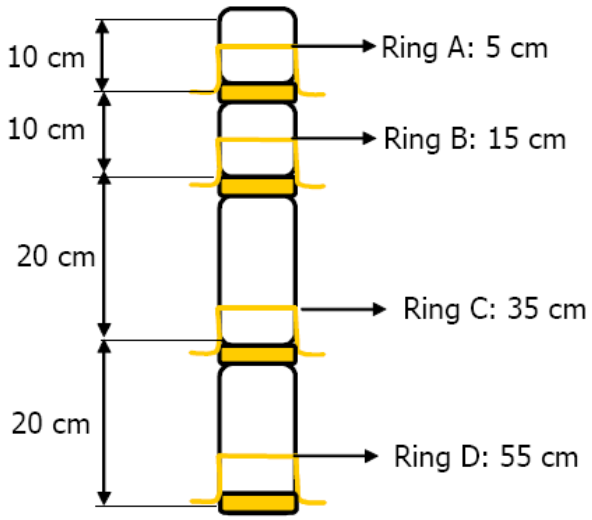

Figure 10 – Column length of 60 cm with the ring D placed at 55 cm [5].

The column tube which contains the packings is covered by a chamber called as “jacket” used for circulation of the cooling water. The outside of the column tube contains 4 set of grooves. Each set of groove had its own inlet and outlet of 6 mm O.D. for inflow and outflow of cooling water constructed on the external wall of the jacket. The grooves help in increasing the heat transfer area and generating turbulence in the cooling water. The excellent conductivity of the aluminum together with the special design of the jacket is considered to be sufficient so that the heat transfer on the cooling side is not limiting the heat transfer process. The water flows in and out of each set of groove in cross-flow mode. In total there are 24 inlets and 24 outlets in the six column modules. A detailed photo of the complete column is provided in the next figure.

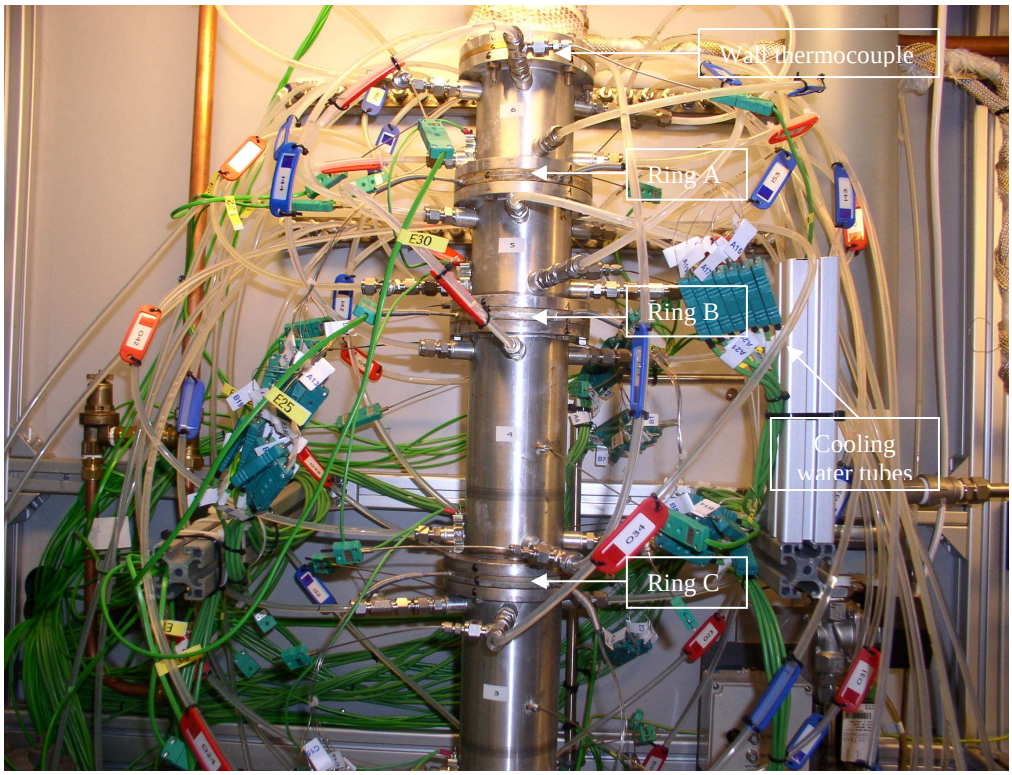

Figure 11 – Photo of the column with the rings, cooling water inlets and outlets and wall thermocouples.

The OCFS and CCFS packings are 5 cm in height with a diameter typically between 4.9 and 5.0 cm (less than 5.0 cm to fit inside the column tube) can be packed into the column (20 modules in the 1 m column). These packings are anisotropic in nature. This means that these packings do not have the same properties in different radial directions. Therefore the heat distribution will not be the same thus obtaining different profiles along different angular positions at the same axial position. Therefore the rings have radial temperature sensors in three different circumferential directions (see figure 14). A thermocouple ring has 21 thermocouples of 0.5 mm diameter, having an accuracy of +/- 1°C, placed in three angular positions in the same plane (R1=0°, R2=90°, R3=135°). Each

angular position contains seven thermocouples with 2 mm length. The distance between the thermocouples is chosen depending on how close they are to the edge. Since the measurements near the edge are more important, due to the strong wall heat transfer resistance, more thermocouples are placed near the edge than near the centre [5], as can be seen in figure 12.

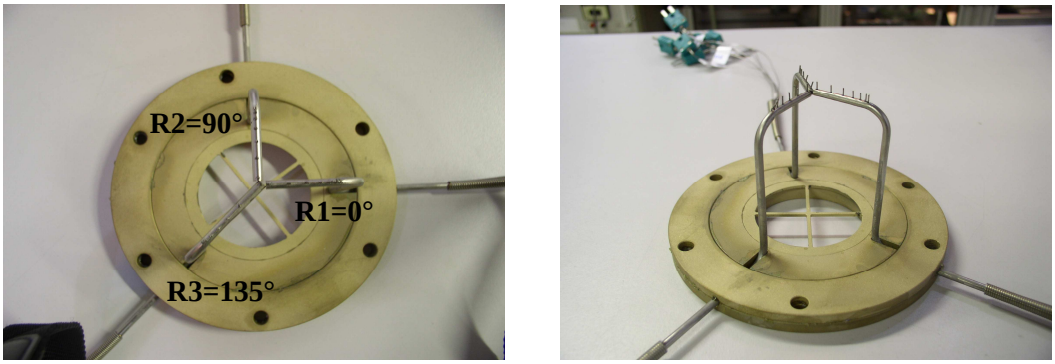

Figure 12 – Top view of the ring and side view of the ring.

Four such rings were placed at different axial positions of the column. In total there are 84 thermocouples installed to measure the radial and axial profiles. The radial positions and the distances from the edge are given in table 3.1.

Table 3.1 – Radial positions on each angular position with distances of each radial position from the centre of the axis.

Radial positions	**R1 axis** (+/- 0.2 mm)	**R2 axis** (+/- 0.2 mm)	**R3 axis** (+/- 0.2 mm)
r1	3	3	0
r2	9	9	9
r3	14	14	14
r4	18	18	18
r5	21	21	21
r6	23	23	23
r7	24	24	24

Besides these, 24 thermocouples are provided to measure the temperature of the cooling water at the inlet and outlet of the jacket to see that these temperatures are maintained constant; 2 thermocouples are placed in 2 inlets and 2 thermocouples are placed in 2 outlets of each module [21]. 16 thermocouples are placed in the wall along the length of the column to measure the wall temperatures. The 20 cm modules are fitted with 3 thermocouples and the 10 cm modules are fitted

with 2 thermocouples. The distance of each wall thermocouple from the bottom of the column is given in table 3.2.

Table 3.2 – Wall thermocouples positions from the top of the column [5].

Module	Number of thermocouples	Axial distance (cm)
6	1	0
5 & 6	2	10
4 & 5	2	20
4	1	30
3 & 4	2	40
3	1	50
2 & 3	2	60
2	1	70
1 & 2	2	80
1	1	90
1	1	100

So in total the heat transfer column is equipped with 128 thermocouples.

In appendix A is presented the process scheme of the heat transfer unit and a list of equipment code and valves for the heat transfer set-up with a brief description of each one.

A precolumn or calming column of 80 cm in length, also made of aluminum, is placed on the top of the heat transfer column to stabilize the temperature and flow profiles. The liquid is distributed on the top of the calming zone with a showerhead consisting of 51 points with the point diameter of 0.5 mm. The gas enters through 4 inlets to ensure its equal distribution in the packing. The column is designed for co-current flow gas and liquid.

A gas/liquid separation zone is in the bottom of the heat transfer column. In this zone the gas is separated from the liquid and escapes to the surroundings via the ventilator and the liquid goes back to X8 (see appendix A) and stays in circulation.

The set-up can be divided in three sections: (i) liquid flow loop, (ii) gas flow zone and (iii) cooling water flow loop (see figure 13).

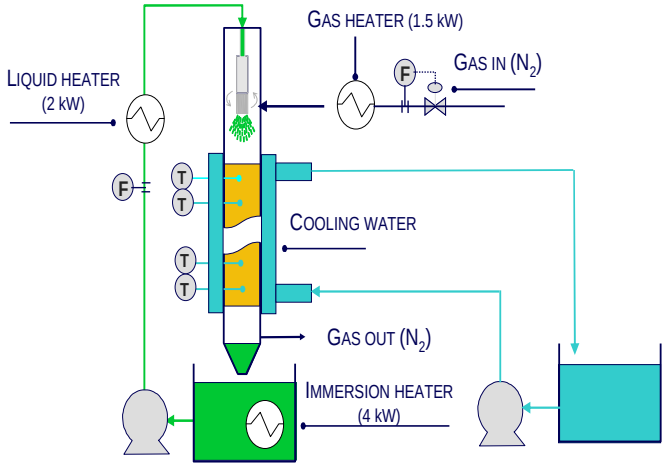

Figure 13 – Schematic representation of the heat transfer set-up [5].

Liquid Flow Loop

The process liquid, ISOPAR-M (a mixture of isoparaffins typically in the diesel range), is stored at atmospheric pressure in X8. In table 3.3 some properties of ISOPAR-M are given.

Table 3.3 – Properties (20°C and 1 atm) of ISOPAR-M used in this experimental work [25].

	Molar mass (kg/mol)	Density (kg/m^3)	Viscosity (mm^2/s)	Surface Tension (N/m)	Flash Point (°C)	Flammable Limits
ISOPAR-M	192	789	3.80	0.0275	81	LEL: 0.5% UEL: 4.8%

The liquid is heated to 50°C (10°C below the operating temperature) in X8 by an immersion heater EH-1. The liquid level and the pressure in the cooling vessel (X8) are indicated and controlled with LIL-1 and PI-2, respectively. The liquid is pumped to the top of the precolumn with the gear pump X3. A manual valve MV-9 is placed in the liquid line to regulate the flowrate by creating a leak flow, which prevents the pump from running dry.

The liquid is heated to the operating temperature (60°C) in EH-2. The reason why two heaters were installed instead of just one is that as the liquid cools down as it flows through the column, there is a considerable drop in temperature, which cannot be predetermined; due to this uncertainty it is preferred to have an immersion heat in the liquid tank (which will heat up the liquid from room temperature to 50°C) and the remaining temperature rise is provided by a flow heater placed in the liquid line from the pump to the column (EH-2). This way the heating load is divided between two heaters and a better temperature control can be achieved on the liquid coming out of the flow heater. After the liquid enters in the top of the precolumn and passes through the precolumn and the heat transfer column the gas/liquid mixture enters in the gas/liquid separation zone where they will be separated. Finally the liquid goes back to X8.

Gas Flow Zone

Nitrogen was chosen as process gas because it is inert in nature and it does not react with ISOPAR-M. The nitrogen is obtained from the net supply. Before it enters in the precolumn it passes through a mass flow controller (FIC) and through a heat exchanger (EH-3) that heats the gas flow from room temperature to 60°C. After leaving the heat transfer column the gas/liquid mixture is separated in the gas/liquid separation zone, it is first cooled to condense ISOPAR-M, and then the gas escapes to the surroundings.

Cooling Water Loop

The cooling water is storage in X9. The water is pumped to the jacket of the heat transfer tube with the centrifugal pump X10. The X10 suction line is divided in 24 inlets lines that are connected to the column and there are 24 cooling water outlets from the column that are joined in one line out of the set-up. Thus the cooling water is discharged in only one line to X9.

The inlet and outlet temperatures of the cooling water in the jacket are measured and the flowrate is large enough such that there is a maximum 1°C between the inlet and the outlet temperatures.

3.2 Experimental Procedure

The column is pre-wetted for a period of 45 minutes with a high liquid velocity (u_L = 21 mm/s) and a low gas velocity (u_G = 0.17 m/s) to ensure fast spreading and wetting of the packing. After the pre-wetting process, the heaters are switched on to heat up the gas and the liquid. Also the cooling water flow is started.

Measurements were carried out starting from the lowest to the highest liquid velocity (6.05 – 25 mm/s) at different gas velocities (0.4 – 2.6 m/s). Each experiment lasts 5 minutes and was duplicated, with an interval of 2 minutes. When the velocity of the gas or the liquid was changed 15 minutes were waited to reach the new steady state.

The radial and axial temperature profiles are recorded in real time, with an interval of 3 seconds, by LabView®.

The first packing to be analyzed was the OCFS. It was decided to study first how the orientation of the packing influences the heat transfer, starting with the packings turned 90° into each other and then 0°. After that the influence of the gap between the edge of the packing and the reactor wall (small, medium and big gap) was studied. For each type of experiment (orientation or gap) 16

experiments were performed (see table 3.6). 4 of the 16 experiments were repeated in the following day to ensure the reproducibility of the results and sometimes verify unexpected results.

Table 3.6 – Combinations with gas and liquid velocities that were made for each experiment.

u_L (mm/s) \ u_G (m/s)	**0.4**	**1.1**	**1.8**	**2.6**
6	*1	*2	*3	*4
12	*5	*6	*7	*8
18	*9	*10	*11	*12
25	*13	*14	*15	*16

* Experiment number

The same procedure that was used on the OCFS packings was used for the CCFS packings.

The procedure to dismount and mount the set-up, including testing for leaks in the cooling water and the column, takes approximately one day.

4. Data Analysis

The experimental measurements in the OCFS and CCFS packings were done with the same type of liquid (ISOPAR-M) and gas (nitrogen) with different ranges of gas and liquid flow.

Calibration of the liquid pump was done (see appendix B).

LabView® records the radial and axial temperatures every 3 seconds. The average temperature was calculated for each thermocouple in each experiment over a period of 5 minutes.

The overall heat transfer coefficient (U_{ov}) was calculated by the overall energy balance for a system in co-current - equation (10) - using Excel®. This balance takes into account all the heat transfer in the column from the first ring to the last ring. The overall heat transfer coefficient was calculated for four different ranges: from A-ring to D-ring – $U_{ov(AD)}$, from A-ring to B-ring – $U_{ov(AB)}$, from B-ring to C-ring – $U_{ov(BC)}$ and from C-ring to D-ring – $U_{ov(CD)}$. Since ring A is placed only after 5 cm of the heat transfer column where cooling starts, the temperature profile is not yet fully developed and therefore high heat transfer rates are obtained for the section AB; at the outside of D-ring the temperature of the liquid and the gas is very similar with the temperature of the cooling water therefore low heat transfer rates are obtained for the section CD. $U_{ov(BC)}$ was chosen as a reference to analyze all data. An important reason for this was to compare the results of this work with the results of previous research.

The error of U_{ov} was calculated by error propagation of equation (10) (see appendix C1). The error of U_{est} was calculated by error propagation of equation (6) (see appendix C2).

The equation that was used to calculate the overall heat transfer coefficient is a function of the density and heat capacity of gas and liquid. These properties are a function of the temperature. To calculate the density of the nitrogen the ideal gas equation was used, for the liquid the following equation was used [26]:

$$\rho = -0.3367\,T + 885.97 \tag{12}$$

Since the temperature range of the experiments is very small (20 – 60°C) the heat capacities of the liquid and the gas were considered constant at T = 20°C [$Cp_{ISOPAR\text{-}M}$ = 2170 J/(kg.K); Cp_{N2} = 1130 J/kg.K)] [21], [26]. The value of heat capacity of nitrogen for the same conditions found in the literature [27] [Cp_{N2} = 1039.7 J/kg.K)] was not the same as the one that was used. However, the first value that was mentioned was used so it was possible to compare the present results with previous results obtained from other researchers.

Equation (2) is solved using MatLab® (see the code in DVD: code of MatLab; regress_pde.m) to fit the computed temperatures profiles inside the packed bed to the experimental ones and the two parameters, $\lambda_{e,r}$ and α_w, are obtained by minimization of the sum of the squared errors between the computed temperatures profiles and the experimental ones. Since the previous researchers used Athena® to calculate the $\lambda_{e,r}$ and α_w values, the Athena® program was also used to solved the equation (2) for some experiments. Since this program used the same equations as MatLab® the results should be the same. For both programs the 95% confidence intervals for $\lambda_{e,r}$ and α_w are obtained from the parameter estimation.

Since the 2-D pseudo-homogeneous is a relative complicated model the simplified 2-D pseudo-homogeneous model – see equation (13) - was also used to calculate the parameters $\lambda_{e,r}$ and α_w (see the code in DVD – code of MatLab; regress_T.m). Equation (13) can be derived from equation (2) if a parabolic radial temperature profile is assumed [23]. The 95% confidence intervals for $\lambda_{e,r}$ and α_w are obtained from the parameter estimation.

$$\frac{T - T_w}{\overline{T} - T_w} = \frac{U_{est}}{\alpha_w} - \frac{U_{est}\,D}{\lambda_r}\left[\left(\frac{r}{D}\right)^2 - \frac{1}{4}\right] \tag{13}$$

5. Results and Discussion

The OCFS packings were measured and were classified in 3 categories (small, medium and big) according to the gap between the packings and the reactor wall (see figure 14 and table 4.1). Since only 24 CCFS packings exist (the exactly number that is needed to perform experiments) they were not measured and classified.

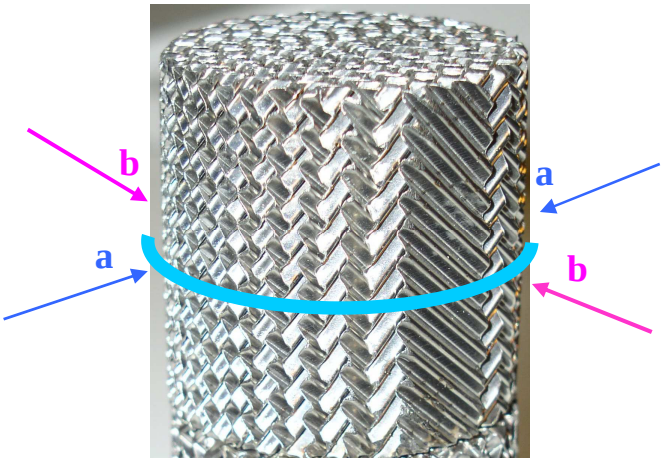

Figure 14 – Representation of *a* and *b* directions.

Table 5.1 – Average and standard deviation of *a* and *b* and range of the gap of the three types of OCFS packings.

	Small_gap	Medium_gap	Big_gap
average_*a* (cm)	4.99	4.97	4.95
average_*b* (cm)	4.75	4.74	4.72
standard-deviation_a	0.014	0.011	0.020
standard-deviation_b	0.015	0.0094	0.019
Range of the gap (%)	4.8 – 5.6	5.8 – 6.0	6.1 – 7.9

a and *b* were also measured on the top of the packings and it was concluded that for the *a* direction the value obtained was the same as in the centre. However for the *b* direction it had a difference of 0.08 cm, 0.09 cm and 0.12 cm respectively for the OCFS packings with a small, medium and big gap.

Before starting to investigate the influence of the orientation and the gap on the heat transfer performance some previous results were reproduced. To reproduce those results the minimum and maximum value of liquid and gas velocities that the previous researcher used were chosen. Each experiment was done in duplicate, with an interval of 2 minutes (see appendix D). In the next table are presented the results that were obtained.

Table 5.2 – Results obtained for the overall heat transfer coefficient for the OCFS packings for this research ($U_{ov\_average}$) and previous research ($U_{ov\_previous\_res}$) with the respective deviations (difference = ($\max U_{ov} - \min U_{ov}$)/$\max U_{ov}$; ΔU = ($U_{ov\_average} - U_{ov\_previous\_res}$) / $U_{ov\_average}$).

u_L (mm/s)	u_G (m/s)	$U_{ov\_average}$ (W m^{-2}K^{-1})	Difference (%)	$U_{ov\_previous\_res}$ (W m^{-2} K^{-1})	ΔU (%)
22	0.4	896	3	885	1
22	2.6	997	1	967	3
6.05	2.6	644	1	479	26
6.05	0.4	597	1	375	37

It was concluded that in this research a different category of OCFS packings was used than in the previous research; in this research packings that have a small gap were used and in the previous research packings with a medium gap were used. For high liquid velocities both type of packings are completely wet and the behaviour of the fluid flows are very similar which consequently makes the overall heat transfer coefficient be comparable (see the following two recordings: OCFS_90°_small-gap_high gas/liquid velocities and OCFS_medium-gap_high gas/liquid velocities). However, for low liquid velocities the OCFS packings with a medium gap have much more stagnant bubbles in the gap between the packing and the column than the ones with a small gap (see figure 15) which makes the overall heat transfer coefficient decrease (see also see the following two recordings: OCFS_90°_small-gap_low gas/liquid velocities and OCFS_medium-gap_low gas/liquid velocities).

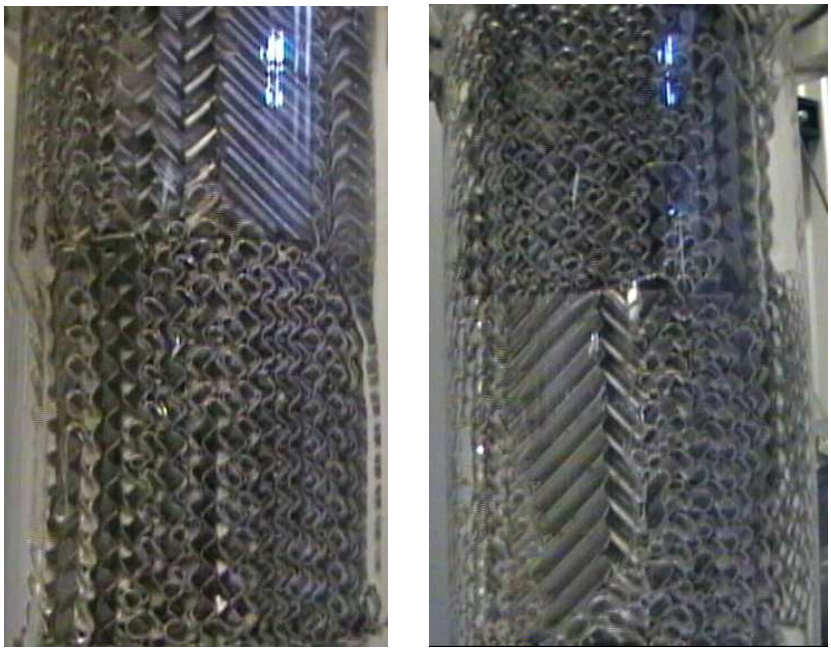

Figure 15 – Snapshots of the recordings of OCFS_90°_small-gap_low gas/liquid velocities (left) and OCFS_medium-gap_low gas/liquid velocities (right).

5.1 OCFS PACKINGS

5.1.1 – Orientation

To study the orientation in the OCFS packings the values of the overall heat transfer coefficient was compared for 0° and 90°. The maximum difference between the duplicate experiments was 6% for the packings turned 90° into each other and 4% for the packings turned 0° into each other while the average difference between the duplicate experiments was 2% for both orientations (see appendix E1). In the next figures are presented the results that were obtained (the values of $\lambda_{e,r}$ and α_w represented in the graphs were calculated with the 2-D pseudo-homogeneous model - see appendix E2).

It is possible to conclude that for every condition of gas and liquid velocities the packings turned 90° into each other are always better than the packings turned 0° into each other ($U_{ov\_90^o}$ always better than the $U_{ov\_0^o}$). Since the packings are anisotropic when the orientation is changed a better mixing is obtained because the liquid that is going in bypass through the gap is obligated to pass through the channels in the next packing.

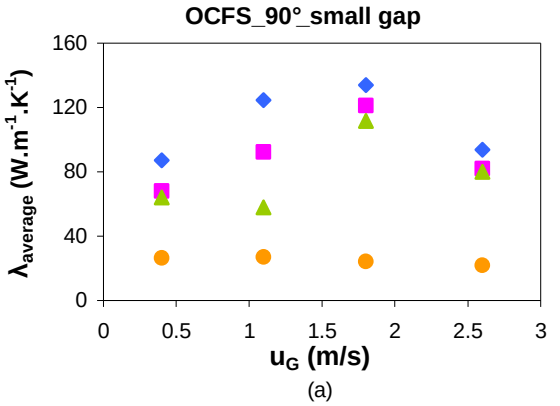

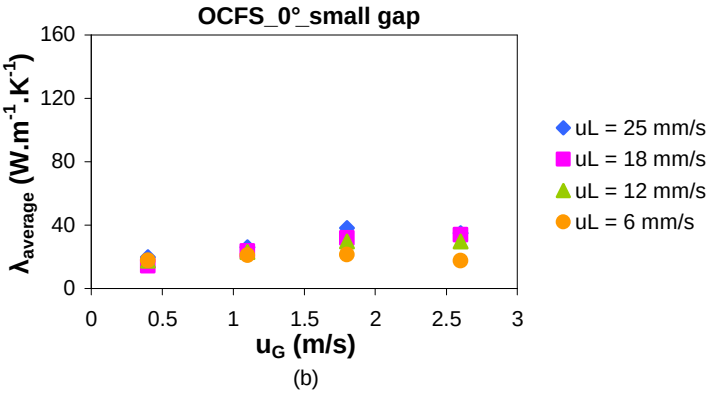

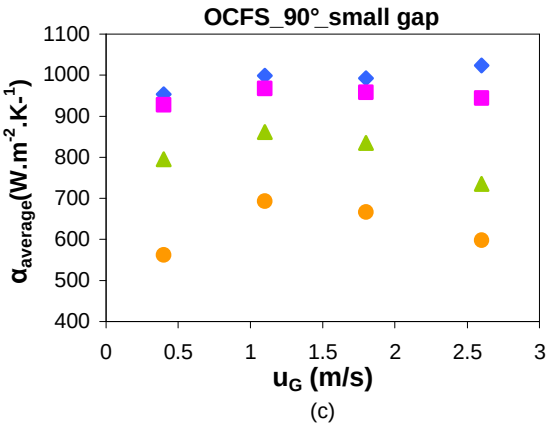

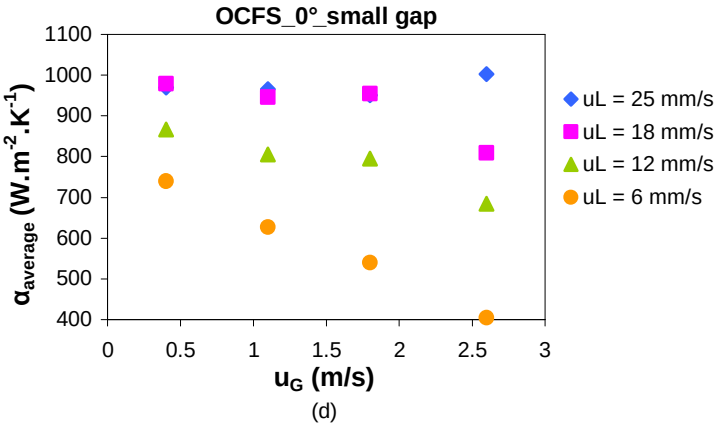

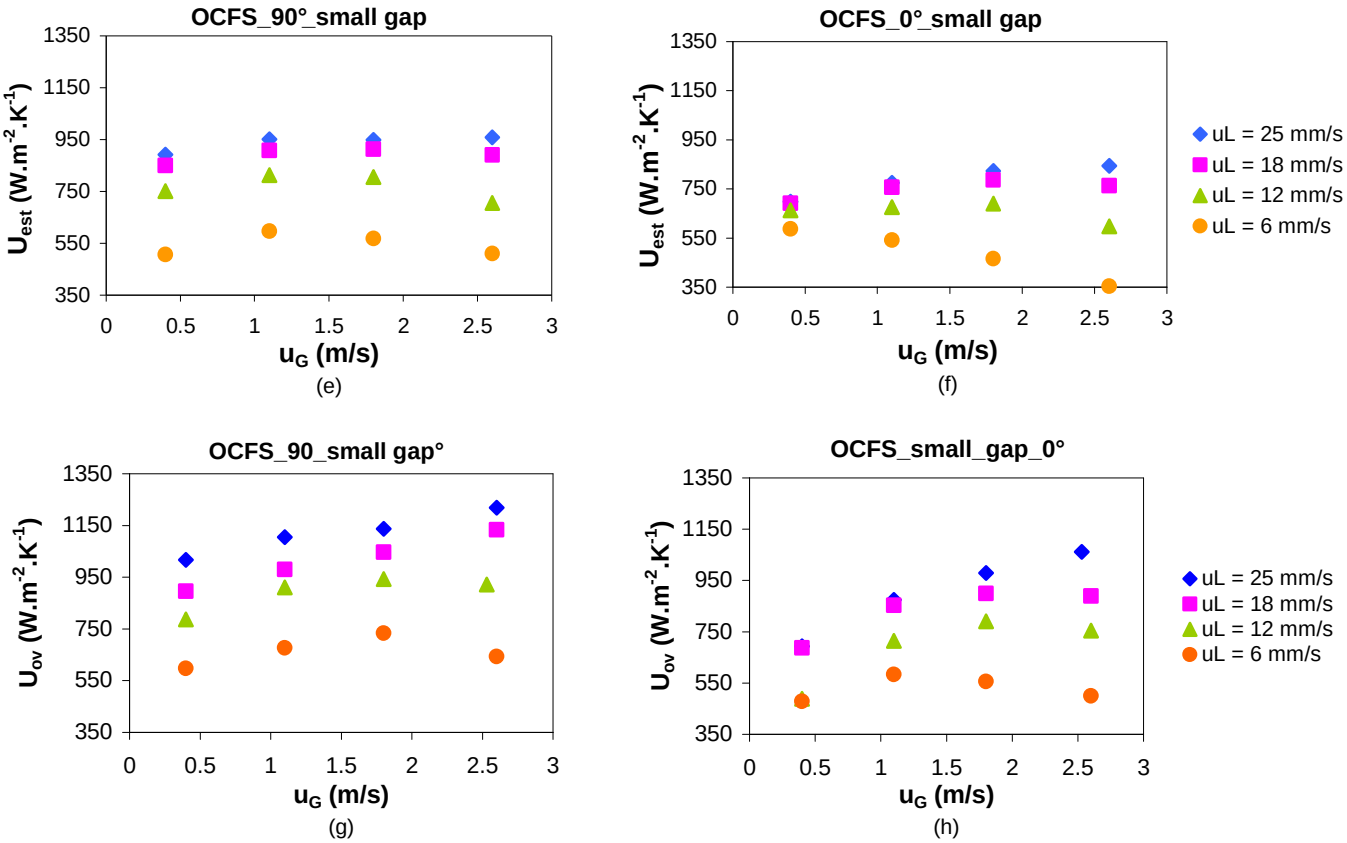

Figure 16 – Profiles obtained for $\lambda_{average}$, $\alpha_{average}$, $U_{estimate}$ and $U_{overall}$ as a function of gas velocity for the OCFS packings with a small gap turned into 90° ((a),(c),(e),(g)) and 0° ((b),(d),(f),(h)) into each other.

The λ_{static} is the conductive component of the heat transport. The λ_{static} in OCFS packings is estimated to be between 8 – 10 ($W.m^{-1}.K^{-1}$) [21]. Thus in this case the convective contribution is highly significant as concluded from the values of $\lambda_{e,r}$ that were obtained, particularly for the packings turned 90º into each other. The graph of $\lambda_{e,r}$ versus gas velocity for different liquid velocities shows an increasing trend until a certain gas velocity and then a decreasing trend (this effect is better visualized in graph (a)). So, it is possible to conclude that $\lambda_{e,r}$ increases in the stratified wavy flow regime and decreases in the annular regime (see figure 17).

This means that the radial convection of liquid is higher at low gas velocities due to the presence of mixing of the liquid by the gas in the stratified wavy flow regime. At high gas velocities the liquid slugs are destroyed forming a thin liquid film on the gap with the gas flowing through the channels of the packing. Therefore the intense mixing attributed to the liquid slugs is lost resulting in a decrease in the $\lambda_{e,r}$ values. The large confidence intervals particularly at high values of $\lambda_{e,r}$ indicate that the radial temperatures profiles are very flat and hence estimation of $\lambda_{e,r}$ can be inaccurate (see appendix E2).

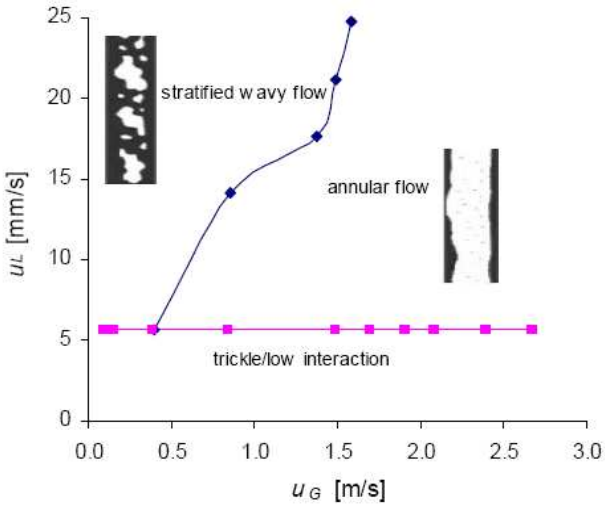

Figure 17 – Flow – map of liquid velocity versus gas velocity for OCFS packings [21].

The graph of α_w versus gas velocity does not show a strong dependence on the gas velocity for high and medium liquid velocities. The heat transfer at the wall is dominated partly by conduction through the liquid film which flows in the gap between the packing and the reactor wall and partly by the turbulence generated near the wall as a result of convection of the liquid in the radial direction. The small increase or decrease in α_w values with the gas velocity for high and medium liquid velocities indicates that both conductive and convective transport of heat at the wall does not change with the gas velocity. However, for low liquid velocities the value of α_w strongly depends on the gas velocity, especially when the packings are turned 0º into each other, because when this velocity is increased more and bigger stagnant bubbles are formed. Since the velocity of the liquid is low the bubbles will not be pushed forward, which consequently decreases the value of α_w as the gas has poorer heat transfer properties than the liquid.

The graph of U_{est} versus gas velocity shows a similar behavior with the graph of α_w versus gas velocity. This is due to the fact that $\lambda_{e,r}$ is very high and consequently α_w becomes the rate limiting factor (to compare directly the values of $\lambda_{e,r}$ and α_w we have to multiply $\lambda_{e,r}$ by 4 and divide by R – see equation (6)).

Just like was mentioned before, it is very difficult to fit the parameters $\lambda_{e,r}$ and α_w in equation (2) since the packings present a very flat radial temperature profile. Therefore the confidence intervals of those parameters are very large. Since equation (6) uses those parameters to calculate the value of U_{est} this value was expected not to be reliable. Comparison between the values of U_{ov} and U_{est} shows that they are not the same; generally U_{est} is smaller than U_{ov}. So it is possible to conclude that this value is not reliable.

To verify the reproducibility of the results that were previously obtained some experiments were repeated in a different day for the OCFS packings turned 0° into each other (see appendix E1). In table 5.3 are presented the results that were obtained.

Table 5.3 – Comparison between the results obtained for the overall heat transfer coefficient for OCFS packings for 0° in two different days and the respective deviation (difference = $U_{ov\_0°\_1}{}^{st}{}_{day}$ - $U_{ov\_0°\_2}{}^{nd}{}_{day}$).

		U_{ov_BC} (W.m^{-2}.K^{-1})		
u_L (mm/s)	u_G (m/s)	1st day	2nd day	Difference (%)
25	0.4	693	668	4
18	1.1	853	830	3
12	1.8	791	760	4
6	2.6	500	498	0

Since the maximum error that was obtained was 4% the reproducibility of the results was verified.

In the next figure are shown the temperatures profiles of R1, R2 and R3 for each ring for the OCFS packings turned 90° into each other with low gas and low liquid velocity.

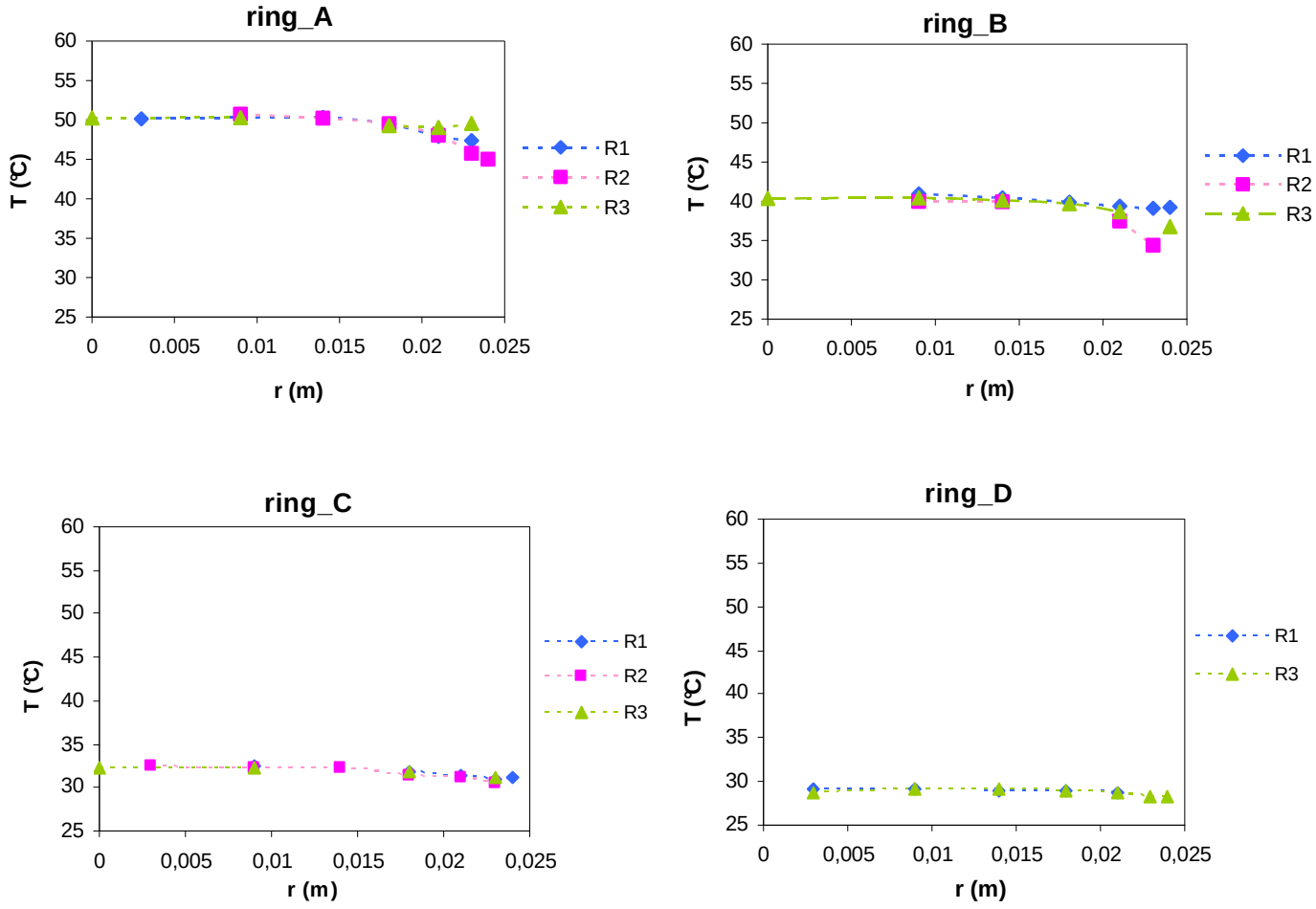

Figure 18 – Temperatures profiles of R1, R2 and R3 for each ring for the OCFS packings with a small gap turned 90° into each other with u_L equal to 6.05 mm/s and u_G equal to 0.4 m/s.

These temperatures profiles are for a specific experiment and a specific type of packing however this is a representative example of all the experiments and packings (OCFS and CCFS) since the behaviour of the other radial temperature profiles are similar.

It can be seen, particularly in the figures of ring A and ring B, that the temperature drop near the wall is smaller for R2 than for R1 indicating a better heat transfer along R2 as compared to R1. The heat transfer along the R1 axis is mainly convective since this axis is parallel to the gas and liquid flow (see figure 19). So in this direction a good radial mixing is achieved and consequently all the fluid will be at the same temperature, thus a flat radial temperature profile will be achieved. The length of the two corrugated metal sheets between which the thermocouples of R1 axis are placed is about the same as the diameter of the packing (see figure 19) so the fluid will only hit the wall once. Since the heat transfer just takes place at the wall, the temperature drop near the wall will be high. The heat transfer along R2 axis is mainly conductive since this axis is perpendicular to the gas and liquid flow (see figure 19). The thermocouples of the R2 axis are placed in different spaces of the corrugated sheets. Also the width of the sheets goes on decreasing along the R2 axis away from the centre. As it is possible to see in figure 19, as the width decreases the number of times that the fluid will hit the wall increases. This results in a better heat removal at the wall along R2 axis which consequently leads to a lower temperature drop near the wall.

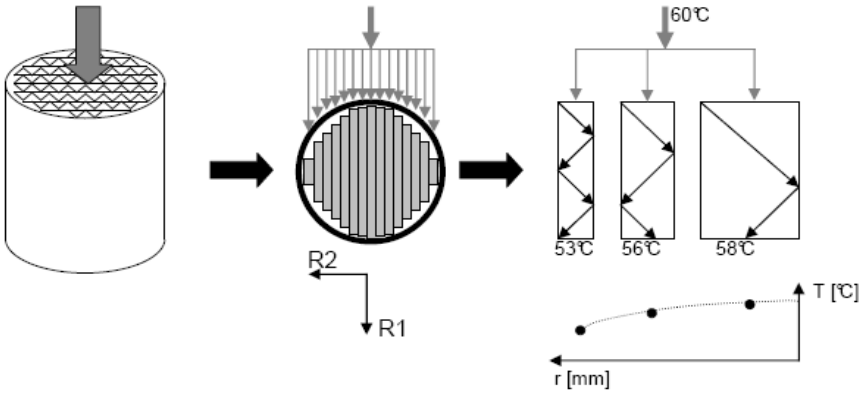

Figure 19 – Sketch of a structured packing and how the profile in R2 direction would look like due to the placement of the thermocouples [21].

5.1.2 – Gap

The values of the overall heat transfer coefficient were compared for the three types of OCFS packings. The maximum difference between the duplicate experiments was 2% for the OCFS packings with a medium gap, 6% for the OCFS packings with a small gap and 7% for the ones with a big gap while the average difference between the duplicate experiments was 1% for the OCFS packings with a small and a medium gap and 2% for the ones with a big gap (see appendix F1).

In the next figure are presented the results that were obtained. The graphs of α_w and U_{ov} versus gas velocity are given since those are the important ones to be analyzed. The graphs of $\lambda_{e,r}$ and U_{est} versus gas velocity are given in appendix F1. The values of $\lambda_{e,r}$ and α_w represented in the graphs were calculated with the 2-D pseudo-homogeneous model - see appendix F2.

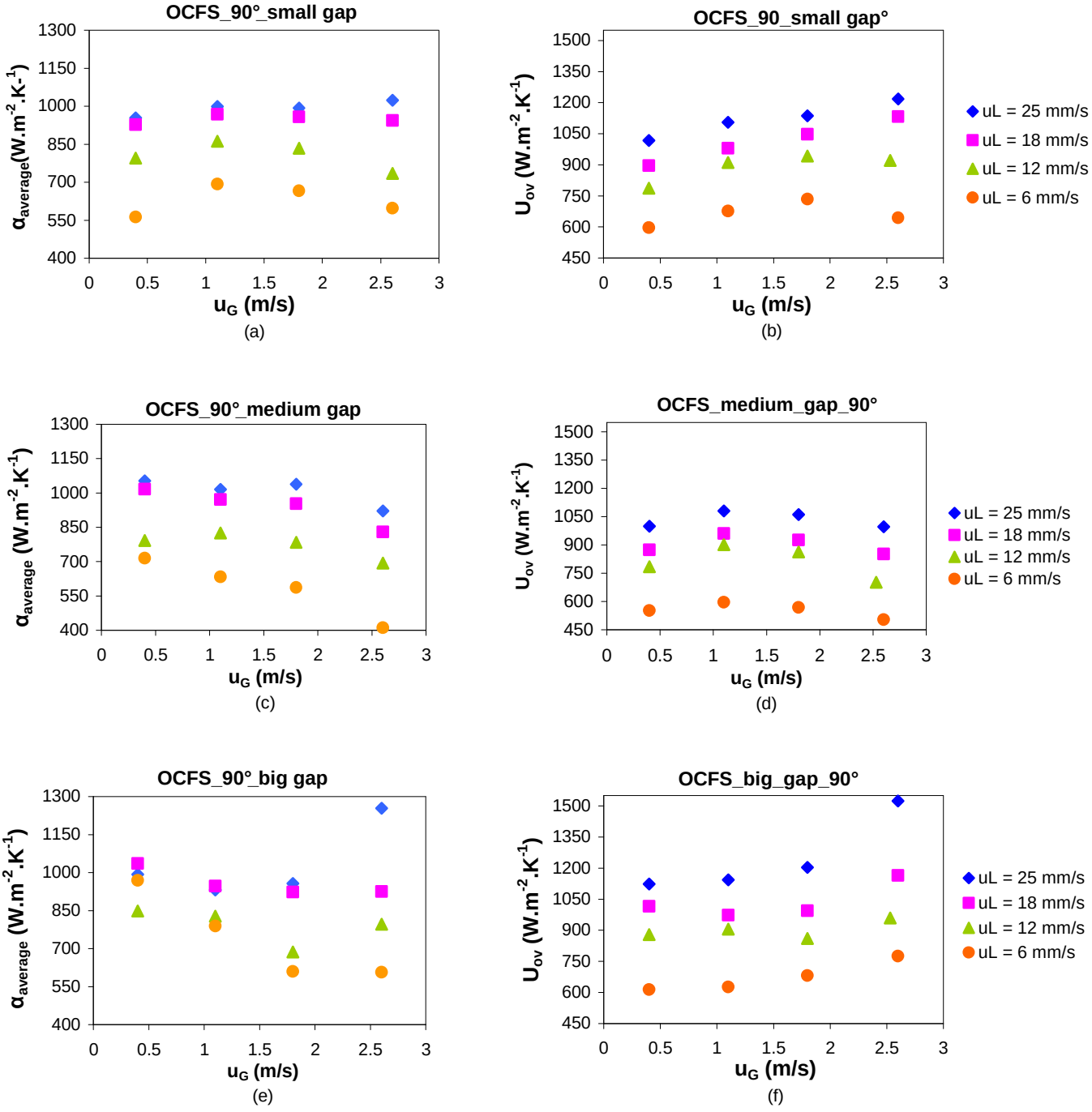

Figure 20 – Profiles obtained for $\alpha_{average}$ and $U_{overall}$ as a function of gas velocity for the OCFS packings with a small ((a),(b)), medium ((c),(d)) and big gap ((e),(f)) turned into 90° into each other.

In general the OCFS packings with the higher value of U_{ov} are the ones that have a big gap. When the column is filled with packings with a small and a medium gap it is not completely wet in some parts of the gap (see figure 21) which makes the α_w decrease, since the gas has poorer heat

transfer properties than the liquid, and consequently the U_{ov} (see also the difference in the following two recordings: OCFS_big_gap_low gas/liquid velocities and OCFS_small_gap_90°_low gas/liquid velocities).

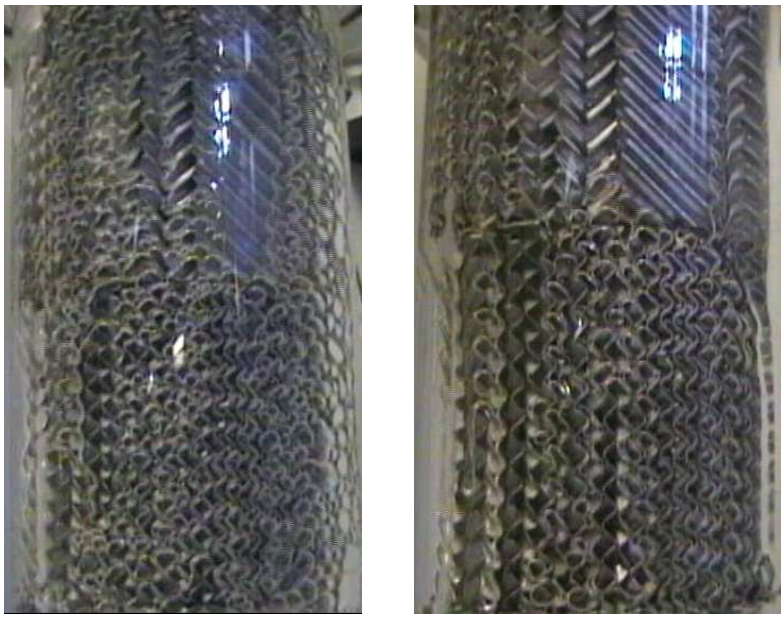

Figure 21 - Snapshots of the recordings of OCFS_big_gap_low gas/liquid velocities (left) and OCFS_small_gap_90°_low gas/liquid velocities (right).

However, for medium gas velocities and for low and medium liquid velocities the OCFS packings with a big gap are worse than the ones that have a small gap (see figure 22) because they have lots of stagnant bubbles which makes the U_{ov} decrease (see also the difference in the following two recordings: OCFS_big_gap_low liquid and medium gas velocities and OCFS_small_gap_90°__medium gas and low liquid velocities).

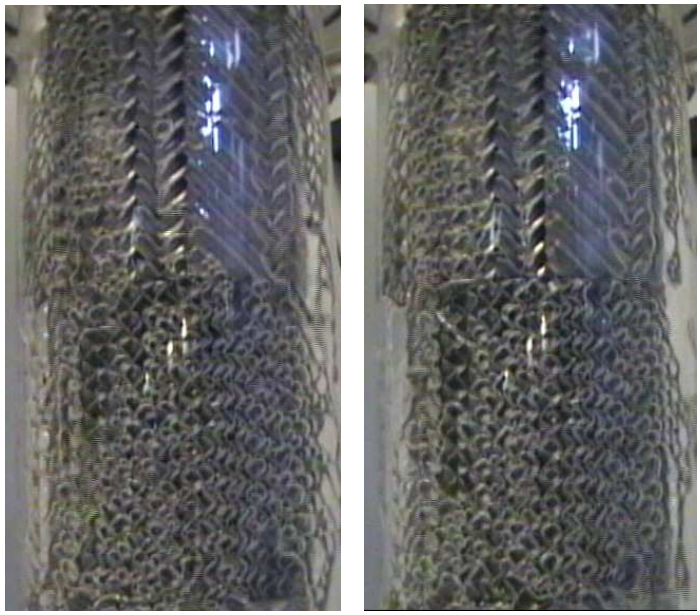

Figure 22 - Snapshots of the recordings of OCFS_big_gap_low liquid and medium gas velocities (left) and OCFS_small_gap_90°__medium gas and liquid velocities (right).

It is possible to conclude that for every condition of gas and liquid velocities the OCFS packings that have a medium gap are the worst.

Just like was mentioned before the λ_{static} in OCFS packings is estimated to be between 8 – 10 ($W.m^{-1}.K^{-1}$) [21]. So in this case the convective contribution is highly significant as concluded from the values of $\lambda_{e,r}$ that were obtained. The graph of $\lambda_{e,r}$ versus gas velocity for different liquid velocities (see appendix F3) shows an increasing trend until a certain gas velocity and then a decreasing trend - this effect is especially visualized in graph (a) and (b). So, it is possible to concluded that $\lambda_{e,r}$ increases in the stratified wavy flow regime and decreases in the annular regime (see figure 17), for the same reasons that were already mentioned before (see chapter 5.1.1).

The large confidence intervals particularly at high values of $\lambda_{e,r}$ indicate that the profiles are very flat and hence estimation of $\lambda_{e,r}$ can be inaccurate (see appendix F2).

The graph of α_w versus gas velocity shows a strong dependence on the gas velocity, particularly for the OCFS packings with a medium and a big gap. This is related with the number and the size of bubbles that are stagnant in the gap between the packing and the reactor wall. For the packings with a medium and a big gap it possible to see that when the velocity of the gas is increased, more and bigger stagnant bubbles are formed which consequently makes the value of α_w decrease. However, for high liquid velocity and high gas velocity, the packings with a big gap have the higher value of α_w. This happens due to the size of the gap; since these packings present a big gap the stagnant bubbles will be able to moved forward which consequently improves the value of α_w.

The graph of U_{est} versus gas velocity (see appendix F3) shows a similar behavior with the graph of α_w versus gas velocity. This is due to the reasons that were already mentioned before (see chapter 5.1.1).

Just like was mentioned before, it is very difficult to fit the parameters $\lambda_{e,r}$ and α_w in equation (2) since the packings present a very flat radial temperature profile. Therefore the confidence intervals of those parameters are very large. Since equation (6) uses those parameters to calculate the value of U_{est} this value was expected not to be reliable. Comparison between the values of U_{ov} and U_{est} shows that they are not the same; usually U_{est} is smaller than U_{ov}. Thus it is possible to conclude that this value is not reliable.

To verify the reproducibility of the results that were previously obtained some experiments were repeated in a different day for the OCFS packings with a big gap turned 90° into each other (see appendix F1). In table 4.4 are presented the results that were obtained.

Since the maximum error that was obtained was 2%, the reproducibility of the results was verified.

Table 5.4 – Comparison between the results obtained for the U_{ov} for OCFS packings with a big gap turned 90° into each other in 2 different days and the respective deviation (difference = $U_{ov\_0°\_1}{}^{st\ day}$ - $U_{ov\_0°\_2}{}^{nd\ day}$).

		U_{ov_BC} (W.m^{-2}.K^{-1})		
u_L (mm/s)	u_G (m/s)	1st day	2nd day	Difference (%)
12	0.4	879	857	2
6	1.1	626	622	1
	1.8	681	667	2

5.2 CCFS PACKINGS

To investigate how the orientation influences the overall heat transfer coefficient in the CCFS packings experiments with packings 0° and 90° into each other were done. The maximum difference between the duplicate experiments was 5% for the packings turned 90° into each other and 3% for the packings turned 0° into each other while the average difference between the duplicate experiments was 1% for both orientations (see appendix G1). In next figure are presented the results that were obtained (the values of $\lambda_{e,r}$ and α_w represented in the graphs were calculated with the 2-D pseudo-homogeneous model - see appendix G2).

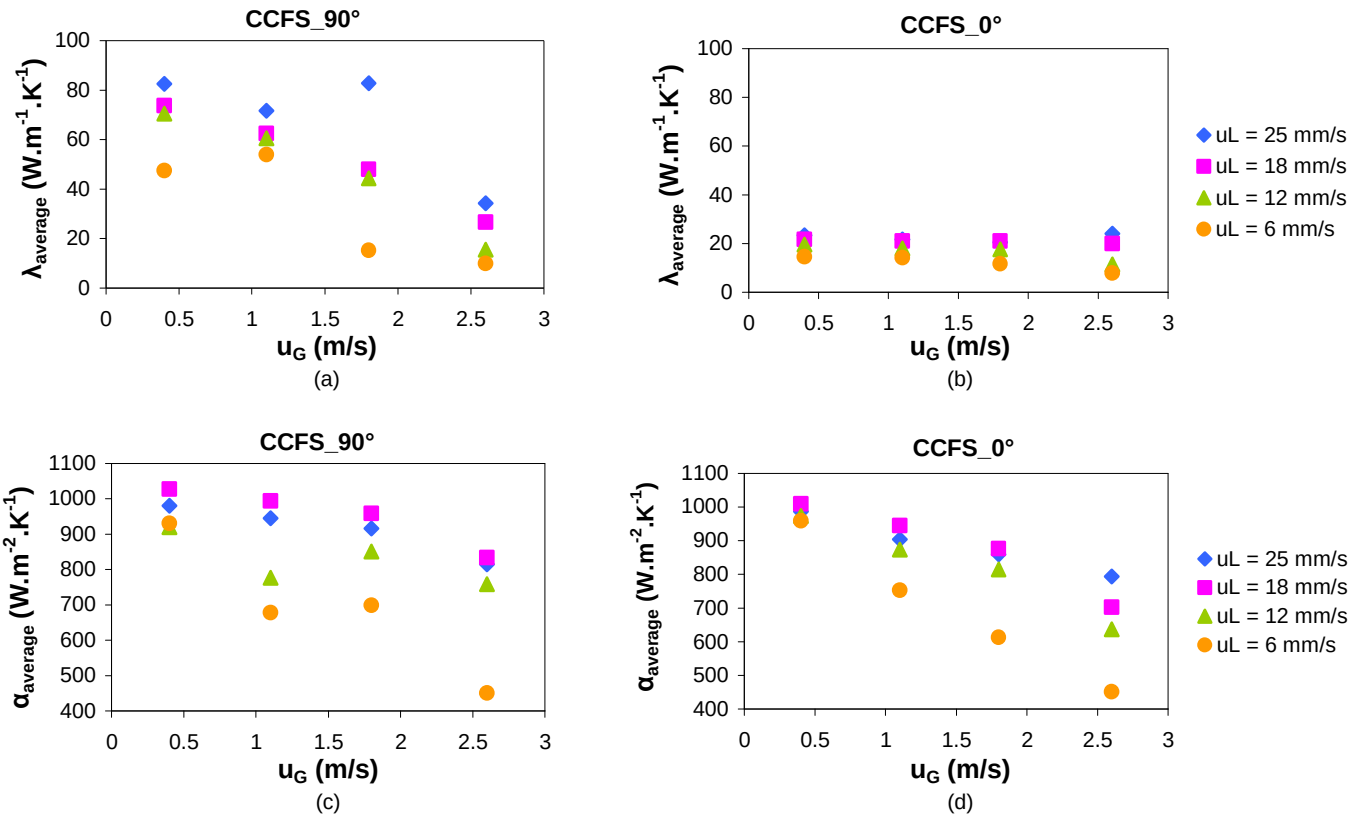

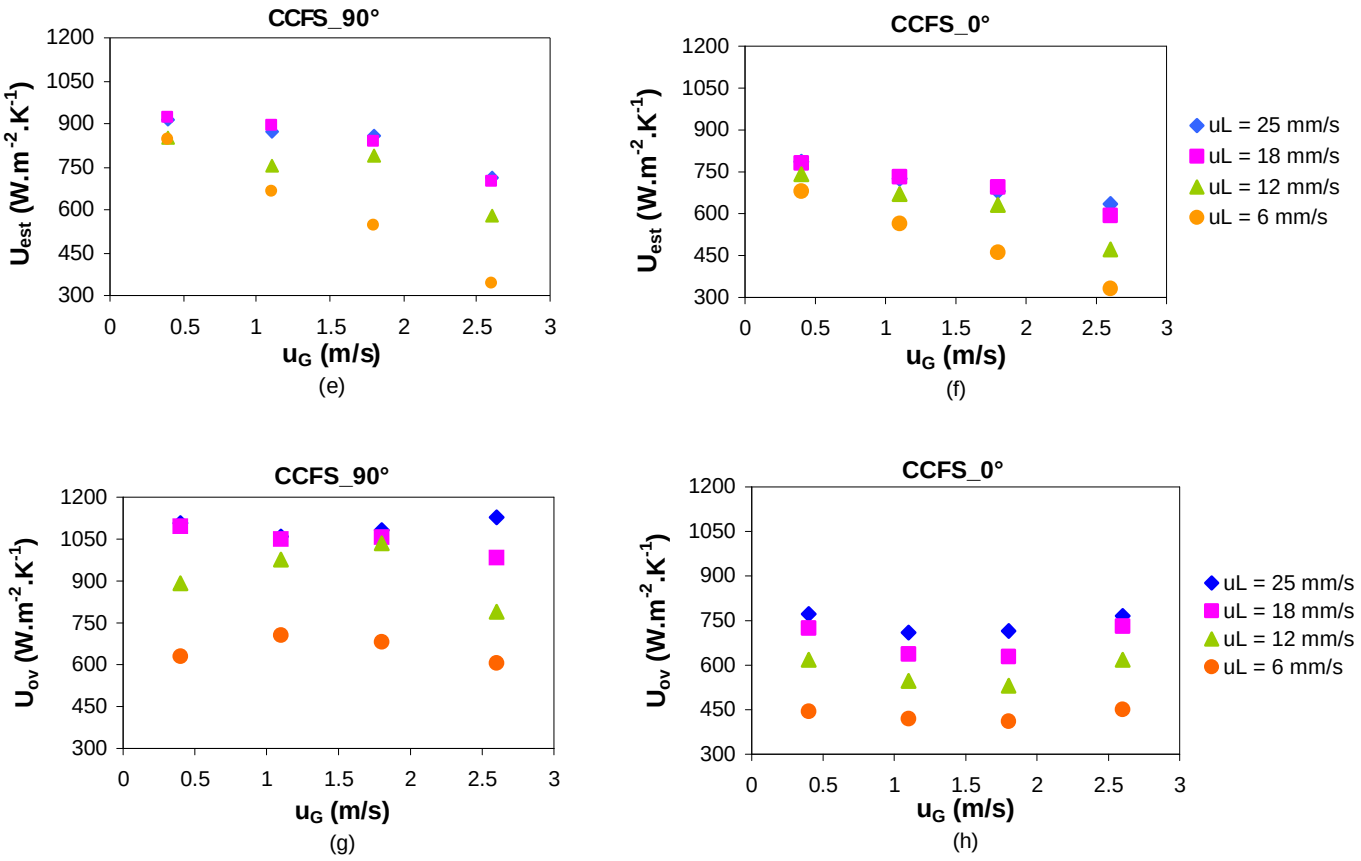

Figure 23 – Profiles obtained for $\lambda_{average}$, $\alpha_{average}$, $U_{estimate}$ and $U_{overall}$ as a function of gas velocity for the CCFS packings turned into 90° ((a),(c),(e),(g)) and 0° ((b),(d),(f),(h)) into each other.

It is possible to conclude that for every condition of gas and liquid velocities the packings turned 90° into each other is always better than the packings turned 0° into each other ($U_{ov\_90^o}$ is always better than the $U_{ov\_0^o}$ - see appendix G1, table G3). Just like was said before since the packings are anisotropic when the orientation is changed a better mixing is obtained because the liquid that is going in bypass through the gap is obligated to pass through the channels in the next packing.

The λ_{static} in CCFS packings is estimated to be between 4 – 6 (W.m^{-1}.K^{-1}) [21]. Thus in this case the convective contribution is highly significant as concluded from the values of $\lambda_{e,r}$ that were obtained, particularly for the packings turned 90º into each other. The graph of $\lambda_{e,r}$ versus gas velocity for different liquid velocities shows an increasing trend until a certain gas velocity and then a decreasing trend (this effect is only visualized in graph (a)). So it is possible to conclude once more that $\lambda_{e,r}$ increases in the stratified wavy flow regime and decreases in the annular regime (see figure 24) because of the same reasons that were already mentioned before for the OCFS packings (see chapter 5.1.1). However, this graph does not show a definite trend due to the relatively large confidence intervals obtained from the parameter estimation (see appendix G2).

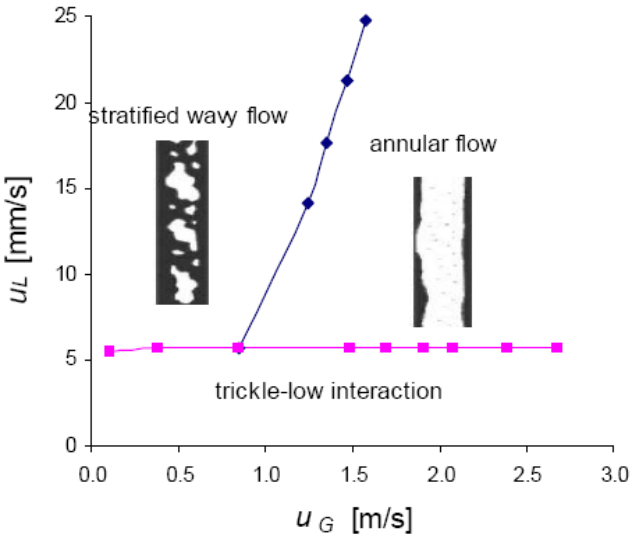

Figure 24 – Flow – map of liquid velocity versus gas velocity for OCFS packings [21].

The graphs of α_w versus gas velocity show a dependence on the gas velocity, mainly for low liquid velocities. When the gas velocity is increased more and bigger stagnant bubbles are formed. Since the velocity of the liquid is low the bubbles will not be pushed forward. In view of the fact that the gas has poorer heat transfer properties than the liquid the value of α_w decreases.

The graph of U_{est} versus gas velocity shows a similar behavior with the graph of α_w versus gas velocity. This is due to the fact that $\lambda_{e,r}$ is very high and consequently α_w becomes the rate limiting factor - see equation (6).

Comparison between the values of U_{ov} and U_{est} shows that they are not the same; in general U_{est} is smaller than to U_{ov}. Thus it is possible to concluded that this value is not reliable for the reasons that were already mentioned before (see chapter 5.1.2).

5.3 Comparison between the type of packings

From the previous sections it was concluded that the orientation that provides the best overall heat transfer coefficient was 90° for both type of packings that were studied. It was also concluded that the OCFS packings with the best overall heat transfer coefficient were the ones that have a big gap between the packing and the reactor wall. Therefore in this sections the heat transfer performance of CCFS and OCFS packings with a big gap will be compared. The heat transfer performance of those two packings will also be compared with the one of glass beads.

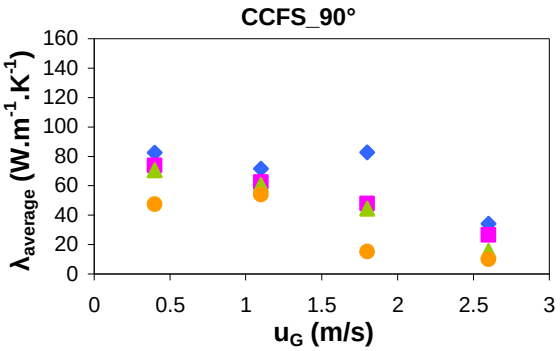
CCFS_90°
λaverage (W.m-1.K-1)
uG (m/s)

(a)

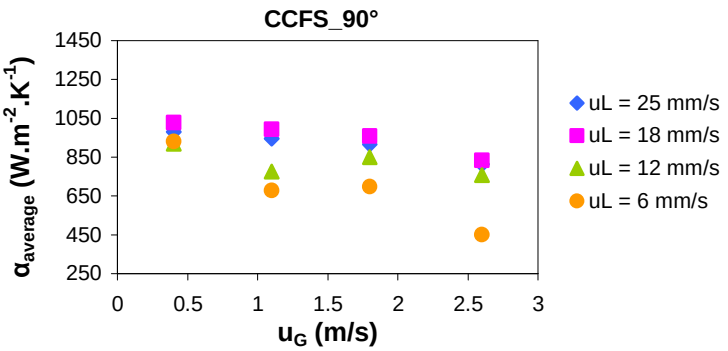
CCFS_90°
αaverage (W.m-2.K-1)
uG (m/s)
uL = 25 mm/s
uL = 18 mm/s
uL = 12 mm/s
uL = 6 mm/s

(b)

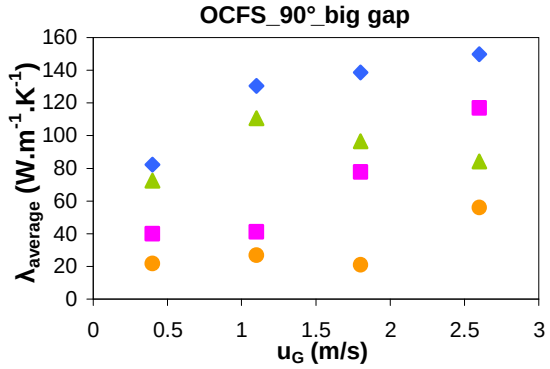
OCFS_90°_big gap
λaverage (W.m-1.K-1)
uG (m/s)

(c)

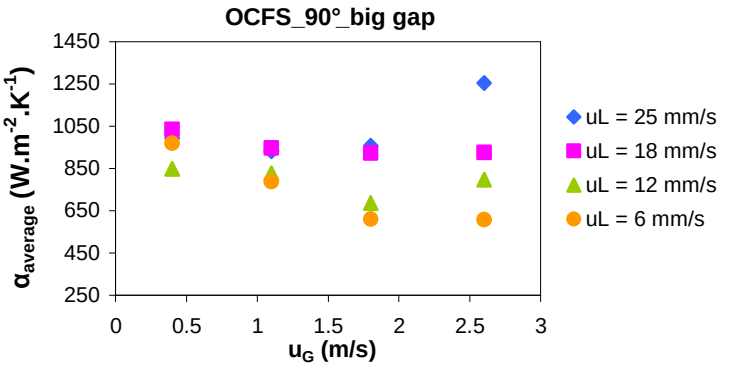
OCFS_90°_big gap
αaverage (W.m-2.K-1)
uG (m/s)
uL = 25 mm/s
uL = 18 mm/s
uL = 12 mm/s
uL = 6 mm/s

(d)

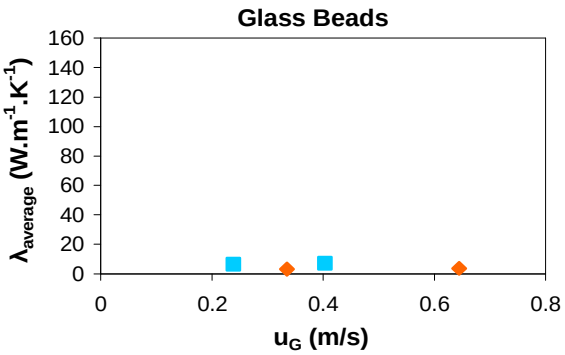
Glass Beads
λaverage (W.m-1.K-1)
uG (m/s)

(e)

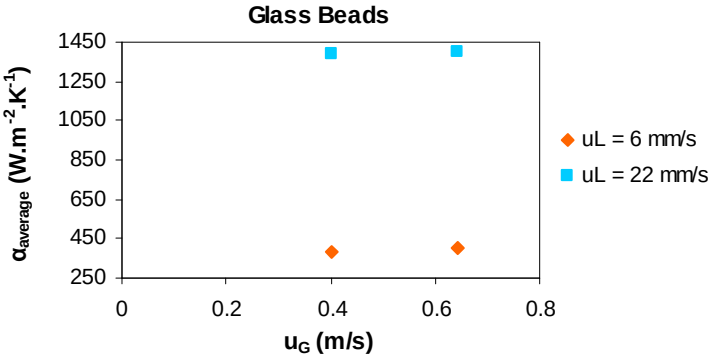
Glass Beads
αaverage (W.m-2.K-1)
uG (m/s)
uL = 6 mm/s
uL = 22 mm/s

(f)

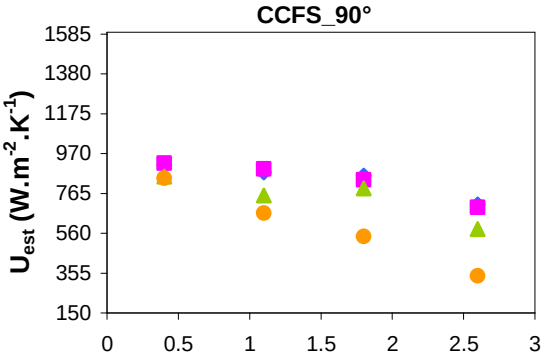
CCFS_90°
Uest (W.m-2.K-1)
uG (m/s)

(g)

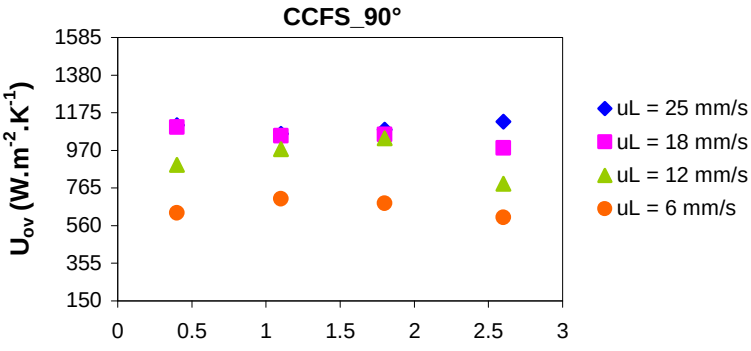
CCFS_90°
Uov (W.m-2.K-1)
uG (m/s)
uL = 25 mm/s
uL = 18 mm/s
uL = 12 mm/s
uL = 6 mm/s

(h)

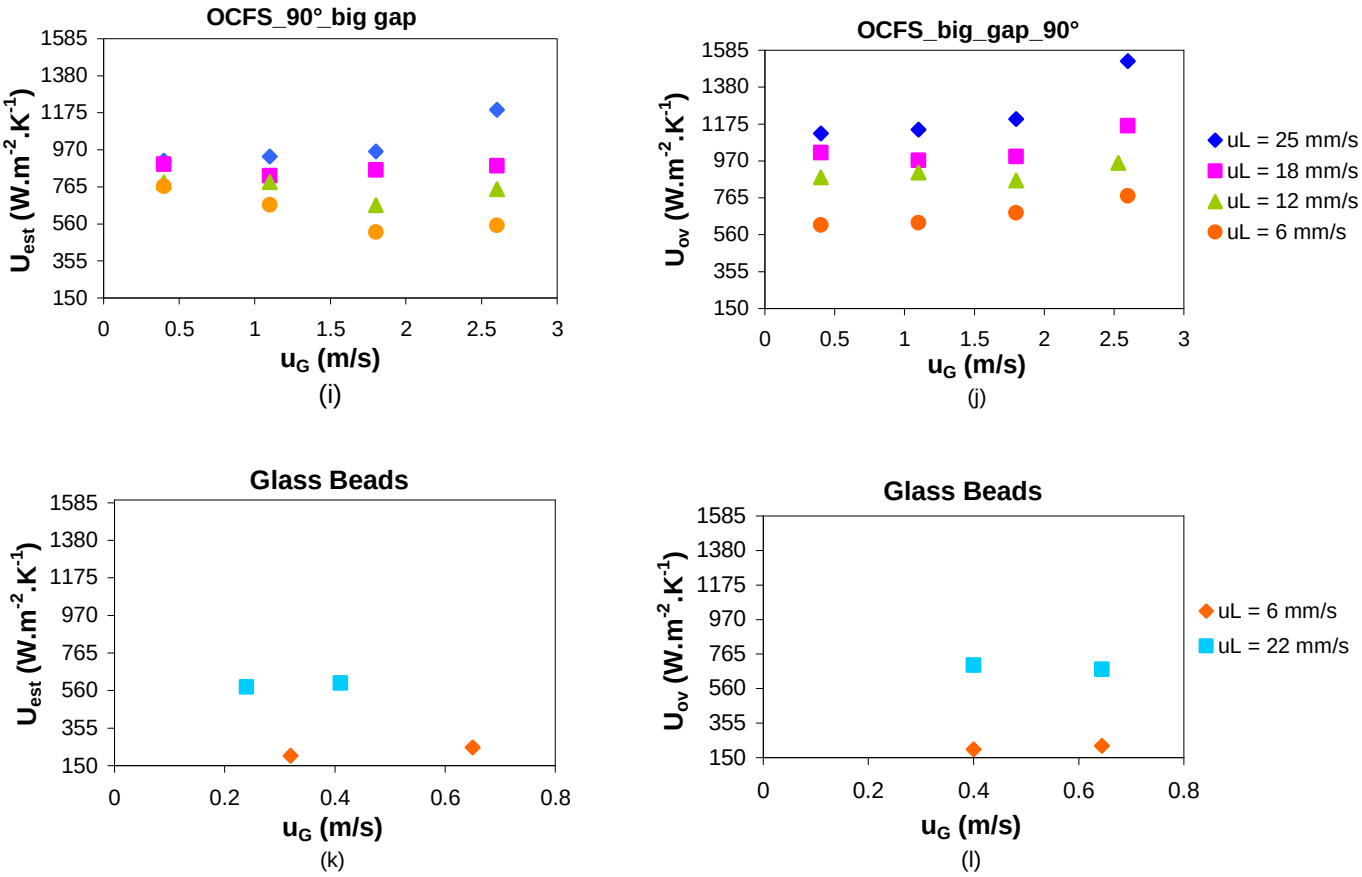

Figure 25 – Comparison between the profiles obtained for $\lambda_{average}$, $\alpha_{average}$, $U_{estimate}$ and $U_{overall}$ as a function of gas velocity for the CCFS packings ((a),(b),(g),(h)), for the OCFS packings ((c),(d),(i),(j)) with a big gap (both packings turned 90°) and for glass beads [23] ((e),(f),(k),(l)). Note: The x axis of figures glass beads are different.

Comparing the graphs of $\lambda_{e,r}$ versus gas velocity it is possible to conclude that the value of $\lambda_{e,r}$ is much higher for structured packings (OCFS and CCFS) than for glass beads. This is due to the significant contribution of the radial convective component in addition to the improved static conductivity which depends mainly on the geometry of the matrix and the conductive properties of the material (stainless steel is much more conductive than glass). Comparing the values of $\lambda_{e,r}$ for the OCFS and CCFS packings it is possible to conclude that for low gas velocities (u_G = 0.4 m/s) the CCFS packings have a higher value of $\lambda_{e,r}$ while for medium and high gas velocities the OCFS packings presents the highest value. A possible explanation for this effect of gas velocity can be given from the flow regime visualization experiments. Since no flow regime visualization experiments were performed the conclusions of the previous researcher will be mentioned. The channels of the CCFS packings have a large surface area (bigger than the surface area of the OCFS packings). With the addition of gas, especially at low gas velocities, well defined liquid waves, slugs, are formed in the small channels [21]. On the other hand, in OCFS at low gas velocities the previous researcher observed that the liquid waves were not as well defined mainly due to the

interaction between adjacent channels [21]. Consequently the radial mixing in OCFS packings is lower at low gas velocities than in CCFS. At high gas velocities in CFFS packings the annular flow pattern of the liquid destroyed radial mixing in the spaces between the sheets leading to lower values of $\lambda_{e,r}$. In OCFS packings the annular flow pattern also takes place but the radial mixing is still comparatively high due to the gas-gas interaction and also the gas-liquid interaction in the adjacent channels [21].

Comparing the graphs of α_w versus gas velocity it is possible to conclude that for low liquid velocities the OCFS and CCFS packings present a higher value of α_w compared to glass beads. However for high liquid velocities glass beads present the highest value of α_w. The glass beads perform very well at high liquid velocities due to higher convective flow at the wall leading to the formation of liquid eddies which can transfer heat very efficiently [23]. The values of α_w are very similar for the OCFS with a big gap and CCFS packings. However, for high gas velocities the value of α_w is clearly higher for the OCFS then for the CCFS packings. Since the OCFS packings have a larger gap between the packing and the reactor wall than the CCFS packings, with high gas velocity the stagnant bubbles will be able to move forward which consequently improves the value of α_w.

The graphs of U_{est} versus gas velocity show a similar behavior with the graphs of α_w versus gas velocity. In the case of OCFS and CCFS packings this is due to the fact that $\lambda_{e,r}$ is very high and consequently α_w becomes the rate limiting factor (to compare directly the values of $\lambda_{e,r}$ and α_w we have to multiple $\lambda_{e,r}$ by 4 and divide by R – see equation (6)). For glass beads the rate limiting factor is $\lambda_{e,r}$ that is why the values of U_{est} are not so big as the values of α_w.

Comparison between the values of U_{ov} and U_{est} shows that for OCFS and CCFS packings they are not the same; in general U_{est} is smaller than U_{ov}. Thus it is possible to conclude that this value is not reliable for the reasons that were already mentioned before (see chapter 5.1.1). However, for the glass beads the values of U_{ov} and U_{est} are very similar. This is due to the fact that for glass beads it is very easy to fit the parameters $\lambda_{e,r}$ and α_w in equation (2) since they present a parabolic radial temperature profile; therefore the confidence intervals of those parameters are very small. Since the equation to estimate U_{est} - equation (6) – uses those parameters this value is expected to be reliable and consequently very similar to U_{ov}.

Comparing the graphs of U_{ov} versus gas velocity it is very clear that the OCFS and CCFS packings are better than the glass beads since they have a better overall heat transfer coefficient. For the OCFS and CCFS packings the values of U_{ov} are very similar. However for high gas velocities the OCFS are clearly better than the CCFS packings which is in agreement with the higher value of α_w.

5.4 Error analysis

Just like was mentioned before the confidence intervals of U_{ov} were calculated by error propagation of equation (10) (see appendix C1). For all the experiments that were done the error obtained for U_{ov} was always smaller than 5%. Since the errors were so small the error for each U_{ov} value was not given individually. The reason why these errors were so small is because the deviation of the temperatures (T_w, T_{out} and T_{in}) – see equation C3 - are also very small.

Since the 2-D pseudo-homogeneous model can not fit the experimental points, the values of $\lambda_{e,r}$ and α_w that are obtained are not the correct ones. As a result the value of U_{est} that is obtained is not correct. This is the reason why the value of U_{est} is not a good representation of U_{ov}. For this reason the error of U_{est} was not analyzed.

5.5 Comparison between the models

To calculate the $\lambda_{e,r}$ and α_w parameters two models were used: the simplified 2-D pseudo-homogeneous model and the 2-D pseudo-homogeneous model (the assumptions of each model were already mentioned before). For both models MatLab® was used to fit the computed temperature profiles inside the packed bed to the experimental ones and the two parameters, $\lambda_{e,r}$ and α_w, are obtained by minimization of the sum of the squared errors between the computed temperatures profiles and the experimental ones. In the next figure is presented a representative example of the results that were obtained. Since the previous researcher used also the 2-D PH model but used the Athena® program to fit the computed temperature profiles inside the packed bed to the experimental ones in the next figure that fit is also represented.

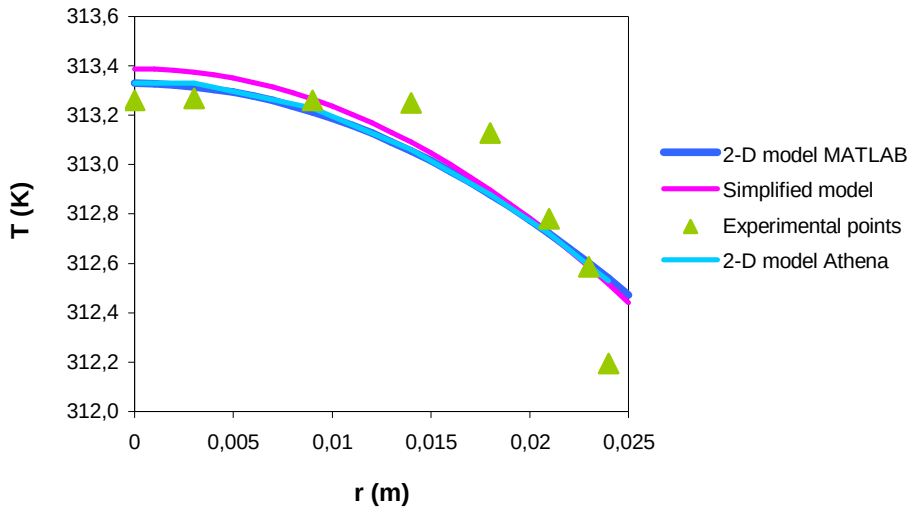

Figure 26 – Representation of the experimental points obtained for the ring C for the OCFS turned 90° into each other and the fit of the two models that were used to calculate the $\lambda_{e,r}$ and α_w parameters (u_G = 1.5m/s ; u_L = 18mm/s).

Table 5.5 – Sum of the squared residuals (SSres) obtained for each model that were used.

Model	Program used	SSres
2-D PH	MatLab	0.230
	Athena	0.223
Simplified 2-D PH	MatLab	0.213

As is possible to see neither model fit the experimental points. Since the radial temperature profile in the OCFS and CCFS packings are very flat it is very difficult to fit a model to those points. The model that presents the minimum residual value is the simplified 2-D model so, in this case, the simplified 2-D model is better than the 2-D PH model. The residual values of 2-D pseudo-homogeneous model calculated with MatLab® and Athena® programs are practically the same (3% different). Applying the Kolmogorov-Smirnov (KS) test to the residual values it is possible to concluded with 95% confidence that the residual values present a trend thus they are not normally distributed. Therefore once more it is achievable to say that both models are not adequate for the obtained experimental radial temperature profiles and consequently for the OCFS packings. It is also expected that these models will not be adequate for the CCFS packings. A new or an improved model should be developed to apply in this type of packings. Since the values of $\lambda_{e,r}$ are relatively high compared to α_w, the α_w parameter becomes the rate limiting factor. Thus the new model that must be developed or improved should give more importance to the α_w parameter.

5.5.1 – Athena and MatLab programs

As was seen before the residual values of MatLab and Athena for the specific experiment shown in figure 26 are very similar. In the next table are presented the results that were obtained for that specific experiment.

Table 5.6 – Values of $\lambda_{e,r}$ and α_w parameters obtained with MatLab and Athena programs for an representative experiment (u_G = 1.5m/s ; u_L = 18mm/s).

MATLAB						ATHENA					
λ (W.m^{-1}.K^{-1})	**λ_{min}**	**λ_{max}**	**α (W.m^{-2}.K^{-1})**	**α_{min}**	**α_{max}**	**λ (W.m^{-1}.K^{-1})**	**+- λ**	**α (W.m^{-2}.K^{-1})**	**+- α**	**Δλ**	**Δα**
198	196	200	1012	1009	1014	142	50	923	23	29	9

As it is possible to see in table 5.5 for this experiment the difference between the sum of the squared residuals of both programs were very similar. However the difference between the solutions of MatLab and Athena programs is 29% and 9% for $\lambda_{e,r}$ and α_w parameters, respectively. In figure 27

a) is represented the calculated temperature profiles obtained from MatLab for the fitted $\lambda_{e,r}$ and α_w parameters of the two programs (see table 5.6). For all the experiments that were done the average difference between the solutions of MatLab and Athena is 32% and 5% for $\lambda_{e,r}$ and α_w parameters, respectively. Since both programs used the same model to calculate the parameters (2-D PH model) and the difference of the sum of the squared residuals between them was small (3%) it was investigated how the radial temperatures profiles changed with the value of $\lambda_{e,r}$ - see figure 27 b.

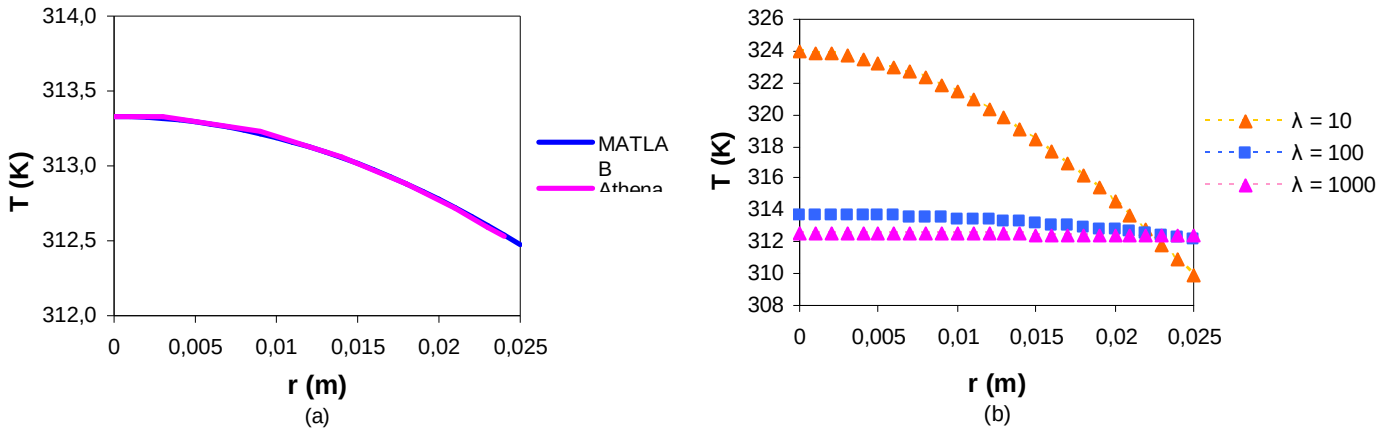

Figure 27 – a) Representation of the fit of the Athena and MatLab programs for the OCFS packings turned 90° into each other for a specific experiment (u_G = 1.5m/s;u_L = 18mm/s) ; b) sensitivity of the radial temperature profiles with $\lambda_{e,r}$.

As it is possible to see in figure 27 a) the fit of both programs are very similar. The small difference can be related to the intrinsic options to solve the model for each program. This is the reason why the difference between the sum of the squared residuals of the two models is so small.

To analyze the sensitivity of the 2-D PH model with the $\lambda_{e,r}$ parameter - see figure 27 b) – the same value of α_w was used (α_w = 968 $W.m^{-2}.K^{-1}$). It is possible to conclude that when the value of $\lambda_{e,r}$ is very low it will influence the fit significantly. However if the value of $\lambda_{e,r}$ is not very small ($\lambda_{e,r} \geq 100$ $W.m^{-1}.K^{-1}$) the fits will be very similar independent of the $\lambda_{e,r}$ value and even that difference between the fits is practically in the range of the error of the thermocouples that were used. This is generally the case in the experiments that were performed. This means that if the value of $\lambda_{e,r}$ will be equal or larger than 100 $W.m^{-1}.K^{-1}$ it will be very difficult to estimate that parameter since it practically does not have influence on the radial temperature profile behaviour so its value could be anything between 100 and infinity.

6. Conclusions

For both types of structured packings that were studied it was found that 90° alternating rotation of the packings is always better than 0° alternating rotation. Since the packings are anisotropic when the orientation is changed a better mixing is obtained.

Generally the OCFS packings with the higher value of U_{ov} are the ones that have a big gap. When the column is filled with packings with a small and a medium gap it is not completely wet in some parts of the gap which makes the α_w decrease, since the gas has poorer heat transfer properties than the liquid, and consequently the U_{ov}. However, for medium gas velocities and for low and medium liquid velocities the OCFS packings with a big gap are worse than the ones that have a small gap because they have lots of stagnant bubbles which makes the U_{ov} decrease. For every condition of gas and liquid velocities the OCFS packings with a medium gap are the worst packings since they have the smallest values of overall heat transfer coefficient. It can be concluded that the size of the gap plays an important role in the heat transfer performance.

In terms of the $\lambda_{e,r}$ parameter for the OCFS and CCFS packings this value is always higher than glass beads and than the value of λ_{static}. This means that the radial convective contribution is highly significant compared to the improved static conductivity which depends mainly on the geometry of the matrix and the conductive properties of the material (stainless steel is much more conductive than glass). For low gas velocities the CCFS packings have the highest value of $\lambda_{e,r}$ while for medium and high liquid velocities the OCFS packings present the highest value.

Relating to the value of α_w for low liquid velocities the OCFS and CCFS packings present the highest values compared to glass beads. However for high liquid velocities glass beads present the highest value of α_w. The glass beads perform very well at high liquid velocities due to higher convective flow at the wall leading to the formation of liquid eddies which can transfer heat very efficiently. The values of α_w are very similar for the OCFS packings with a big gap and CCFS packings. However for high gas velocities the value of α_w is clearly higher for these type of OCFS packings than for the CCFS packings. Since the OCFS packings have a larger gap between the packing and the reactor wall than the CCFS packings, with high gas velocity the stagnant bubbles will be able to move forward which consequently improves the value of α_w.

For the OCFS and CCFS packings the graph of U_{est} versus gas velocity shows a similar behaviour with the graph of α_w versus gas velocity. This is due to the fact that $\lambda_{e,r}$ is very high and consequently α_w becomes the rate limiting factor. For glass beads the rate limiting factor is $\lambda_{e,r}$.

For glass beads the values of U_{ov} and U_{est} are very similar. This is due to the fact that for glass beads it is very easy to fit the parameters $\lambda_{e,r}$ and α_w in the 2-D pseudo-homogeneous model

since they present a parabolic radial temperature profile. Since the equation to estimate U_{est} uses those parameters this value is reliable and consequently very similar to U_{ov}. However for the OCFS and CCFS packings these parameters are very difficult to estimate since those packings present a very flat radial temperature profile. Since the equation to estimate U_{est} uses those parameters this value is not reliable and consequently different from the value of U_{ov}.

The OCFS and the CCFS packings are better than glass beads since the value of U_{ov} for those packings is always higher than the one for glass beads. For the OCFS and CCFS packings the values of U_{ov} are very similar. However for high gas velocities the OCFS packings with a big gap are clearly better than the CCFS packings which is in agreement with the higher value of α_w.

The simplified 2-D PH model and the 2-D PH model were used to fit the experimental points. However, neither of these models are a good model for the structured packings that were studied since they do not fit the experimental points. Since the radial temperature profile in the OCFS and CCFS packings are very flat it is very difficult to fit a model to those points. If the value of $\lambda_{e,r}$ is large the fits will be very independent of the value of $\lambda_{e,r}$.

7. Recommendations for Future Work

To verify the conclusions that were obtained in this research additional measurements should be done even with different velocities of gas and liquid.

Because no time was left, the influence of the fit in the CCFS packings was not studied. This influence should also be studied in the following researches. Comparison between the influence of the fit in the OCFS packings should be compared with the conclusions that will be obtained for the influence of the fit in the CCFS packings. It is expected that the influence of the gap in this type of packings is in the same order of magnitude as the OCFS packings.

To have more accuracy in the results that were obtained and consequently in the parameters that were calculated more thermocouples should be added to each arm in each ring. Since it is already known that the $\lambda_{e,r}$ parameter is very high therefore α_w is the rate limiting factor it is more significant to add more thermocouples between the edge of the packing and the wall than in the centre of the packing or use a different type of sensors that has a smaller error.

Since the tank of the cooling water does not have a cooling system the temperature of the cooling water slowly heats up during the day (the difference can even be 10°C). To have exactly the same conditions for all the experiments and consequently to have a more uniform temperature at the wall in the column during every day an effective cooling system should be designed.

A new or an improved model should be developed to apply to this type of structured packings since both models that were used do not fit the experimental points. Since the values of $\lambda_{e,r}$ are very high α_w becomes the rate limiting factor. Thus the new model that must be developed should not take into account the $\lambda_{e,r}$ value or should give more importance to the α_w parameter.

Residence time distributions experiments should be performed to investigate the plug flow behaviour of the column.

On this research it was concluded that the OCFS packings with a big gap have better heat transfer characteristics. Thus new experiments should be performed with OCFS packings with a bigger gap since that phenomena was not investigated. An optimal value for the gap is expected.

If it is possible OCFS and CCFS packings should be manufacture with a material more conductive than stainless steel, like carbon or copper. That will improve the heat transfer.

It was concluded that alternating the orientation of the packing increases the heat transfer. If it is possible to decrease the height of the packings the orientation will be changed more times than before. As a result better heat transfer is expected.

Try to improve the $\lambda_{e,r}$ in the y direction (R2 axis).

8. Bibliography

[1] Roberts, P., *The End of Oil*, Houghton Mifflin Company, New York, 2004

[2] Mesheryakov, V. D., Kirillow, V. A., Kuzin, N. A., *A Multifunctional Reactor with a Regular Catalyst packing for Fischer-Tropsch Synthesis*, Chem. Eng. Sci. 54, 1999, pp 1375-1381

[3] Krishna, R., Sie, S. T., *Design and scale-up of the Fischer-Tropsch bubble column slurry reactor*, Fuel Proc. Techn. 64, 2000, 73

[4] Moulijn, J. A., Makkee, M., van Diepen, A., *Chemical Process Technology*, John Wiley & Sons Ltd, 2001

[5] Pangarkar, K., *Draft Article – Heat Transfer Results for Glass Beads and Structured Packings*, 2007

[6] Schildhauer, T., Newson, E., Wokaun, A., *Improvements of the heat transfer in catalytic fixed bed reactors by means of structured packings*, Laboratory from Energy and Material Cycles, Paul Scherrer Institute, Switzerland

[7] Kroschwitz, I., Howe-Grant, M., *Kirk - Othmer encyclopedia of chemical technology*, Wiley & Sons, New York, fourth edition, 1996

[8] Steynberg, A., Dry, M., *Fischer-Tropsch Technology – studies in surface science and catalysis*, 2004

[9] *Shell Gas to Liquid 2004*, http://www.shell.com/home/content/shellgasandpower-en/products_and_services/what_is_gtl/dir_what_is_gtl_1205.html, visited in May 2008

[10] Deugd, R.M., *Fischer-Tropsch Synthesis Revisited; Efficiency and Selectivity Benefits from Imposing Temporal and/or Spatial Structure in the Reactor*; 2004

[11] G.P. Van der Laan and A.A.C.M. Beenackers, *Kinetics and Selectivity of the Fischer-Tropsch Synthesis: A Literature Review*, Catal. Rev. –Sci. Eng. 41 (1999)

[12] Ciobica, I.M., *The Molecular Basis of the Fischer-Tropsch Reaction*, PhD thesis, 2002

[13] Vannice, M. A., *J. Catal.*, 1975, 37, 449

[14] Khodakov, A. Y., Chu, W., Fongarland, P., *Advances in the Development of Novel Cobalt Fischer-Tropsch Catalysts for Synthesis of Long-Chain Hydrocarbons and Clean Fuels*, Chemical Reviews 107 (5), pp. 1692-1744

[15] Anderson, R. B., *Catalysts for the Fischer-Tropsch Synthesis*, vol. 4, Van Nostrand Reinhold, New York, 1956

[16] Deugd, R. M., Kapteijn, F., Moulijn, J. A., *Trends in Fischer-Tropsch reactor technology – opportunities for structured reactors*, Catalysis, vol. 26, Nos. 1-4, December 2003

[17] Schulz, H., *Trends in Research and Development of Coal Conversion to liquid fuels and Basic Chemicals in Europe*, Pure & Appl. Chem. 51, 1979, pp 2225

[18] Post, M. F. M., Van't Hoog, A. C., Minderhoud, J. K., Sie, S. T., *Diffusion Limitations in Fischer-Tropsch Catalysts*, Aiche Journal, vol. 35, No.7, pp. 1107-1114, 1989

[19] Krishna, R., Sie, S., *Strategies for multiphase reactor selection*, Chem. Eng. Sci. 49, 1994, 4029

[20] Spiegel, L., Meier, W., *Distillation columns with structured packings in the next decade*, Chemical Engineering Research and Design, volume 81, issue 1, 2003, pp. 39-47

[21] Pangarkar, K., *Review – Structured Packings for Multiphase Fixed Bed Reactors: Hydrodynamics, Mass Transfer and Heat Transfer*, TUDelft, 2008

[22] von Scala, C., Wehrli, M., Gaiser, G., *Heat transfer measurements and simulation of KATAPAK-M® catalyst supports*, Chemical Engineering Science 54, pp. 1375-1381,1999

[23] Behrens, M., Saraber, P. P., Jansen, H., Olujic, Z., *Performance Characteristics of a Monolith-like Structured Packing*, Chem. Biochem. Eng. Q., 2001, 15, 49-57

[24] Schildhauer, T. J., *Untersuchungen zur Verbesserung des Wärmeübergangs in katalytischen Festbettreaktoren für Energiespeicheranwendungen*, Ph.D – thesis No 14301, ETH, Zürich, Switzerland, 2001

[25] *ISOPAR-M: U.S. Material Safety Data Sheets*, European Science Foundation, 2003

[26] Calvo, S. C., *Graduation Report: Heat transfer measurements in structured packings*, Delft University of Technology, Process and Products Engineering Group, 2006

[27] http://www.engineeringtoolbox.com/nitrogen-d_977.html, visited in June 2008

APPENDICES

Appendix A

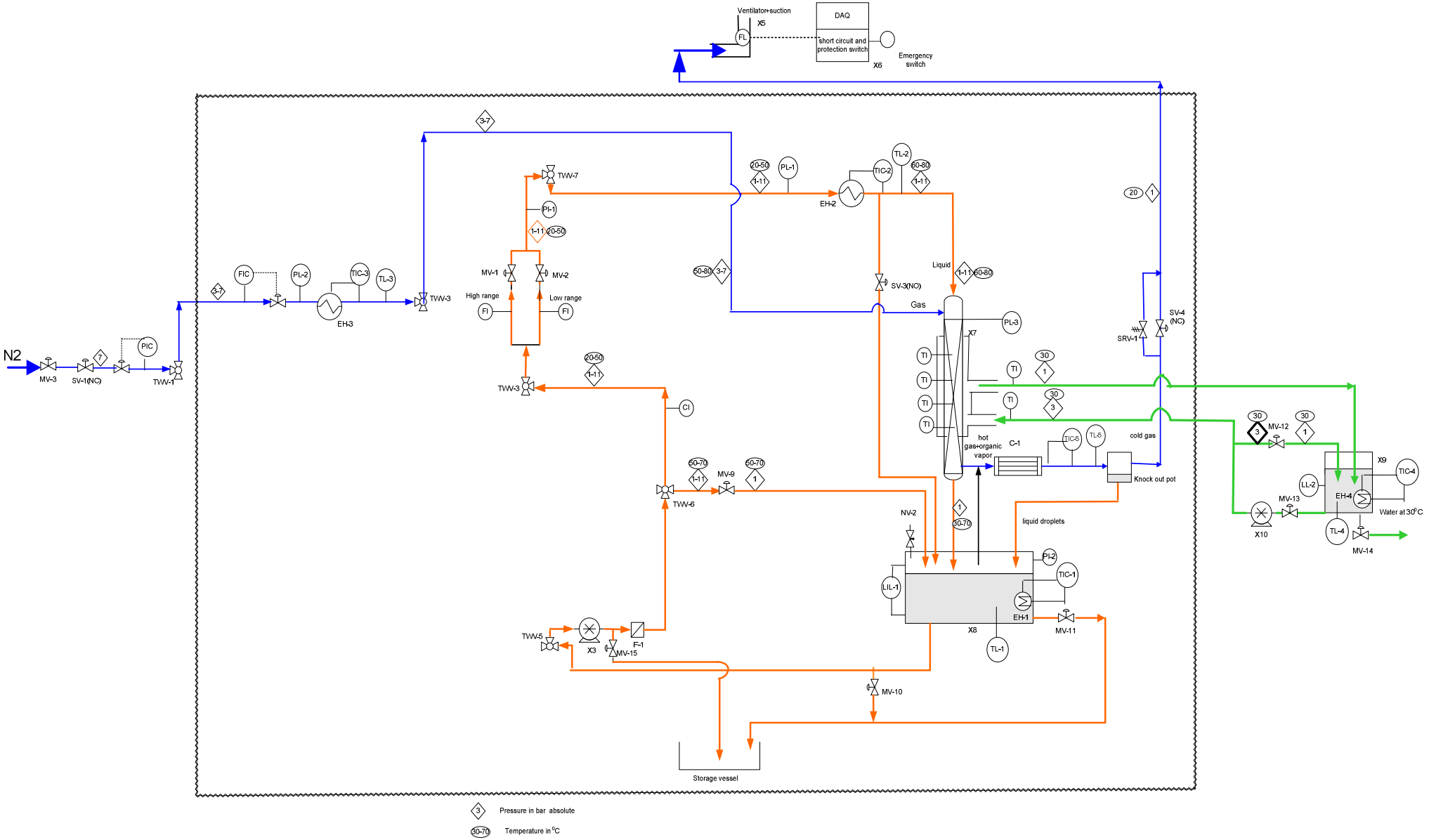

Figure A1 – Process scheme of the heat transfer unit.

Table A1 – List of equipment code of heat transfer set-up and brief description of each one [27].

Equipment Code	Description
C-1	Condenser for the hot gas leaving the column
DAQ	Data acquisition box
EH-1	Immersion heater for the liquid (from room temperature to 50°C)
EH-2	Electric flow heater for the liquid (from 50°C to 60°C)
EH-3	Electric flow heater for the gas
F-1	Filter for the liquid from the pump
FI	Flow indicator
FIC	Flow indicator controller
LIL-1	Level indicator and switch (limiter) for the cooling vessel (X8)
LL-2	Level switch (limiter) for the collecting vessel (X9)
PI	Pressure indicator
PIC	Pressure indicator controller
PI-2	Pressure gauge for the storage vessel for the process liquid
PL-1	Pressure switch (limiter) for EH-2
PL-2	Pressure switch (limiter) for EH-3
PL-3	Pressure switch (limiter) for X7
TI	Temperature indicator
TIC-1 and TL-1	Temperature indicator controller + limiter for EH-1
TIC-2 and TL-2	Temperature indicator controller + limiter for EH-2
TIC-3 and TL-3	Temperature indicator controller + limiter for EH-3
TIC-4 and TL-4	Temperature indicator controller + limiter for EH-4
TL-5	Temperature limiter for C-1
X3	Pump for the column
X5	Ventilator
X6	DAQ + short circuit protection box + emergency switch
X7	Column for measurements (precolumn + heat transfer column + gas/liquid separation zone)
X8	Storage vessel for the liquid
X9	Collecting vessel for the cooling water
X10	Centrifugal pump for the cooling water

Table A2 – List of the valves for the heat transfer set-up and brief description of each one [27].

Equipment Code	Description
MV-1	Manual valve for the high flow sensor
MV-2	Manual valve for the low flow sensor
MV-3	Manual valve to open the nitrogen net line
MV-9	Manual valve for the gear pump X3
MV-10	Manual valve to drain the liquid from the suction side of the pump X3
MV-11	Manual valve to drain the liquid from the storage vessel X8
MV-12	Manual valve for the centrifugal pump X10
MV-13	Manual valve to control the flowrate of the cooling water
MV-14	Manual valve to drain the cooling water tank X9
SV-1	Magnetic solenoid valve (NC) to open the nitrogen line from the net
SV-3	Magnetic solenoid valve(NO) to release the liquid from the EH-2 to X8
SV-4	Magnetic solenoid valve(NO) to close the system at the gas exit line going to the suction

Appendix B

Table B1 - Parameters measured that were necessary to make the calibration of the pump of the liquid.

Pump rate (%)	time (s)	Volume (mL)	$V_{average}$ (mL)	Q (mL/s)	Q (L/h)	$Q_{average}$ (L/h)	error (%)
0	60	750	753	13	45	45.2	0.7
	60	755		13	45		
10	40	680	678	17	61	61.0	0.7
	40	675		17	61		
20	40	930	925	23	84	83.3	1.1
	40	920		23	83		
40	25	875	880	35	126	126.7	1.1
	25	885		35	127		
50	20	820	825	41	148	148.5	1.2
	20	830		42	149		

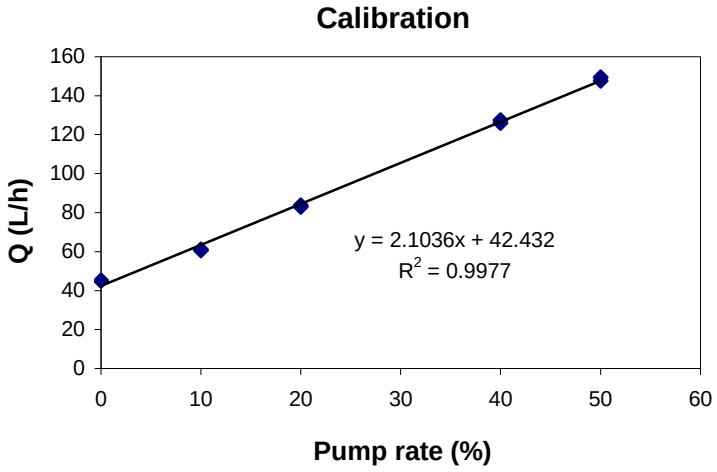

Figure B1 – Representation of the calibration of the liquid pump.

Appendix C

Appendix C1 – Derivation of the error of U_{ov}

$$U_{ov} = \frac{MCp\left(T_{m,in} - T_{m,out}\right)}{2\pi rL\,\Delta T_{LM}} = \frac{\left(u_L\rho_L C_{p,L} + u_G\rho_G C_{p,G}\right)\left(T_{m,in} - T_{m,out}\right)}{2\pi rL\,\Delta T_{LM}} \qquad (C1)$$

and

$$\Delta T_{LM} = \frac{\left(T_{m,in} - T_w\right) - \left(T_{m,out} - T_w\right)}{\ln\dfrac{\left(T_{m,in} - T_w\right)}{\left(T_{m,out} - T_w\right)}} \qquad (C2)$$

$$\Delta U_{ov} = \sqrt{\left(\frac{MCp}{2\pi RL}\frac{\partial U_{ov}}{\partial T_w}\Delta T_w\right)^2 + \left(\frac{MCp}{2\pi RL}\frac{\partial U_{ov}}{\partial T_{m,in}}\Delta T_{m,in}\right)^2 + \left(\frac{MCp}{2\pi RL}\frac{\partial U_{ov}}{\partial T_{m,out}}\Delta T_{m,out}\right)^2} \qquad (C3)$$

where:

$$\frac{\partial U_{ov}}{\partial T_w} = -\frac{1}{\left(T_{m,in} - T_w\right)} + \frac{1}{\left(T_{m,out} - T_w\right)} \qquad (C4)$$

$$\frac{\partial U_{ov}}{\partial T_{m,in}} = \frac{1}{\left(T_{m,in} - T_w\right)} \qquad (C5)$$

$$\frac{\partial U_{ov}}{\partial T_{m,out}} = \frac{1}{\left(T_{m,out} - T_w\right)} \qquad (C6)$$

and ΔT_w, $\Delta T_{m,in}$ and $\Delta T_{m,out}$ are equal to 0.0546. These values represent the standard deviation of the measurements during 6 hours.

Appendix C2 – Derivation of the error of U_{est}

$$U_{est} = \left(\frac{1}{\alpha_w} + \frac{R}{4\lambda_{e,r}} \right)^{-1} \tag{C7}$$

$$\Delta U_{est} = \sqrt{\left(\frac{\partial U_{est}}{\partial \alpha_w} \Delta \alpha_w \right)^2 + \left(\frac{\partial U_{est}}{\partial \lambda_{e,r}} \Delta \lambda_{e,r} \right)^2} \tag{C8}$$

where:

$$\frac{\partial U_{est}}{\partial \alpha_w} = \frac{4\lambda_{e,r}\alpha_w R - 4\lambda_{e,r}\left(4\lambda_{e,r} + R\alpha_w\right)}{\left(4\lambda_{e,r} + R\alpha_w\right)^2} \tag{C8}$$

$$\frac{\partial U_{est}}{\partial \lambda_{e,r}} = \frac{16\lambda_{e,r}\alpha_w - 4\alpha_w\left(4\lambda_{e,r} + R\alpha_w\right)}{\left(4\lambda_{e,r} + R\alpha_w\right)^2} \tag{C9}$$

So:

$$\Delta U_{est} = \sqrt{\left(\frac{4\lambda_{e,r}\alpha_w R - 4\lambda_{e,r}\left(4\lambda_{e,r} + R\alpha_w\right)}{\left(4\lambda_{e,r} + R\alpha_w\right)^2} \Delta \alpha_w \right)^2 + \left(\frac{16\lambda_{e,r}\alpha_w - 4\alpha_w\left(4\lambda_{e,r} + R\alpha_w\right)}{\left(4\lambda_{e,r} + R\alpha_w\right)^2} \Delta \lambda_{e,r} \right)^2} \tag{C10}$$

Appendix D

Table D1 – Results obtained for the overall heat transfer coefficient for OCFS packings with a small gap turned 90° into each other and the respective deviation.

		U_{ov} (W.m^{-2}.K^{-1})								$U_{average}$ (W.m^{-2}.K^{-1})				Deviation (%)			
u_L (mm/s)	u_G (m/s)	A-B		B-C		A-D		C-D		A-B	B-C	A-D	C-D	AB	BC	AD	CD
6	0.4	837	767	600	593	520	503	368	369	802	597	512	368	8	1	3	0
	2.6	843	925	640	648	588	620	401	423	884	644	604	412	9	1	5	5
22	0.4	1299	1322	881	911	921	933	729	720	1310	896	927	724	2	3	1	1
	2.6	1260	1277	994	997	1080	1079	805	807	1269	997	1079	806	1	1	0	0

Appendix E

Appendix E1 – Results obtained for the OCFS with a small gap turned into 90° and 0° into each other (U_{ov}).

Table E1 – Results obtained for the overall heat transfer coefficient for OCFS packings with a small gap turned 90° into each other and the respective deviation.

		U_{ov} (W.m^{-2}.K^{-1})									$U_{average}$ (W.m^{-2}.K^{-1})							Deviation (%)							
u_L (mm/s)	u_G (m/s)	A-B			B-C			A-D			C-D			A-B	B-C	A-D	C-D	minAB	maxAB	minBC	maxBC	minAD	maxAD	minCD	maxCD
25	0.4	998	993	1009	1020	1023	1009	905	905	919	702	707	709	1000	1017	910	706	0	2	0	1	0	2	0	1
	1.1	1058	1053	1038	1112	1097	1106	955	947	952	734	730	748	1049	1105	951	737	0	2	0	1	0	1	1	2
	1.8	1050	1045	1069	1126	1123	1161	971	972	983	781	793	777	1055	1137	975	784	0	2	0	3	0	1	1	2
	2.6	1133	1132	1103	1226	1230	1200	1037	1031	1017	829	818	832	1123	1218	1029	827	0	3	0	2	1	2	0	2
18	0.4	862	861	---	894	897	---	774	775	---	714	717	---	862	895	774	715	0		0		0		0	
	1.1	935	937	912	997	997	947	843	841	818	743	743	742	928	980	834	743	0	3	0	5	0	3	0	0
	1.8	991	988	987	1041	1061	1040	883	881	883	749	734	760	989	1047	882	748	0	0	0	2	0	0	1	3
	2.6	972	965	1049	1138	1128	1133	924	924	952	737	752	780	996	1133	934	757	1	8	0	1	0	3	2	6
12	0.4	741	741	747	763	759	811	642	646	664	583	599	605	743	787	650	596	0	1	0	6	1	3	1	4
	1.1	783	783	---	905	917	---	710	710	---	634	632	---	783	911	710	633	0		1		0		0	
	1.8	796	797	792	939	939	950	717	717	715	636	639	630	795	943	717	635	0	1	0	1	0	0	0	1
	2.6	691	689	---	914	929	---	675	671	---	605	612	---	690	921	673	608	0		2		1		1	
6	0.4	837	887	---	600	593	---	520	504	---	368	369	---	862	597	512	368	6		1		3		0	
	1.1	795	876	871	671	674	683	628	656	653	391	395	385	847	676	646	391	1	9	1	2	0	4	1	3
	1.8	761	774	---	738	730	---	660	657	---	431	429	---	767	734	659	430	2		1		0		0	
	2.6	843	925	---	640	648	---	588	620	---	401	423	---	884	644	604	412	9		1		5		5	

Table E2 – Results obtained for the overall heat transfer coefficient for OCFS packings with a small gap turned 0° into each other and the respective deviation.

		U_{ov} (W.m^{-2}.K^{-1})												$U_{average}$ (W.m^{-2}.K^{-1})				Deviation (%)							
u_L (mm/s)	u_G (m/s)	A-B			B-C			A-D			C-D			A-B	B-C	A-D	C-D	minAB	maxAB	minBC	maxBC	minAD	maxAD	minCD	maxCD
25	0.4	1050	1051	1059	681	692	694	659	658	665	480	465	492	1053	693	661	479	0	1	0	2	0	1	2	5
	1.1	1122	1120	1110	878	878	866	749	752	751	486	483	490	1118	874	751	486	0	1	0	1	0	0	1	1
	1.8	1121	1126	1120	979	986	973	862	858	856	656	644	651	1122	979	858	650	0	0	1	1	0	1	1	2
	2.6	1073	1127	---	1062	1104	---	982	1012	---	758	780	---	1100	1062	997	769		5		4		3		3
18	0.4	1103	1089	1100	685	689	687	642	646	639	405	409	404	1097	687	642	406	0	1	0	1	1	1	0	1
	1.1	906	910	909	850	854	854	750	754	756	529	531	537	908	853	753	532	0	0	0	0	0	1	0	1
	1.8	902	905	909	904	891	905	836	836	838	700	710	703	905	900	836	704	0	1	0	2	0	0	0	1
	2.6	991	987	983	884	884	900	864	861	863	740	737	730	987	889	863	736	0	1	0	2	0	0	0	1
12	0.4	857	858	859	493	490	482	567	564	575	479	472	505	858	489	569	485	0	0	1	2	1	2	1	7
	1.1	761	761	756	728	700	718	714	711	699	635	655	614	760	715	708	635	0	1	1	4	0	2	3	6
	1.8	794	786	772	799	803	772	733	733	716	600	606	601	784	791	727	602	1	3	0	4	0	2	0	1
	2.6	745	743	---	754	755	---	711	710	---	620	618	---	744	754	710	619		0		0		0		0
6	0.4	739	708	710	481	482	474	508	498	493	391	384	380	719	479	499	385	0	4	0	2	1	3	1	3
	1.1	686	682	625	582	594	575	533	542	511	390	402	375	664	584	529	389	1	9	1	3	2	6	3	7
	1.8	560	572	559	559	552	555	493	496	493	383	392	388	564	556	494	388	0	2	1	1	0	1	1	2
	2.6	466	466	461	501	497	503	461	462	461	406	415	407	464	500	461	409	0	1	0	1	0	0	0	2

Table E3 – Results obtained for the overall heat transfer coefficient for OCFS packings for 0° and 90° and the respective deviation ($\Delta U = U_{ov\_average\_90°} - U_{ov\_average\_0°}$).

u_L (mm/s)	u_G (m/s)	$U_{ov\_average\_0°}$ (W m^{-2} K^{-1})	$U_{ov\_average\_90°}$ (W m^{-2} K^{-1})	ΔU (%)
25	0.4	693	1017	32
	1.1	874	1105	21
	1.8	979	1137	14
	2.6	1062	1218	13
18	0.4	687	895	23
	1.1	853	980	13
	1.8	900	1047	14
	2.6	889	1133	22
12	0.4	489	787	38
	1.1	715	911	22
	1.8	791	943	16
	2.6	761	921	17
6	0.4	479	597	20
	1.1	584	676	14
	1.8	556	734	24
	2.6	500	644	22

Table E4 – Results obtained for the overall heat transfer coefficient for OCFS packings with a small gap turned 0°into each other and the respective deviation (second day).

		U_{ov} (W.m^{-2}.K^{-1})								$U_{average}$ (W.m^{-2}.K^{-1})				Deviation (%)			
u_L (mm/s)	u_G (m/s)	A-B		B-C		A-D		C-D		A-B	B-C	A-D	C-D	AB	BC	AD	CD
25	0.4	960	948	664	672	661	647	528	511	954	668	654	519	1	1	2	3
18	1.1	766	770	812	807	643	645	469	479	768	809	644	474	1	1	0	2
12	1.8	619	623	758	762	625	626	582	581	621	760	626	582	1	0	0	0
6	2.6	411	407	501	503	408	407	390	387	409	502	407	389	1	0	0	1

Appendix E2 – Results obtained for the OCFS with a small gap turned 90° and 0° into each other for the simplified 2-D PH model and for the 2-D PH model.

Table E5 - Results obtained for the OCFS with a small gap turned 90° into each other (λ and α for the simplified 2-D PH model).

u_L	u_G	$\lambda a_{e,r}$	$\lambda a_{e,r\ min}$	αa	αa_{min}	αa_{max}	$\lambda b_{e,r}$	$\lambda b_{e,r\ min}$	αb	αb_{min}	αb_{max}	$\lambda c_{e,r}$	$\lambda c_{e,r\ min}$	αc	αc_{min}	αc_{max}	$\lambda d_{e,r}$	$\lambda d_{e,r\ min}$	$\lambda d_{e,r\ max}$	α_d	αd_{min}	αd_{max}
(mm/s)	(m/s)	($W.m^{-1}.K^{-1}$)		($W.m^{-2}.K^{-1}$)			($W.m^{-1}.K^{-1}$)		($W.m^{-2}.K^{-1}$)			($W.m^{-1}.K^{-1}$)		($W.m^{-2}.K^{-1}$)			($W.m^{-1}.K^{-1}$)			($W.m^{-2}.K^{-1}$)		
25	0.4	88	54	1073	1015	1139	83	51	1067	1015	1123	159	87	1100	1050	1156	57	45	79	1024	987	1064
	1.1	280	102	1111	1056	1172	149	70	1136	1077	1201	303	145	1168	1128	1210	81	61	120	1060	1026	1095
		301	102	1133	1073	1200	150	71	1162	1101	1230	278	147	1192	1155	1231	90	68	131	1110	1078	1143
	1.8	340	108	1140	1080	1205	149	71	1174	1112	1242	299	154	1183	1148	1221	91	69	136	1126	1093	1161
		349	97	1181	1107	1264	179	93	1199	1153	1249	142	98	1260	1220	1303	78	58	118	1127	1087	1171
		387	103	1273	1192	1367	169	92	1302	1250	1358	121	90	1356	1315	1401	81	60	125	1205	1159	1254
	2.6	422	105	1275	1193	1369	170	92	1306	1253	1363	112	91	1376	1345	1408	76	57	112	1200	1156	1248
		410	106	1240	1164	1327	182	96	1265	1217	1318	163	112	1296	1258	1336	83	63	124	1210	1167	1255
18	0.4	74	44	1115	1036	1207	59	40	1127	1064	1199	74	52	1005	960	1053	36	28	50	1136	1065	1218
		224	78	1122	1047	1207	131	72	1154	1103	1209	241	114	1041	1001	1085	49	37	74	1155	1090	1228
	1.1	234	80	1126	1052	1211	129	73	1161	1111	1215	244	114	1046	1005	1090	49	36	73	1148	1084	1221
		127	68	1114	1053	1183	73	48	1162	1102	1229	97	65	1045	1001	1093	40	31	55	1165	1097	1242
		284	82	1158	1076	1252	122	68	1204	1147	1267	170	105	1106	1071	1144	50	39	70	1177	1120	1242
	1.8	310	80	1154	1068	1256	101	52	1217	1133	1314	115	88	1134	1105	1164	49	36	77	1150	1079	1230
		327	81	1154	1068	1255	99	53	1220	1142	1310	123	92	1150	1120	1182	48	35	75	1135	1066	1214
	2.6	351	82	1193	1101	1302	110	60	1258	1187	1338	137	100	1227	1195	1261	56	42	86	1169	1110	1235
12	0.4	53	33	976	900	1066	37	28	1008	951	1073	51	38	869	828	914	21	16	30	1032	932	1154
		67	43	943	891	1002	37	28	1012	955	1076	49	36	865	821	914	21	16	29	1061	955	1194
		103	46	932	859	1020	62	41	976	929	1028	90	50	885	830	948	25	18	39	1059	948	1200
	1.1	139	50	981	896	1084	98	56	1011	962	1065	169	72	964	906	1030	28	20	45	1123	1005	1273
		129	49	987	902	1091	98	53	1014	959	1076	180	76	970	913	1034	28	20	46	1124	1000	1284
		306	61	998	908	1108	72	41	1081	1006	1167	103	63	1022	971	1080	28	20	49	1134	1007	1297
	1.8	324	62	1001	912	1110	72	41	1086	1012	1171	109	67	1019	972	1070	28	19	49	1143	1009	1319
		351	63	994	905	1102	72	41	1080	1008	1161	114	72	1027	985	1074	27	18	54	1127	978	1329
	2.6	482	56	870	788	970	171	56	899	840	966	296	142	947	921	976	42	28	80	967	894	1054
		291	56	941	853	1049	132	51	976	907	1057	207	102	978	940	1018	38	25	76	983	895	1089

Table E5 - Results obtained for the OCFS with a small gap turned 90° into each other (λ and α for the simplified 2-D PH model) – cont.

u_L	u_G	$\lambda a_{e,r}$	$\lambda a_{e,r\ min}$	αa	αa_{min}	αa_{max}	$\lambda b_{e,r}$	$\lambda b_{e,r\ min}$	αb	αb_{min}	αb_{max}	$\lambda c_{e,r}$	$\lambda c_{e,r\ min}$	αc	αc_{min}	αc_{max}	$\lambda d_{e,r}$	$\lambda d_{e,r\ min}$	$\lambda d_{e,r\ max}$	α_d	αd_{min}	αd_{max}
(mm/s)	(m/s)	($W.m^{-1}.K^{-1}$)		($W.m^{-2}.K^{-1}$)			($W.m^{-1}.K^{-1}$)		($W.m^{-2}.K^{-1}$)			($W.m^{-1}.K^{-1}$)		($W.m^{-2}.K^{-1}$)			($W.m^{-1}.K^{-1}$)			($W.m^{-2}.K^{-1}$)		
6	0.4	57	36	791	745	843	29	17	861	763	989	16	13	701	657	752	10	7	15	816	672	1038
		48	24	721	650	810	29	12	759	615	990	18	14	632	578	698	9	7	14	824	662	1089
	1.1	40	25	925	840	1029	36	19	918	799	1079	35	20	789	704	899	14	9	26	781	646	987
		31	16	870	727	1082	35	21	830	748	931	44	25	750	684	831	15	10	31	750	627	934
	1.8	46	23	779	690	894	32	20	824	755	908	60	32	821	745	915	17	11	37	802	668	1004
		47	24	794	704	911	31	20	846	769	939	61	32	806	732	896	16	11	32	807	682	990
	2.6	68	30	750	678	840	35	18	819	718	953	31	22	811	747	887	19	14	31	714	646	798
		41	25	936	838	1060	38	20	933	814	1093	29	19	841	749	958	17	12	26	801	712	917

Table E6 - Results obtained for the OCFS with a small gap turned 0° into each other (λ and α for the simplified 2-D PH model).

u_L	u_G	$\lambda a_{e,r}$	$\lambda a_{e,r\ min}$	αa	αa_{min}	αa_{max}	$\lambda b_{e,r}$	$\lambda b_{e,r\ min}$	αb	αb_{min}	αb_{max}	$\lambda c_{e,r}$	$\lambda c_{e,r\ min}$	$\lambda c_{e,r\ max}$	αc	αc_{min}	αc_{max}	$\lambda d_{e,r}$	$\lambda d_{e,r\ min}$	$\lambda d_{e,r\ max}$	α_d	αd_{min}	αd_{max}
(mm/s)	(m/s)	($W.m^{-1}.K^{-1}$)		($W.m^{-2}.K^{-1}$)			($W.m^{-1}.K^{-1}$)		($W.m^{-2}.K^{-1}$)			($W.m^{-1}.K^{-1}$)			($W.m^{-2}.K^{-1}$)			($W.m^{-1}.K^{-1}$)			($W.m^{-2}.K^{-1}$)		
25	0.4	204	130	1233	1198	1269	63	37	1344	1207	1517	14	12	16	1096	991	1228	9	7	13	1126	870	1596
		136	98	1062	1039	1087	52	30	1158	1034	1315	13	11	16	990	882	1127	9	7	14	1119	849	1639
	1.1	528	204	1227	1191	1266	54	35	1417	1299	1558	19	16	23	1231	1118	1370	8	7	11	939	773	1196
	1.8	410	222	1041	1024	1058	70	35	1124	1019	1254	31	26	39	1283	1194	1386	15	12	20	1271	1093	1517
	2.6	534	241	1122	1100	1144	69	40	1227	1130	1341	28	23	34	1469	1353	1608	14	11	19	1385	1150	1742
18	0.4	96	72	1166	1127	1208	32	27	1383	1301	1477	9	7	12	1376	1061	1957	5	4	8	1264	846	2495
	1.1	170	96	996	960	1035	44	22	1112	962	1317	18	15	24	1342	1165	1582	9	7	10	1681	1344	2245
		168	116	946	929	965	42	23	1061	934	1228	16	12	23	1273	1053	1608	7	6	8	1445	1174	1878
	1.8	112	73	978	945	1014	44	22	1064	920	1260	22	18	27	1313	1196	1457	12	9	16	1688	1285	2460
		115	76	981	949	1014	45	22	1067	924	1262	22	18	26	1336	1223	1473	11	9	16	1697	1289	2481
	2.6	330	175	1017	996	1039	52	27	1132	1001	1301	26	23	30	1203	1147	1265	13	10	19	1636	1251	2364
		330	176	1022	1001	1043	53	27	1135	1006	1301	26	23	30	1183	1126	1246	13	10	19	1650	1263	2382
12	0.4	53	42	943	911	977	26	18	1065	930	1246	9	7	13	877	684	1224	11	8	19	2337	1398	7127
	1.1	64	42	826	786	870	37	18	874	750	1047	16	14	19	1143	1038	1273	9	7	14	1532	1091	2572
	1.8	73	48	841	805	880	63	25	863	743	1029	18	16	21	1196	1098	1314	10	8	14	1584	1180	2411
		87	60	816	791	844	36	16	893	752	1098	19	16	22	1130	1034	1245	10	8	14	1500	1117	2281
	2.6	162	96	774	755	794	44	18	844	712	1037	22	17	31	1025	920	1157	11	8	17	1440	1061	2244

Table E6 - Results obtained for the OCFS with a small gap turned 0° into each other (λ and α for the simplified 2-D PH model) – cont.

u_L	u_G	$\lambda a_{e,r}$	$\lambda a_{e,r\ min}$	αa	αa_{min}	αa_{max}	$\lambda b_{e,r}$	$\lambda b_{e,r\ min}$	αb	αb_{min}	αb_{max}	$\lambda c_{e,r}$	$\lambda c_{e,r\ min}$	$\lambda c_{e,r\ max}$	αc	αc_{min}	αc_{max}	$\lambda d_{e,r}$	$\lambda d_{e,r\ min}$	$\lambda d_{e,r\ max}$	α_d	αd_{min}	αd_{max}
(mm/s)	(m/s)	($W.m^{-1}.K^{-1}$)		($W.m^{-2}.K^{-1}$)			($W.m^{-1}.K^{-1}$)		($W.m^{-2}.K^{-1}$)			($W.m^{-1}.K^{-1}$)			($W.m^{-2}.K^{-1}$)			($W.m^{-1}.K^{-1}$)			($W.m^{-2}.K^{-1}$)		
6		41	23	829	738	947	32	17	847	732	1005	13	10	19	663	580	774	7	5	10	1322	858	2877
	0.4	37	23	802	727	895	24	13	852	717	1051	11	9	15	692	608	804	6	4	9	1399	874	3509
		39	28	800	755	850	21	13	892	771	1058	10	8	12	717	644	808	6	5	10	1273	830	2730
	1.1	42	34	770	746	795	36	15	786	662	967	13	10	17	876	761	1033	7	5	11	1275	856	2499
		38	31	708	686	732	34	14	719	605	885	12	10	16	856	750	996	7	5	11	1065	770	1726
	1.8	33	25	647	619	679	37	15	638	546	767	13	11	15	792	727	870	8	6	12	986	752	1434
	2.6	41	29	540	517	564	28	9	560	440	771	15	11	26	648	560	767	8	6	12	909	712	1258

Table E7 - Results obtained for the OCFS with a small gap turned 90° into each other ($\lambda_{average}$, $\alpha_{average}$ and U_{est} for the 2-D PH model).

u_L (mm/s)	u_G (m/s)	λ ($W.m^{-1}.K^{-1}$)	λ_min ($W.m^{-1}.K^{-1}$)	λ_max ($W.m^{-1}.K^{-1}$)	α ($W.m^{-2}.K^{-1}$)	α_min ($W.m^{-2}.K^{-1}$)	α_max ($W.m^{-2}.K^{-1}$)	U_{est} ($W.m^{-2}.K^{-1}$)	U_{est}_min ($W.m^{-2}.K^{-1}$)	U_{est}_max ($W.m^{-2}.K^{-1}$)	$\lambda_{average}$ ($W.m^{-1}.K^{-1}$)	$\alpha_{average}$ ($W.m^{-2}.K^{-1}$)	U_{est}_average ($W.m^{-2}.K^{-1}$)
25	0.4	87	77	123	953	921	987	892	857	940	87	953	892
	1.1	125	85	223	999	963	1035	951	899	1006	125	999	951
	1.8	134	84	230	992	956	1026	948	893	998	134	992	948
		134	84	236	993	957	1031	949	893	1004			
	2.6	94	76	152	1029	989	1069	963	915	1024	94	1024	958
		93	75	159	1018	974	1062	953	901	1019			
18	0.4	68	59	79	928	898	976	850	820	906	68	928	850
	1.1	92	66	150	968	930	1006	908	855	966	92	968	908
		92	66	154	968	932	1006	908	856	967			
	1.8	121	119	123	958	956	960	913	910	915	121	958	913
		78	68	126	972	932	1012	902	858	964			
	2.6	82	72	132	944	906	984	879	840	940	82	944	890
12	0.4	64	30	102	782	744	820	739	644	781	64	795	751
		64	30	102	781	745	821	738	645	782			
		64	42	112	824	786	866	776	704	826			
	1.1	58	42	340	837	791	887	817	708	873	58	862	813
		58	48	94	886	842	954	809	759	897			
	1.8	112	110	114	838	836	840	801	798	803	112	835	806
		113	42	300	831	785	881	810	703	865			
	2.6	80	40	222	709	671	747	690	607	732	80	735	705
		80	42	158	761	723	803	720	653	778			
6	0.4	27	19	41	692	652	736	595	537	662	27	562	506
		25	11	501	433	381	493	418	313	490			
	1.1	29	21	39	700	668	734	609	557	657	27	693	597
		25	17	37	686	646	732	586	522	651			
	1.8	24	18	34	666	628	706	569	516	625	24	666	568
		24	18	34	666	628	706	568	516	625			
	2.6	21	15	33	577	539	617	493	440	552	22	598	511
		23	15	33	620	588	654	529	472	582			

Table E8 - Results obtained for the OCFS with a small gap turned 0° into each other ($\lambda_{average}$, $\alpha_{average}$ and U_{est} for the 2-D PH model)

u_L (mm/s)	u_G (m/s)	λ ($W.m^{-1}.K^{-1}$)	λ_min ($W.m^{-1}.K^{-1}$)	λ_max ($W.m^{-1}.K^{-1}$)	α ($W.m^{-2}.K^{-1}$)	α_min ($W.m^{-2}.K^{-1}$)	α_max ($W.m^{-2}.K^{-1}$)	U_{est} ($W.m^{-2}.K^{-1}$)	U_{est}_min ($W.m^{-2}.K^{-1}$)	U_{est}_max ($W.m^{-2}.K^{-1}$)	$\lambda_{average}$ ($W.m^{-1}.K^{-1}$)	$\alpha_{average}$ ($W.m^{-2}.K^{-1}$)	$U_{est\_average}$ ($W.m^{-2}.K^{-1}$)
25	0.4	21	13	31	1019	901	1119	697	629	913	20	969	698
		18	10	28	920	816	1034	698	540	840			
	1.1	26	14	38	966	860	1088	775	621	923	26	966	775
	1.8	38	24	62	951	869	1041	823	709	942	38	951	823
	2.6	35	21	53	1002	906	1106	844	714	978	35	1002	844
18	0.4	14	8	20	979	859	1117	691	514	828	14	979	691
	1.1	26	16	40	1004	898	1112	809	665	947	24	946	757
		21	11	33	888	786	1000	705	543	841			
	1.8	32	20	44	949	871	1031	783	685	899	32	954	787
		32	20	44	960	882	1042	791	691	908			
	2.6	34	20	156	815	743	893	769	603	862	34	809	763
		34	20	158	802	730	880	757	594	850			
12	0.4	18	12	26	866	788	906	662	559	744	18	866	662
	1.1	23	18	40	805	751	863	676	596	760	23	805	676
	1.8	30	23	63	804	746	864	707	620	796	30	795	690
		30	20	48	785	733	841	674	596	758			
	2.6	32	18	54	704	650	760	619	530	699	30	685	598
		27	15	43	666	624	724	577	495	655			
6	0.4	18	12	28	748	670	808	592	497	685	18	740	587
		18	12	26	732	662	790	582	492	664			
	1.1	22	17	39	641	605	675	552	495	609	21	627	541
		20	16	36	614	578	650	531	472	584			
	1.8	21	13	33	540	504	580	466	406	523	21	540	466
	2.6	18	10	30	404	376	432	353	304	396	18	404	353

Table E9 – Comparison between the values obtained with the simplified and the 2-D PH model for the OCFS packings with a small gap turned 90° into each other.

		2-D model		Simplified 2-D model			
u_L (mm/s)	u_G (m/s)	$\lambda_{average}$ ($W.m^{-1}.K^{-1}$)	$\alpha_{average}$ ($W.m^{-2}.K^{-1}$)	$\lambda_{average}$ ($W.m^{-1}.K^{-1}$)	$\alpha_{average}$ ($W.m^{-2}.K^{-1}$)	$\Delta\lambda$ (%)	$\Delta\alpha$ (%)
25	0.4	87	953	159	1100	45	13
	1.1	125	999	303	1168	59	14
	1.8	134	992	240	1211	44	18
	2.6	94	1024	132	1343	29	24
18	0.4	63	928	74	1005	14	8
	1.1	92	968	194	1044	52	7
	1.8	77	966	136	1130	43	14
	2.6	82	944	137	1227	40	23
12	0.4	64	795	63	873	-1	9
	1.1	58	862	175	967	67	11
	1.8	112	835	109	1023	-3	18
	2.6	80	735	251	962	68	24
6	0.4	27	562	17	667	-57	16
	1.1	27	693	39	770	30	10
	1.8	24	666	61	814	60	18
	2.6	22	598	30	826	27	28

Table E10 – Comparison between the values obtained with the simplified and the 2-D PH model for the OCFS packings with a small gap turned 0° into each other.

		2-D model		Simplified 2-D model			
u_L (mm/s)	u_G (m/s)	$\lambda_{average}$ ($W.m^{-1}.K^{-1}$)	$\alpha_{average}$ ($W.m^{-2}.K^{-1}$)	$\lambda_{average}$ ($W.m^{-1}.K^{-1}$)	$\alpha_{average}$ ($W.m^{-2}.K^{-1}$)	$\Delta\lambda$ (%)	$\Delta\alpha$ (%)
25	0.4	20	969	13	1043	-46	7
	1.1	26	966	19	1231	-39	22
	1.8	38	951	31	1283	-23	26
	2.6	35	1002	28	1469	-27	32
18	0.4	14	979	9	1376	-59	29
	1.1	24	946	17	1308	-38	28
	1.8	32	954	22	1325	-48	28
	2.6	34	809	26	1193	-30	32
12	0.4	18	866	9	877	-102	1
	1.1	23	805	16	1143	-45	30
	1.8	30	795	18	1163	-62	32
	2.6	30	685	22	1025	-34	33
6	0.4	18	740	11	691	-58	-7
	1.1	21	627	13	866	-65	28
	1.8	21	540	13	792	-70	32
	2.6	18	404	15	648	-14	38

Appendix F

Appendix F1 – Results obtained for the OCFS with a small, medium and a big gap turned into 90° into each other (U_{ov}).

Table F1 – Results obtained for the overall heat transfer coefficient for OCFS packings with a medium gap turned 90° into each other and the respective deviation.

		U_{ov} (W.m^{-2}.K^{-1})								$U_{average}$ (W.m^{-2}.K^{-1})				Deviation (%)			
u_L (mm/s)	u_G (m/s)	A-B		B-C		A-D		C-D		A-B	B-C	A-D	C-D	AB	BC	AD	CD
25	0.4	1104	1106	1006	992	914	908	746	747	1105	999	911	747	0	1	1	0
	1.1	1065	1072	1083	1077	928	930	755	762	1069	1080	929	758	1	0	0	1
	1.8	1192	1191	1071	1052	988	984	856	863	1191	1061	986	859	0	2	0	1
	2.6	1335	1335	1000	994	968	960	833	818	1335	997	964	826	0	1	1	2
18	0.4	958	972	873	875	785	800	703	712	965	874	792	707	1	0	2	1
	1.1	1003	1004	961	961	846	843	753	750	1003	961	845	751	0	0	0	1
	1.8	1074	1073	920	932	879	879	827	820	1073	926	879	824	0	1	0	1
	2.6	1150	1152	848	856	870	870	825	815	1151	852	870	820	0	1	0	1
12	0.4	804	804	788	781	682	679	596	596	804	784	680	596	0	1	0	0
	1.1	892	892	904	898	763	762	674	668	892	901	762	671	0	1	0	1
	1.8	992	1002	862	864	793	797	712	720	997	863	795	716	1	0	0	1
	2.6	840	838	699	704	704	705	712	715	839	702	704	714	0	1	0	0
6	0.4	572	600	553	551	432	435	406	380	586	552	433	393	5	0	1	6
	1.1	653	640	602	590	478	478	423	444	647	596	478	433	2	2	0	5
	1.8	658	670	565	571	497	497	476	463	664	568	497	470	2	1	0	3
	2.6	605	607	508	499	470	467	439	437	606	503	468	438	0	2	1	0

Table F2 – Results obtained for the overall heat transfer coefficient for OCFS packings with a big gap turned 90° into each other and the respective deviation.

		U_{ov} (W.m^{-2}.K^{-1})								$U_{average}$ (W.m^{-2}.K^{-1})				Deviation (%)			
u_L (mm/s)	u_G (m/s)	A-B		B-C		A-D		C-D		A-B	B-C	A-D	C-D	AB	BC	AD	CD
25	0.4	1025	1040	1101	1145	921	932	685	669	1033	1123	927	677	1	4	1	2
	1.1	1020	980	1130	1157	925	932	691	708	1000	1144	928	699	4	2	1	2
	1.8	977	997	1207	1199	952	961	731	753	957	1203	957	742	2	1	1	3
	2.6	1263	1266	1526	1522	1185	1184	887	892	1264	1524	1185	890	0	0	0	0
18	0.4	1171	1164	1020	1011	1029	1033	882	898	1167	1016	1031	890	1	1	0	2
	1.1	924	925	980	967	831	831	728	715	925	974	831	722	0	1	0	2
	1.8	1008	998	989	1000	894	890	712	724	1003	995	892	718	1	1	1	2
	2.6	1049	1047	1162	1167	963	961	751	748	1048	1165	962	750	0	0	0	0
12	0.4	872	863	875	883	743	745	604	607	868	879	744	606	1	1	0	1
	1.1	856	867	905	906	744	744	608	605	862	906	744	606	1	0	0	0
	1.8	623	633	779	803	637	657	574	602	628	861	647	588	2	3	3	5
	2.6	695	750	954	965	785	799	790	795	722	960	792	792	7	1	2	1
6	0.4	892	858	613	616	510	506	339	345	875	615	508	342	4	0	1	2
	1.1	833	786	616	636	531	524	416	412	810	626	527	414	6	3	1	1
	1.8	720	680	706	656	542	482	466	395	700	681	512	430	6	7	11	15
	2.6	651	763	751	801	594	622	571	546	707	776	608	558	15	6	5	4

Table F3 – Results obtained for the overall heat transfer coefficient for OCFS packings with a big gap turned 90° into each other and the respective deviation (second day).

		U_{ov} (W.m^{-2}.K^{-1})								$U_{average}$ (W.m^{-2}.K^{-1})				Deviation (%)			
u_L (mm/s)	u_G (m/s)	A-B		B-C		A-D		C-D		A-B	B-C	A-D	C-D	AB	BC	AD	CD
12	0.4	1045	1042	846	868	731	727	626	640	1043	857	729	633	0	3	0	2
6	1.1	830	802	624	620	600	594	516	512	816	622	597	514	3	1	1	1
	1.8	721	744	662	672	517	488	469	466	732	667	503	468	3	2	6	1

Table F4– Average of the results obtained for the overall heat transfer coefficient for the three types of OCFS packings with the best orientation (90º) and the respective deviation (*ΔU1 = $U_{ov\_big\_gap}$ - $U_{ov\_medium\_gap}$, ΔU2 = $U_{ov\_small\_gap}$ - $U_{ov\_medium\_gap}$ and ΔU3 = $U_{ov\_big\_gap}$ - $U_{ov\_small\_gap}$*).

u_L (mm/s)	u_G (m/s)	$U_{ov\_medium\_gap}$ (W m^{-2} K^{-1})	$U_{ov\_big\_gap}$ (W m^{-2} K^{-1})	$U_{ov\_small\_gap}$ (W m^{-2} K^{-1})	ΔU1	ΔU2	ΔU3
25	0.4	999	1123	1017	11	2	9
	1.1	1080	1144	1105	6	2	3
	1.8	1061	1203	1137	12	7	6
	2.6	997	1524	1218	35	18	20
18	0.4	874	1016	895	14	2	12
	1.1	961	974	980	1	2	-1
	1.8	926	995	1047	7	12	-5
	2.6	852	1165	1133	27	25	3
12	0.4	784	879	787	11	0	10
	1.1	901	906	911	1	1	-1
	1.8	863	861	943	0	8	-9
	2.6	702	960	921	27	24	4
6	0.4	552	615	597	10	9	3
	1.1	596	626	676	5	12	-8
	1.8	568	681	734	17	23	-8
	2.6	503	776	644	35	22	17

Appendix F2 – Results obtained for the OCFS with a small, medium and a big gap turned 90° into each other for the simplified and the 2-D PH model.

Table F5 - Results obtained for the OCFS with a small gap turned 90° into each other (λ and α for the simplified 2-D PH model).

u_L	u_G	$\lambda a_{e,r}$	$\lambda a_{e,r\ min}$	αa	αa_{min}	αa_{max}	$\lambda b_{e,r}$	$\lambda b_{e,r\ min}$	αb	αb_{min}	αb_{max}	$\lambda c_{e,r}$	$\lambda c_{e,r\ min}$	αc	αc_{min}	αc_{max}	$\lambda d_{e,r}$	$\lambda d_{e,r\ min}$	$\lambda d_{e,r\ max}$	α_d	αd_{min}	αd_{max}
(mm/s)	(m/s)	($W.m^{-1}.K^{-1}$)		($W.m^{-2}.K^{-1}$)			($W.m^{-1}.K^{-1}$)		($W.m^{-2}.K^{-1}$)			($W.m^{-1}.K^{-1}$)		($W.m^{-2}.K^{-1}$)			($W.m^{-1}.K^{-1}$)			($W.m^{-2}.K^{-1}$)		
25	0.4	88	54	1073	1015	1139	83	51	1067	1015	1123	159	87	1100	1050	1156	57	45	79	1024	987	1064
	1.1	280	102	1111	1056	1172	149	70	1136	1077	1201	303	145	1168	1128	1210	81	61	120	1060	1026	1095
		301	102	1133	1073	1200	150	71	1162	1101	1230	278	147	1192	1155	1231	90	68	131	1110	1078	1143
	1.8	340	108	1140	1080	1205	149	71	1174	1112	1242	299	154	1183	1148	1221	91	69	136	1126	1093	1161
		349	97	1181	1107	1264	179	93	1199	1153	1249	142	98	1260	1220	1303	78	58	118	1127	1087	1171
		387	103	1273	1192	1367	169	92	1302	1250	1358	121	90	1356	1315	1401	81	60	125	1205	1159	1254
	2.6	422	105	1275	1193	1369	170	92	1306	1253	1363	112	91	1376	1345	1408	76	57	112	1200	1156	1248
		410	106	1240	1164	1327	182	96	1265	1217	1318	163	112	1296	1258	1336	83	63	124	1210	1167	1255
18	0.4	74	44	1115	1036	1207	59	40	1127	1064	1199	74	52	1005	960	1053	36	28	50	1136	1065	1218
		224	78	1122	1047	1207	131	72	1154	1103	1209	241	114	1041	1001	1085	49	37	74	1155	1090	1228
	1.1	234	80	1126	1052	1211	129	73	1161	1111	1215	244	114	1046	1005	1090	49	36	73	1148	1084	1221
		127	68	1114	1053	1183	73	48	1162	1102	1229	97	65	1045	1001	1093	40	31	55	1165	1097	1242
		284	82	1158	1076	1252	122	68	1204	1147	1267	170	105	1106	1071	1144	50	39	70	1177	1120	1242
	1.8	310	80	1154	1068	1256	101	52	1217	1133	1314	115	88	1134	1105	1164	49	36	77	1150	1079	1230
		327	81	1154	1068	1255	99	53	1220	1142	1310	123	92	1150	1120	1182	48	35	75	1135	1066	1214
	2.6	351	82	1193	1101	1302	110	60	1258	1187	1338	137	100	1227	1195	1261	56	42	86	1169	1110	1235
12	0.4	53	33	976	900	1066	37	28	1008	951	1073	51	38	869	828	914	21	16	30	1032	932	1154
		67	43	943	891	1002	37	28	1012	955	1076	49	36	865	821	914	21	16	29	1061	955	1194
		103	46	932	859	1020	62	41	976	929	1028	90	50	885	830	948	25	18	39	1059	948	1200
	1.1	139	50	981	896	1084	98	56	1011	962	1065	169	72	964	906	1030	28	20	45	1123	1005	1273
		129	49	987	902	1091	98	53	1014	959	1076	180	76	970	913	1034	28	20	46	1124	1000	1284
		306	61	998	908	1108	72	41	1081	1006	1167	103	63	1022	971	1080	28	20	49	1134	1007	1297
	1.8	324	62	1001	912	1110	72	41	1086	1012	1171	109	67	1019	972	1070	28	19	49	1143	1009	1319
		351	63	994	905	1102	72	41	1080	1008	1161	114	72	1027	985	1074	27	18	54	1127	978	1329
	2.6	482	56	870	788	970	171	56	899	840	966	296	142	947	921	976	42	28	80	967	894	1054
		291	56	941	853	1049	132	51	976	907	1057	207	102	978	940	1018	38	25	76	983	895	1089

Table F5 - Results obtained for the OCFS with a small gap turned 90° into each other (λ and α for the simplified 2-D PH model) – cont.

u_L	u_G	$\lambda a_{e,r}$	$\lambda a_{e,r\ min}$	αa	αa_{min}	αa_{max}	$\lambda b_{e,r}$	$\lambda b_{e,r\ min}$	αb	αb_{min}	αb_{max}	$\lambda c_{e,r}$	$\lambda c_{e,r\ min}$	αc	αc_{min}	αc_{max}	$\lambda d_{e,r}$	$\lambda d_{e,r\ min}$	$\lambda d_{e,r\ max}$	α_d	αd_{min}	αd_{max}
(mm/s)	(m/s)	($W.m^{-1}.K^{-1}$)		($W.m^{-2}.K^{-1}$)			($W.m^{-1}.K^{-1}$)		($W.m^{-2}.K^{-1}$)			($W.m^{-1}.K^{-1}$)		($W.m^{-2}.K^{-1}$)			($W.m^{-1}.K^{-1}$)			($W.m^{-2}.K^{-1}$)		
6	0.4	57	36	791	745	843	29	17	861	763	989	16	13	701	657	752	10	7	15	816	672	1038
		48	24	721	650	810	29	12	759	615	990	18	14	632	578	698	9	7	14	824	662	1089
	1.1	40	25	925	840	1029	36	19	918	799	1079	35	20	789	704	899	14	9	26	781	646	987
		31	16	870	727	1082	35	21	830	748	931	44	25	750	684	831	15	10	31	750	627	934
	1.8	46	23	779	690	894	32	20	824	755	908	60	32	821	745	915	17	11	37	802	668	1004
		47	24	794	704	911	31	20	846	769	939	61	32	806	732	896	16	11	32	807	682	990
	2.6	68	30	750	678	840	35	18	819	718	953	31	22	811	747	887	19	14	31	714	646	798
		41	25	936	838	1060	38	20	933	814	1093	29	19	841	749	958	17	12	26	801	712	917

Table F6 - Results obtained for the OCFS with a medium gap turned 90° into each other (λ and α for the simplified 2-D PH model).

u_L	u_G	$\lambda a_{e,r}$	$\lambda a_{e,r\ min}$	αa	αa_{min}	αa_{max}	$\lambda b_{e,r}$	$\lambda b_{e,r\ min}$	αb	αb_{min}	αb_{max}	$\lambda c_{e,r}$	$\lambda c_{e,r\ min}$	αc	αc_{min}	αc_{max}	$\lambda d_{e,r}$	$\lambda d_{e,r\ min}$	$\lambda d_{e,r\ max}$	α_d	αd_{min}	αd_{max}
(mm/s)	(m/s)	($W.m^{-1}.K^{-1}$)		($W.m^{-2}.K^{-1}$)			($W.m^{-1}.K^{-1}$)		($W.m^{-2}.K^{-1}$)			($W.m^{-1}.K^{-1}$)		($W.m^{-2}.K^{-1}$)			($W.m^{-1}.K^{-1}$)			($W.m^{-2}.K^{-1}$)		
25	0.4	234	124	1432	1376	1494	61	30	1603	1361	1951	89	43	992	917	1081	61	45	95	1160	1099	1228
		242	129	1443	1389	1502	61	29	1619	1370	1978	82	41	974	899	1063	64	47	101	1162	1103	1228
	1.1	559	183	1289	1245	1337	65	32	1444	1259	1692	2870	150	1038	993	1088	98	69	170	1145	1101	1193
		621	203	1303	1262	1347	65	32	1465	1276	1719	5173	157	1032	988	1081	92	65	157	1160	1113	1211
	1.8	402	220	1398	1368	1429	88	45	1492	1353	1662	155	65	1134	1058	1222	92	71	130	1283	1242	1327
		795	245	1376	1337	1418	87	45	1488	1350	1656	288	58	1041	947	1157	93	74	125	1341	1303	1383
	2.6	585	257	1744	1695	1796	102	56	1853	1690	2051	164	53	1011	926	1112	65	49	94	1502	1419	1596
		420	256	1654	1623	1686	120	56	1714	1553	1914	159	62	1052	982	1134	61	45	99	1447	1349	1560
18	0.4	112	73	1273	1212	1339	35	23	1476	1285	1733	69	36	915	842	1001	30	23	43	1330	1200	1490
		115	71	1271	1205	1345	35	22	1472	1276	1740	66	36	912	845	991	32	24	47	1311	1187	1463
	1.1	218	122	1260	1216	1309	51	29	1414	1245	1635	94	40	1018	925	1132	42	32	63	1318	1218	1435
		238	125	1287	1238	1340	52	30	1448	1276	1674	215	62	953	884	1033	43	29	76	1351	1212	1526
	1.8	389	191	1285	1251	1322	79	41	1368	1238	1529	156	57	954	888	1031	43	34	59	1435	1339	1545
		277	121	1310	1248	1377	78	40	1371	1240	1533	122	51	972	902	1054	44	35	61	1434	1336	1546
	2.6	680	231	1462	1418	1510	71	32	1618	1371	1974	122	40	900	813	1007	45	35	61	1393	1305	1494
		289	96	1427	1321	1552	114	42	1438	1265	1666	171	21	758	623	969	51	41	68	1523	1436	1620

Table F6 - Results obtained for the OCFS with a medium gap turned 90° into each other (λ and α for the simplified 2-D PH model) – cont.

u_L	u_G	$\lambda a_{e,r}$	$\lambda a_{e,r\ min}$	αa	αa_{min}	αa_{max}	$\lambda b_{e,r}$	$\lambda b_{e,r\ min}$	αb	αb_{min}	αb_{max}	$\lambda c_{e,r}$	$\lambda c_{e,r\ min}$	αc	αc_{min}	αc_{max}	$\lambda d_{e,r}$	$\lambda d_{e,r\ min}$	$\lambda d_{e,r\ max}$	α_d	αd_{min}	αd_{max}
(mm/s)	(m/s)	($W.m^{-1}.K^{-1}$)		($W.m^{-2}.K^{-1}$)			($W.m^{-1}.K^{-1}$)		($W.m^{-2}.K^{-1}$)			($W.m^{-1}.K^{-1}$)		($W.m^{-2}.K^{-1}$)			($W.m^{-1}.K^{-1}$)			($W.m^{-2}.K^{-1}$)		
12	0.4	84	50	1074	1002	1156	32	20	1210	1065	1402	40	25	851	780	936	18	14	27	1237	1055	1495
		94	56	1072	1009	1143	32	21	1218	1075	1405	40	25	847	778	929	19	15	26	1233	1074	1448
	1.1	262	109	1129	1077	1188	47	27	1276	1126	1472	86	47	918	864	979	24	17	39	1408	1186	1733
		673	266	1109	1089	1131	51	27	1281	1122	1493	86	49	923	874	979	24	17	38	1393	1182	1697
	1.8	735	195	1225	1184	1269	49	20	1409	1111	1923	122	48	885	821	960	23	18	33	1444	1261	1689
		707	217	1244	1208	1282	49	21	1431	1140	1924	280	42	853	761	970	22	17	31	1540	1332	1825
	2.6	-942	342	1047	1012	1084	46	17	1229	946	1755	93	25	618	548	709	30	24	41	1307	1194	1445
		-1365	292	1024	990	1061	44	17	1207	932	1711	114	146	637	595	684	30	23	46	1263	1135	1422
6	0.4	80	44	806	759	860	30	17	893	785	1035	21	11	621	517	776	7	5	12	2557	1131	-9787
		69	35	848	774	938	25	18	967	886	1064	23	14	654	584	741	6	4	8	7688	1775	-3299
	1.1	170	46	893	818	984	31	15	1058	866	1359	20	11	682	562	867	8	6	13	1858	1072	6946
		194	59	887	822	964	27	14	1070	875	1377	27	13	624	537	747	8	6	13	2219	1140	41288
	1.8	100	46	910	836	998	24	11	1099	830	1624	30	16	575	513	656	10	8	15	1589	1131	2671
		213	62	916	844	1002	24	12	1161	873	1732	50	23	539	494	593	10	8	13	1621	1188	2554
	2.6	155	82	815	786	847	26	11	964	717	1471	49	24	472	440	509	16	12	24	891	776	1046
		261	112	806	780	834	26	11	981	730	1494	45	25	490	462	522	15	12	19	875	784	989

Table F7 - Results obtained for the OCFS with a big gap turned 90° into each other (λ and α for the simplified 2-D PH model).

u_L	u_G	$\lambda a_{e,r}$	$\lambda a_{e,r\ min}$	αa	αa_{min}	αa_{max}	$\lambda b_{e,r}$	$\lambda b_{e,r\ min}$	αb	αb_{min}	αb_{max}	$\lambda c_{e,r}$	$\lambda c_{e,r\ min}$	αc	αc_{min}	αc_{max}	$\lambda d_{e,r}$	$\lambda d_{e,r\ min}$	$\lambda d_{e,r\ max}$	α_d	αd_{min}	αd_{max}
(mm/s)	(m/s)	($W.m^{-1}.K^{-1}$)		($W.m^{-2}.K^{-1}$)			($W.m^{-1}.K^{-1}$)		($W.m^{-2}.K^{-1}$)			($W.m^{-1}.K^{-1}$)		($W.m^{-2}.K^{-1}$)			($W.m^{-1}.K^{-1}$)			($W.m^{-2}.K^{-1}$)		
25	0.4	104	76	1095	1064	1129	41	27	1222	1107	1363	45	21	1216	999	1554	42	30	72	1159	1068	1266
		202	146	1126	1108	1144	63	36	1217	1111	1345	64	28	1251	1062	1520	47	32	88	1071	992	1164
	1.1	436	220	1120	1099	1141	68	44	1234	1159	1318	81	35	1235	1082	1437	52	37	87	1103	1037	1179
		439	211	1065	1044	1086	115	49	1114	1029	1214	162	63	1174	1087	1277	54	34	135	1111	1018	1224
	1.8	327	167	1108	1082	1136	129	52	1143	1055	1249	85	50	1308	1215	1417	49	31	106	1188	1079	1320
		692	340	1126	1111	1140	140	53	1176	1081	1290	81	59	1302	1249	1360	46	30	99	1243	1118	1398
	2.6	4415	487	1428	1401	1457	196	59	1510	1356	1704	75	41	1717	1512	1986	43	26	117	1533	1310	1848
		958	186	1466	1399	1540	104	44	1590	1401	1837	69	40	1790	1579	2066	43	26	114	1573	1339	1905
18	0.4	73	49	1161	1096	1234	29	20	1372	1211	1581	36	19	1228	1006	1576	28	21	40	1304	1176	1462
		77	54	1388	1314	1471	29	21	1735	1513	2035	38	22	1447	1209	1802	26	20	37	1654	1447	1929
	1.1	97	64	1077	1028	1130	29	20	1288	1147	1468	38	19	1155	950	1473	29	22	44	1221	1106	1363
		100	65	1068	1020	1121	31	20	1251	1099	1452	37	18	1146	941	1466	29	22	43	1246	1130	1389
	1.8	183	121	1169	1140	1198	56	31	1278	1139	1456	48	23	1219	1023	1508	35	27	50	1226	1138	1329
		421	255	1162	1146	1178	53	36	1341	1246	1453	52	25	1212	1028	1476	38	27	65	1186	1081	1313
	2.6	556	174	1248	1203	1296	104	49	1327	1214	1463	56	28	1313	1131	1566	40	29	64	1267	1164	1390
		838	303	1200	1177	1223	101	47	1290	1181	1422	56	29	1316	1137	1563	41	27	84	1248	1116	1413
12	0.4	173	86	1025	981	1073	46	30	1156	1061	1268	36	19	1005	855	1218	22	17	31	1189	1056	1361
		175	88	1019	977	1065	48	31	1140	1049	1249	39	21	1019	879	1211	21	16	31	1167	1031	1346
	1.1	728	147	989	950	1031	51	33	1127	1045	1223	52	21	989	831	1221	21	14	42	1175	971	1489
		1114	225	994	969	1021	83	26	1054	893	1287	45	20	984	829	1209	21	14	43	1199	984	1533
	1.8	714	161	687	670	704	40	20	791	702	906	70	31	786	717	871	23	15	49	1063	894	1309
		188	105	740	723	758	42	19	833	722	984	77	34	848	773	939	22	15	36	1100	952	1301
	2.6	119	69	775	749	804	34	14	876	707	1154	94	53	1011	956	1073	26	18	46	1499	1255	1862
		103	64	834	804	866	29	16	985	838	1194	94	49	1031	964	1109	23	17	36	1564	1328	1901

Table F7 - Results obtained for the OCFS with a big gap turned 90° into each other (λ and α for the simplified 2-D PH model) – cont.

u_L	u_G	$\lambda a_{e,r}$	$\lambda a_{e,r\ min}$	αa	αa_{min}	αa_{max}	$\lambda b_{e,r}$	$\lambda b_{e,r\ min}$	αb	αb_{min}	αb_{max}	$\lambda c_{e,r}$	$\lambda c_{e,r\ min}$	αc	αc_{min}	αc_{max}	$\lambda d_{e,r}$	$\lambda d_{e,r\ min}$	$\lambda d_{e,r\ max}$	α_d	αd_{min}	αd_{max}
(mm/s)	(m/s)	($W.m^{-1}.K^{-1}$)		($W.m^{-2}.K^{-1}$)			($W.m^{-1}.K^{-1}$)		($W.m^{-2}.K^{-1}$)			($W.m^{-1}.K^{-1}$)		($W.m^{-2}.K^{-1}$)			($W.m^{-1}.K^{-1}$)			($W.m^{-2}.K^{-1}$)		
6	0.4	27	19	1005	901	1137	24	13	1066	861	1397	25	11	840	653	1176	6	5	11	2044	1026	2931
		30	21	950	858	1065	26	13	1006	795	1370	24	14	839	704	1038	7	5	10	1935	1099	2859
	1.1	40	21	875	762	1028	20	12	1046	862	1330	22	13	863	718	1082	8	6	13	1889	1147	3350
		33	19	844	732	998	31	13	850	681	1131	23	13	885	726	1131	8	6	12	1858	1156	3728
	1.8	38	27	1008	927	1104	33	16	1020	842	1292	24	15	841	733	984	9	6	14	2082	1219	3141
		30	23	947	871	1038	25	14	980	820	1220	23	15	791	695	918	8	5	14	2070	1077	2642
	2.6	70	38	812	757	877	27	16	935	806	1112	28	12	900	691	1290	13	9	20	1481	1116	2203
		43	28	936	857	1032	26	16	1044	905	1233	32	17	983	820	1228	11	8	17	1743	1230	2992

Table F8 - Results obtained for the OCFS with a small gap turned 90° into each other ($\lambda_{average}$, $\alpha_{average}$ and U_{est} for the 2-D PH model).

u_L (mm/s)	u_G (m/s)	λ ($W.m^{-1}.K^{-1}$)	λ_min ($W.m^{-1}.K^{-1}$)	λ_max ($W.m^{-1}.K^{-1}$)	α ($W.m^{-2}.K^{-1}$)	α_min ($W.m^{-2}.K^{-1}$)	α_max ($W.m^{-2}.K^{-1}$)	U_{est} ($W.m^{-2}.K^{-1}$)	U_{est}_min ($W.m^{-2}.K^{-1}$)	U_{est}_max ($W.m^{-2}.K^{-1}$)	$\lambda_{average}$ ($W.m^{-1}.K^{-1}$)	$\alpha_{average}$ ($W.m^{-2}.K^{-1}$)	$U_{est\_average}$ ($W.m^{-2}.K^{-1}$)
25	0.4	87	77	123	953	921	987	892	857	940	87	953	892
	1.1	125	85	223	999	963	1035	951	899	1006	125	999	951
	1.8	134	84	230	992	956	1026	948	893	998	134	992	948
		134	84	236	993	957	1031	949	893	1004			
	2.6	94	76	152	1029	989	1069	963	915	1024	94	1024	958
		93	75	159	1018	974	1062	953	901	1019			
18	0.4	68	59	79	928	898	976	850	820	906	68	928	850
	1.1	92	66	150	968	930	1006	908	855	966	92	968	908
		92	66	154	968	932	1006	908	856	967			
	1.8	121	119	123	958	956	960	913	910	915	121	958	913
		78	68	126	972	932	1012	902	858	964			
	2.6	82	72	132	944	906	984	879	840	940	82	944	890
12	0.4	64	30	102	782	744	820	739	644	781	64	795	751
		64	30	102	781	745	821	738	645	782			
		64	42	112	824	786	866	776	704	826			
	1.1	58	42	340	837	791	887	817	708	873	58	862	813
		58	48	94	886	842	954	809	759	897			
	1.8	112	110	114	838	836	840	801	798	803	112	835	806
		113	42	300	831	785	881	810	703	865			
	2.6	80	40	222	709	671	747	690	607	732	80	735	705
		80	42	158	761	723	803	720	653	778			
6	0.4	27	19	41	692	652	736	595	537	662	27	562	506
		25	11	501	433	381	493	418	313	490			
	1.1	29	21	39	700	668	734	609	557	657	27	693	597
		25	17	37	686	646	732	586	522	651			
	1.8	24	18	34	666	628	706	569	516	625	24	666	568
		24	18	34	666	628	706	568	516	625			
	2.6	21	15	33	577	539	617	493	440	552	22	598	511
		23	15	33	620	588	654	529	472	582			

Table F9 - Results obtained for the OCFS with a medium gap turned 90° into each other ($\lambda_{average}$, $\alpha_{average}$ and U_{est} for the 2-D PH model).

u_L (mm/s)	u_G (m/s)	λ ($W.m^{-1}.K^{-1}$)	λ_min ($W.m^{-1}.K^{-1}$)	λ_max ($W.m^{-1}.K^{-1}$)	α ($W.m^{-2}.K^{-1}$)	α_min ($W.m^{-2}.K^{-1}$)	α_max ($W.m^{-2}.K^{-1}$)	U_{est} ($W.m^{-2}.K^{-1}$)	U_{est}_min ($W.m^{-2}.K^{-1}$)	U_{est}_max ($W.m^{-2}.K^{-1}$)	$\lambda_{average}$ ($W.m^{-1}.K^{-1}$)	$\alpha_{average}$ ($W.m^{-2}.K^{-1}$)	$U_{est\_average}$ ($W.m^{-2}.K^{-1}$)
25	0.4	78	47	129	1051	983	1125	964	869	1067	79	1053	965
		80	45	121	1055	985	1129	966	866	1067			
	1.1	118	72	346	1016	958	1078	964	884	1057	116	1015	963
		115	69	341	1014	954	1078	961	878	1057			
	1.8	118	74	258	1048	996	1106	993	919	1077	127	1038	988
		136	72	340	1028	966	1088	982	891	1067			
	2.6	109	43	501	929	831	1037	883	741	1024	111	922	876
		112	42	502	914	822	1012	870	732	999			
18	0.4	69	24	52	1022	954	1090	867	764	964	69	1017	863
		69	23	53	1012	942	1080	858	750	958			
	1.1	78	44	100	974	920	1050	882	814	985	78	971	879
		78	42	110	968	908	1048	877	800	989			
	1.8	87	43	111	951	893	1031	861	790	974	89	953	865
		90	42	120	954	898	1014	868	792	963			
	2.6	81	45	501	836	758	920	812	686	910	81	830	807
		81	33	501	825	755	899	802	661	889			
12	0.4	64	22	124	793	737	853	749	609	818	64	792	748
		64	22	126	791	737	851	747	609	817			
	1.1	79	37	501	838	784	894	820	692	884	81	825	808
		82	52	500	813	759	887	797	696	877			
	1.8	89	59	501	784	732	890	769	679	880	87	784	769
		85	65	501	784	734	896	769	686	886			
	2.6	44	24	88	685	617	745	624	532	708	46	694	634
		48	26	108	702	634	764	643	550	732			

Table F9 - Results obtained for the OCFS with a medium gap turned 90° into each other ($\lambda_{average}$, $\alpha_{average}$ and U_{est} for the 2-D PH model) – cont.

u_L (mm/s)	u_G (m/s)	λ ($W.m^{-1}.K^{-1}$)	λ_min ($W.m^{-1}.K^{-1}$)	λ_max ($W.m^{-1}.K^{-1}$)	α ($W.m^{-2}.K^{-1}$)	α_min ($W.m^{-2}.K^{-1}$)	α_max ($W.m^{-2}.K^{-1}$)	U_{est} ($W.m^{-2}.K^{-1}$)	U_{est}_min ($W.m^{-2}.K^{-1}$)	U_{est}_max ($W.m^{-2}.K^{-1}$)	$\lambda_{average}$ ($W.m^{-1}.K^{-1}$)	$\alpha_{average}$ ($W.m^{-2}.K^{-1}$)	U_{est}_average ($W.m^{-2}.K^{-1}$)
6	0.4	34	28	70	701	653	757	633	570	709	35	715	645
		35	26	64	729	677	791	658	582	734			
	1.1	41	25	161	625	569	685	571	498	667	41	633	578
		42	26	124	641	587	701	585	514	677			
	1.8	29	15	49	584	538	642	518	439	593	29	586	521
		29	13	55	589	535	649	524	426	604			
	2.6	18	8	30	408	370	452	356	287	413	17	411	357
		16	8	28	413	373	457	357	289	415			

Table F10 - Results obtained for the OCFS with a big gap turned 90° into each other ($\lambda_{average}$, $\alpha_{average}$ and U_{est} for the 2-D PH model).

u_L (mm/s)	u_G (m/s)	λ (W.m^{-1}.K^{-1})	λ_min (W.m^{-1}.K^{-1})	λ_max (W.m^{-1}.K^{-1})	α (W.m^{-2}.K^{-1})	α_min (W.m^{-2}.K^{-1})	α_max (W.m^{-2}.K^{-1})	U_{est} (W.m^{-2}.K^{-1})	U_{est}_min (W.m^{-2}.K^{-1})	U_{est}_max (W.m^{-2}.K^{-1})	$\lambda_{average}$ (W.m^{-1}.K^{-1})	$\alpha_{average}$ (W.m^{-2}.K^{-1})	$U_{est\_average}$ (W.m^{-2}.K^{-1})
25	0.4	81	37	85	993	933	1055	892	806	979	82	993	910
		82	60	150	992	926	1036	910	845	993			
	1.1	112	74	274	972	926	1024	922	859	1001	130	932	933
		149	79	347	983	937	1029	944	872	1010			
	1.8	135	75	297	1001	955	1045	957	885	1023	139	957	961
		142	76	340	1009	959	1057	966	889	1037			
	2.6	150	98	398	1254	1196	1312	1192	1111	1286	150	1254	1192
18	0.4	40	28	60	1035	973	1101	890	799	988	40	1035	890
		40	30	58	1034	1178	1330	799	946	1163			
	1.1	40	26	62	948	890	1010	826	733	917	41	947	828
		42	28	66	945	887	1005	829	740	918			
	1.8	72	56	132	922	872	984	853	795	940	78	923	859
		84	64	192	924	876	976	865	807	946			
	2.6	117	73	339	924	876	976	881	815	959	117	926	882
		117	73	337	927	883	975	883	821	958			
12	0.4	73	57	141	850	808	894	792	742	860	73	848	790
		72	58	156	846	804	892	788	740	861			
	1.1	118	58	286	822	784	862	788	723	846	111	828	791
		103	51	289	833	783	887	793	714	870			
	1.8	97	49	215	663	629	699	636	582	685	97	687	664
		96	49	247	710	674	750	692	621	736			
	2.6	84	46	180	785	741	831	742	673	808	84	797	752
		84	42	154	808	764	858	762	686	829			

Table F10 - Results obtained for the OCFS with a big gap turned 90° into each other ($\lambda_{average}$, $\alpha_{average}$ and U_{est} for the 2-D PH model) – cont.

u_L (mm/s)	u_G (m/s)	λ ($W.m^{-1}.K^{-1}$)	λ_min ($W.m^{-1}.K^{-1}$)	λ_max ($W.m^{-1}.K^{-1}$)	α ($W.m^{-2}.K^{-1}$)	α_min ($W.m^{-2}.K^{-1}$)	α_max ($W.m^{-2}.K^{-1}$)	U_{est} ($W.m^{-2}.K^{-1}$)	U_{est}_min ($W.m^{-2}.K^{-1}$)	U_{est}_max ($W.m^{-2}.K^{-1}$)	$\lambda_{average}$ ($W.m^{-1}.K^{-1}$)	$\alpha_{average}$ ($W.m^{-2}.K^{-1}$)	U_{est}_average ($W.m^{-2}.K^{-1}$)
6	0.4	20	12	30	968	962	1166	768	641	938	22	969	769
		23	15	33	969	891	1035	769	650	865			
	1.1	26	16	44	802	738	866	673	573	771	27	789	666
		28	18	46	775	717	837	660	574	752			
	1.8	29	19	45	757	709	819	651	575	735	21	610	515
		13	5	37	464	372	592	379	254	538			
	2.6	84	22	154	541	507	577	520	443	564	56	607	553
		28	18	46	673	629	719	585	516	655			

Table F11 – Comparison between the values obtained with the simplified and the 2-D PH model for the OCFS packings with a small gap turned 90° into each other.

		2-D model		Simplified 2-D model			
u_L (mm/s)	u_G (m/s)	$\lambda_{average}$ ($W.m^{-1}.K^{-1}$)	$\alpha_{average}$ ($W.m^{-2}.K^{-1}$)	$\lambda_{average}$ ($W.m^{-1}.K^{-1}$)	$\alpha_{average}$ ($W.m^{-2}.K^{-1}$)	$\Delta\lambda$ (%)	$\Delta\alpha$ (%)
25	0.4	87	953	159	1100	45	13
	1.1	125	999	303	1168	59	14
	1.8	134	992	240	1211	44	18
	2.6	94	1024	132	1343	29	24
18	0.4	63	928	74	1005	14	8
	1.1	92	968	194	1044	52	7
	1.8	77	966	136	1130	43	14
	2.6	82	944	137	1227	40	23
12	0.4	64	795	63	873	-1	9
	1.1	58	862	175	967	67	11
	1.8	112	835	109	1023	-3	18
	2.6	80	735	251	962	68	24
6	0.4	27	562	17	667	-57	16
	1.1	27	693	39	770	30	10
	1.8	24	666	61	814	60	18
	2.6	22	598	30	826	27	28

Table F12 – Comparison between the values obtained with the simplified and the 2-D PH model for the OCFS packings with a medium gap turned 90° into each other.

		2-D model		Simplified 2-D model			
u_L (mm/s)	u_G (m/s)	$\lambda_{average}$ ($W.m^{-1}.K^{-1}$)	$\alpha_{average}$ ($W.m^{-2}.K^{-1}$)	$\lambda_{average}$ ($W.m^{-1}.K^{-1}$)	$\alpha_{average}$ ($W.m^{-2}.K^{-1}$)	$\Delta\lambda$ (%)	$\Delta\alpha$ (%)
25	0.4	79	1053	86	983	8	-7
	1.1	116	1015	71	1035	-64	2
	1.8	127	1038	221	1088	43	5
	2.6	111	922	161	1032	31	11
18	0.4	69	1017	67	914	-2	-11
	1.1	78	971	155	985	50	1
	1.8	89	953	139	963	36	1
	2.6	81	830	147	829	45	0
12	0.4	64	792	40	849	-59	7
	1.1	81	825	86	921	7	10
	1.8	87	784	201	869	57	10
	2.6	46	694	103	627	56	-11
6	0.4	35	715	22	637	-56	-12
	1.1	41	633	24	653	-76	3
	1.8	29	586	40	557	28	-5
	2.6	17	411	47	481	64	15

Table F13 – Comparison between the values obtained with the simplified and the 2-D PH model for the OCFS packings with a big gap turned 90° into each other.

		2-D model		Simplified 2-D model			
u_L (mm/s)	u_G (m/s)	$\lambda_{average}$ ($W.m^{-1}.K^{-1}$)	$\alpha_{average}$ ($W.m^{-2}.K^{-1}$)	$\lambda_{average}$ ($W.m^{-1}.K^{-1}$)	$\alpha_{average}$ ($W.m^{-2}.K^{-1}$)	$\Delta\lambda$ (%)	$\Delta\alpha$ (%)
25	0.4	82	993	54	1234	-51	20
	1.1	130	932	122	1204	-7	23
	1.8	139	957	83	1305	-66	27
	2.6	150	1254	72	1753	-108	28
18	0.4	40	1035	37	1338	-8	23
	1.1	41	947	38	1151	-9	18
	1.8	78	923	50	1216	-56	24
	2.6	117	926	56	1315	-109	30
12	0.4	73	848	38	1012	-92	16
	1.1	111	828	49	986	-128	16
	1.8	97	687	73	817	-32	16
	2.6	84	797	94	1021	11	22
6	0.4	22	969	25	840	12	-15
	1.1	27	789	23	874	-20	10
	1.8	21	610	23	816	10	25
	2.6	56	607	30	942	-87	36

Appendix F3 – Graphs of $\lambda_{average}$ versus gas velocity and U_{est} versus gas velocity obtained for the three types of OCFS packings.

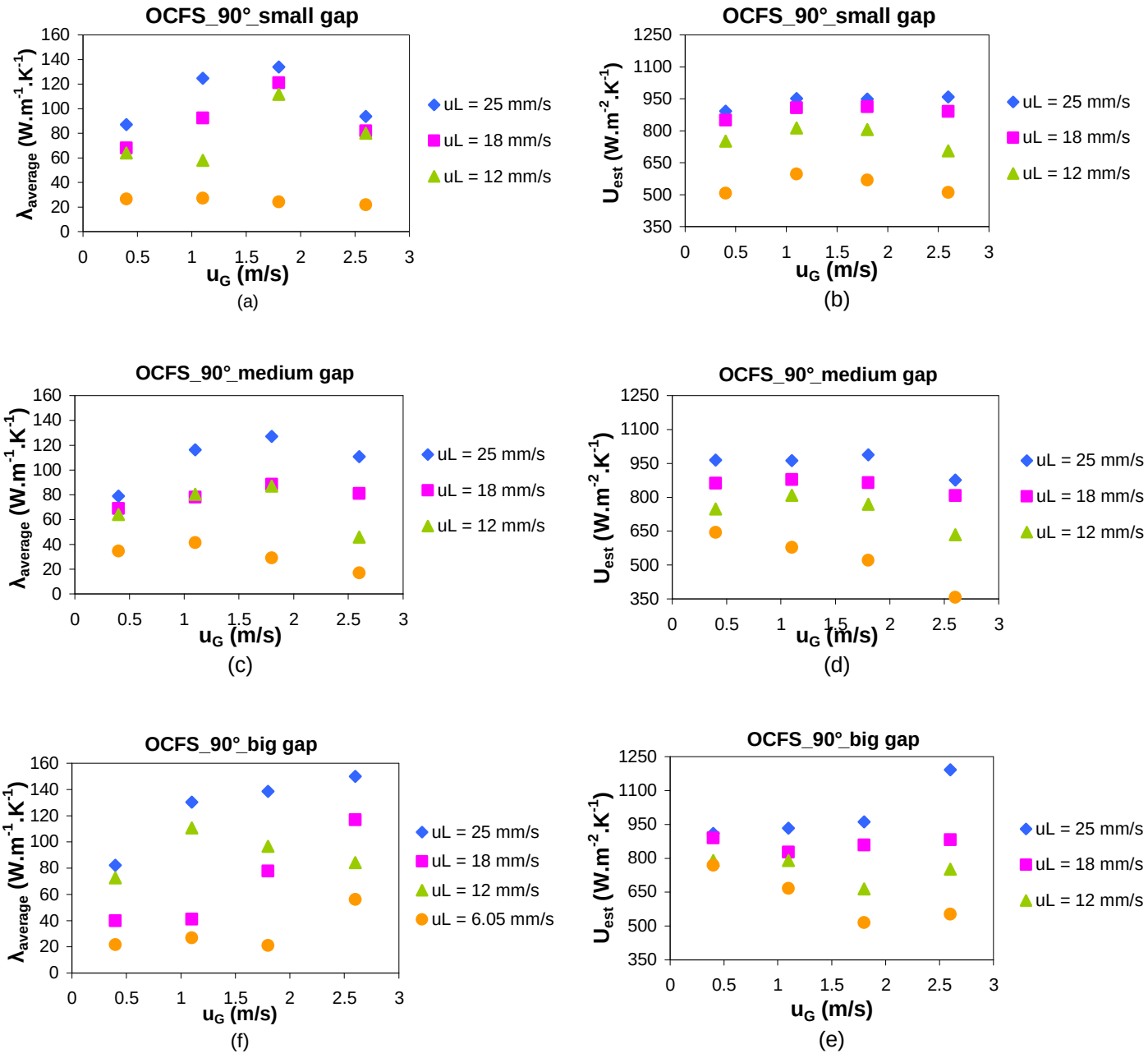

Figure F1 – Profiles obtained for $\lambda_{average}$ and $U_{estimate}$ as a function of gas velocity for the OCFS packings with a small ((a),(b)), medium ((c),(d)) and big gap ((e),(f)) turned into 90° into each other.

Appendix G

Appendix G1 – Results obtained for the CCFS turned into 90° and 0º into each other (U_{ov}).

Table G1 – Results obtained for the U_{ov} for CCFS packings turned 90° into each other and the respective deviation.

		U_{ov} (W.m^{-2}.K^{-1})								$U_{average}$ (W.m^{-2}.K^{-1})				Deviation (%)			
u_L (mm/s)	u_G (m/s)	A-B		B-C		A-D		C-D		A-B	B-C	A-D	C-D	AB	BC	AD	CD
25	0.4	1307	1308	1104	1110	986	980	614	602	1308	1107	983	608	0	1	1	2
	1.1	1303	1301	1061	1058	940	938	583	586	1302	1059	939	584	0	0	0	0
	1.8	1309	1313	1081	1084	947	947	597	583	1311	1082	947	590	0	0	0	2
	2.6	1390	1378	1122	1132	970	969	602	602	1384	1127	969	602	1	1	0	0
18	0.4	1089	1190	1121	1071	911	970	693	740	1139	1096	940	716	9	5	6	6
	1.1	1095	1109	1051	1048	907	918	684	693	1102	1049	913	689	1	0	1	1
	1.8	1125	1130	1059	1055	901	911	628	655	1128	1057	906	641	0	0	1	4
	2.6	1203	1204	974	994	855	867	562	572	1204	984	861	567	0	2	1	2
12	0.4	1025	1000	885	898	806	803	642	657	1013	891	805	650	2	1	0	2
	1.1	999	1010	976	977	800	814	568	596	1005	976	807	582	1	0	2	5
	1.8	1052	1048	1031	1039	851	847	610	611	1050	1035	849	611	0	1	0	0
	2.6	1023	1028	789	789	688	691	461	467	1025	789	690	464	1	0	0	1
6	0.4	848	852	630	630	496	495	336	335	850	630	495	336	1	0	0	0
	1.1	800	771	713	700	543	538	391	387	786	706	540	389	4	2	1	1
	1.8	816	821	686	679	575	575	444	433	818	682	575	438	1	1	0	2
	2.6	712	746	612	599	508	527	364	384	729	606	517	374	4	2	4	5

Table G2 – Results obtained for the U_{ov} for CCFS packings turned 0° into each other and the respective deviation.

		U_{ov} (W.m^{-2}.K^{-1})								$U_{average}$ (W.m^{-2}.K^{-1})				Deviation (%)			
u_L (mm/s)	u_G (m/s)	A-B		B-C		A-D		C-D		A-B	B-C	A-D	C-D	AB	BC	AD	CD
25	0.4	1129	1128	777	768	862	860	762	765	1128	773	861	764	0	1	0	0
	1.1	1092	1096	712	707	876	876	866	869	1094	709	876	867	0	1	0	0
	1.8	1146	1146	715	714	910	904	919	903	1146	714	907	911	0	0	1	2
	2.6	1155	1148	766	766	971	973	1007	1016	1151	766	972	1012	1	0	0	1
18	0.4	1050	1044	720	729	871	869	869	862	1047	725	870	865	1	1	0	1
	1.1	1089	1090	641	635	860	862	896	903	1089	638	861	900	0	1	0	1
	1.8	1123	1131	631	627	845	845	859	859	1127	629	845	859	1	1	0	0
	2.6	891	887	738	725	842	842	873	887	889	731	842	880	0	2	0	1
12	0.4	982	979	617	619	767	758	756	735	980	618	763	745	0	0	1	3
	1.1	938	933	545	549	732	737	763	770	935	547	735	766	0	1	1	1
	1.8	979	980	535	527	746	745	785	786	979	531	745	785	0	1	0	0
	2.6	844	844	620	615	647	649	675	688	844	618	648	682	0	1	0	2
6	0.4	798	784	448	441	553	562	539	547	791	445	557	543	2	2	1	1
	1.1	704	715	422	418	564	560	574	573	710	420	562	573	2	1	1	0
	1.8	670	670	413	410	562	563	615	614	670	411	562	615	0	1	0	0
	2.6	727	727	444	458	534	535	541	537	727	451	535	539	0	3	0	1

Table G3 – Results obtained for the overall heat transfer coefficient for CCFS packings for 0° and 90° and the respective deviation ($\Delta U = U_{ov\_average\_90°} - U_{ov\_average\_0°}$).

u_L (mm/s)	u_G (m/s)	$U_{average\_0°}$ (W m^{-2} K^{-1})	$U_{average\_90°}$ (W m^{-2} K^{-1})	ΔU (%)
25	0.4	773	1107	30
	1.1	709	1059	33
	1.8	714	1082	34
	2.6	766	1127	32
18	0.4	725	1096	34
	1.1	638	1049	39
	1.8	629	1057	41
	2.6	731	984	26
12	0.4	618	891	31
	1.1	547	976	44
	1.8	531	1035	49
	2.6	618	789	22
6	0.4	445	630	29
	1.1	420	706	41
	1.8	411	682	40
	2.6	451	606	26

Appendix G2 – Results obtained for the CCFS turned 90° and 0º into each other for the simplified 2-D PH model and for the 2-D PH model.

Table G4 - Results obtained for the CCFS turned 90° into each other (λ and α for the simplified 2-D PH model).

u_L	u_G	$\lambda a_{e,r}$	$\lambda a_{e,r\ min}$	αa	αa_{min}	αa_{max}	$\lambda b_{e,r}$	$\lambda b_{e,r\ min}$	αb	αb_{min}	αb_{max}	$\lambda c_{e,r}$	$\lambda c_{e,r\ min}$	αc	αc_{min}	αc_{max}
(mm/s)	(m/s)	($W.m^{-1}.K^{-1}$)		($W.m^{-2}.K^{-1}$)			($W.m^{-1}.K^{-1}$)		($W.m^{-2}.K^{-1}$)			($W.m^{-1}.K^{-1}$)		($W.m^{-2}.K^{-1}$)		
25	0.4	146	11	1268	757	3922	65	38	1360	1239	1508	193	78	1192	1109	1289
		232	16	1213	841	2178	61	35	1334	1207	1492	163	66	1194	1098	1309
	1.1	149	16	1216	847	2156	50	25	1354	1147	1650	491	63	1159	1024	1335
		120	11	1322	766	4811	51	26	1461	1239	1779	602	58	1147	999	1345
	1.8	132	13	1305	822	3159	51	25	1447	1222	1774	279	77	1161	1002	1378
		148	14	1319	850	2945	50	25	1480	1241	1833	233	76	1163	997	1395
	2.6	168	131	1400	1379	1423	53	27	1577	1327	1943	89	31	1245	1082	1466
		171	77	1409	1324	1507	52	27	1598	1349	1959	94	25	1249	1037	1571
18	0.4	128	11	1273	747	4310	60	35	1366	1233	1532	122	16	1093	822	1629
		197	19	1318	940	2207	69	38	1428	1285	1607	356	21	1138	885	1592
	1.1	131	10	1186	698	3951	54	29	1287	1138	1482	102	14	1107	804	1775
		115	8	1273	661	1731	61	33	1355	1212	1537	140	16	1106	823	1684
	1.8	237	11	1150	691	3425	43	20	1336	1091	1722	113	15	1138	825	1835
		105	7	1258	610	1986	47	23	1389	1154	1745	108	14	1133	820	1832
	2.6	131	75	1246	1192	1304	36	20	1472	1219	1858	129	14	1032	758	1618
		139	71	1246	1180	1319	37	21	1467	1218	1845	124	14	1074	778	1734
12	0.4	108	7	1167	563	1679	87	31	1191	1026	1419	92	53	938	901	979
		103	7	1157	579	1892	87	33	1176	1030	1372	46	20	959	830	1138
	1.1	109	11	1131	698	2973	91	38	1148	1030	1296	95	14	1009	747	1555
		107	9	1165	665	4722	162	66	1128	1059	1207	213	16	977	746	1415
	1.8	87	6	1188	568	2652	52	25	1265	1077	1530	136	11	1080	714	2215
		90	7	1196	582	2097	52	25	1276	1087	1547	108	12	1080	740	1999
	2.6	115	9	1141	648	4796	25	13	1478	1093	2285	68	7	847	530	2113
		111	8	1155	635	6388	25	13	1493	1094	2352	68	7	850	536	2058

Table G4 - Results obtained for the CCFS turned 90° into each other (λ and α for the simplified 2-D PH model) – cont.

u_L	u_G	$\lambda a_{e,r}$	$\lambda a_{e,r\ min}$	αa	αa_{min}	αa_{max}	$\lambda b_{e,r}$	$\lambda b_{e,r\ min}$	αb	αb_{min}	αb_{max}	$\lambda c_{e,r}$	$\lambda c_{e,r\ min}$	αc	αc_{min}	αc_{max}
(mm/s)	(m/s)	($W.m^{-1}.K^{-1}$)		($W.m^{-2}.K^{-1}$)			($W.m^{-1}.K^{-1}$)		($W.m^{-2}.K^{-1}$)			($W.m^{-1}.K^{-1}$)		($W.m^{-2}.K^{-1}$)		
6	0.4	118	32	1053	915	1241	58	31	1120	1009	1259	11	3	805	341	2253
		90	23	1088	889	1403	68	31	1119	990	1286	11	3	814	356	2845
	1.1	51	5	993	442	4066	37	19	1045	888	1271	19	4	841	458	5186
		63	5	1013	474	7312	40	20	1079	917	1310	19	5	809	495	2208
	1.8	63	6	964	490	2833	22	11	1180	894	1733	30	10	775	597	1103
		60	4	994	416	2565	25	13	1170	911	1636	26	11	783	636	1018
	2.6	59	3	812	288	995	18	8	1025	720	1781	23	6	681	474	1214
		56	3	876	290	855	19	9	1091	775	1841	39	9	677	511	1007

Table G5 - Results obtained for the CCFS turned 0° into each other (λ and α for the simplified 2-D PH model).

u_L	u_G	$\lambda a_{e,r}$	$\lambda a_{e,r\ min}$	αa	αa_{min}	αa_{max}	$\lambda b_{e,r}$	$\lambda b_{e,r\ min}$	αb	αb_{min}	αb_{max}	$\lambda c_{e,r}$	$\lambda c_{e,r\ min}$	αc	αc_{min}	αc_{max}
(mm/s)	(m/s)	($W.m^{-1}.K^{-1}$)		($W.m^{-2}.K^{-1}$)			($W.m^{-1}.K^{-1}$)		($W.m^{-2}.K^{-1}$)			($W.m^{-1}.K^{-1}$)		($W.m^{-2}.K^{-1}$)		
25	0.4	86	69	1147	1120	1176	25	17	1462	1247	1768	17	8	1415	879	3614
		97	69	1131	1092	1174	26	17	1458	1241	1767	17	8	1416	882	3577
	1.1	78	48	1223	1134	1327	28	18	1512	1285	1836	17	8	1245	825	2537
		85	54	1106	1047	1173	25	17	1403	1191	1706	17	8	1236	814	2563
	1.8	92	56	1154	1088	1228	27	18	1464	1238	1793	15	8	1325	836	3195
		90	52	1226	1135	1332	29	19	1528	1289	1878	16	8	1303	830	3033
	2.6	96	60	1297	1217	1388	32	20	1601	1350	1968	17	8	1277	822	2863
		86	51	1281	1184	1395	31	20	1570	1322	1932	17	8	1276	825	2812
18	0.4	77	47	1080	1007	1166	22	15	1411	1184	1746	16	8	1246	801	2810
	1.1	78	42	1080	983	1198	26	14	1286	1013	1760	15	8	1140	794	2019
		78	41	1080	983	1199	26	14	1285	1016	1747	15	8	1132	785	2028
	1.8	93	59	1297	1223	1380	33	10	1474	974	3034	12	6	1059	654	2771
		86	53	1152	1084	1228	24	15	1503	1222	1954	13	7	1150	720	2856
	2.6	95	51	952	893	1020	23	14	1229	1015	1556	17	8	1068	696	2292
		95	50	954	893	1024	24	15	1227	1016	1549	17	8	1069	697	2291
12	0.4	56	41	1005	956	1060	16	11	1433	1125	1971	14	6	1023	624	2841
		54	38	1017	957	1084	15	10	1507	1155	2167	14	6	1002	610	2795
	1.1	45	22	949	804	1157	18	11	1176	908	1667	12	6	975	607	2480
		85	36	853	768	959	18	10	1164	896	1661	12	6	982	608	2541
	1.8	128	43	894	803	1007	18	12	1295	1033	1737	11	5	973	583	2921
		81	40	914	839	1003	18	12	1279	1018	1722	11	5	972	585	2873
	2.6	48	25	910	794	1067	16	10	1233	964	1710	9	4	871	490	3877
		61	36	916	844	1001	16	10	1274	994	1772	9	4	848	487	3284
6	0.4	26	17	876	759	1036	9	6	1313	850	2882	6	3	977	520	8064
	1.1	28	16	806	685	978	11	7	1165	897	1660	7	4	810	484	2481
	1.8	30	16	779	659	953	12	8	1067	840	1463	9	4	655	406	1693
		32	17	774	662	934	12	8	1070	841	1469	9	4	654	404	1713
	2.6	54	29	877	787	989	19	9	1042	729	1821	6	3	817	483	2656
		51	30	879	803	971	19	9	1035	725	1809	6	4	842	500	2660

Table G6 - Results obtained for the CCFS turned 90° into each other ($\lambda_{average}$, $\alpha_{average}$ and U_{est} for the 2-D PH model).

u_L (mm/s)	u_G (m/s)	λ (W.m^{-1}.K^{-1})	λ_min (W.m^{-1}.K^{-1})	λ_max (W.m^{-1}.K^{-1})	α (W.m^{-2}.K^{-1})	α_min (W.m^{-2}.K^{-1})	α_max (W.m^{-2}.K^{-1})	U_{est} (W.m^{-2}.K^{-1})	U_{est}_min (W.m^{-2}.K^{-1})	U_{est}_max (W.m^{-2}.K^{-1})	$\lambda_{average}$ (W.m^{-1}.K^{-1})	$\alpha_{average}$ (W.m^{-2}.K^{-1})	$U_{est\_average}$ (W.m^{-2}.K^{-1})
25	0.4	84	46	220	979	895	1071	913	798	1039	83	981	913
		81	45	217	982	902	1070	913	802	1038			
	1.1	74	38	246	945	843	1057	875	740	1029	72	945	873
		70	34	258	946	832	1070	872	722	1043			
	1.8	82	36	500	916	796	1048	856	699	1034	83	916	857
		83	35	501	917	789	1057	858	692	1043			
	2.6	36	14	144	804	670	956	704	516	918	34	814	709
		33	13	125	825	685	979	713	515	933			
18	0.4	55	31	103	1028	952	1108	921	799	1038	74	1028	921
		92	36	500	1113	1031	1197	1087	874	1179			
	1.1	63	33	89	990	922	1058	887	785	985	63	994	891
		62	31	107	997	923	1075	896	778	1011			
	1.8	48	23	79	957	873	1053	834	706	972	48	959	836
		48	23	79	961	873	1057	838	706	975			
	2.6	26	14	52	834	740	938	694	556	843	27	834	694
		27	15	53	859	767	961	718	581	863			
12	0.4	72	42	216	920	858	1004	851	761	976	70	920	851
		69	39	189	919	840	982	830	740	951			
	1.1	61	39	501	747	687	869	726	619	860	60	776	755
		60	41	501	806	742	900	784	667	890			
	1.8	44	26	84	917	849	989	812	705	921	44	851	791
		250	40	500	784	728	932	769	654	921			
	2.6	16	6	30	752	638	874	577	383	739	16	758	581
		16	8	30	765	655	889	585	433	750			

Table G6 - Results obtained for the CCFS turned 90° into each other ($\lambda_{average}$, $\alpha_{average}$ and U_{est} for the 2-D PH model) – cont.

u_L (mm/s)	u_G (m/s)	λ (W.m^{-1}.K^{-1})	λ_min (W.m^{-1}.K^{-1})	λ_max (W.m^{-1}.K^{-1})	α (W.m^{-2}.K^{-1})	α_min (W.m^{-2}.K^{-1})	α_max (W.m^{-2}.K^{-1})	U_{est} (W.m^{-2}.K^{-1})	U_{est}_min (W.m^{-2}.K^{-1})	U_{est}_max (W.m^{-2}.K^{-1})	$\lambda_{average}$ (W.m^{-1}.K^{-1})	$\alpha_{average}$ (W.m^{-2}.K^{-1})	$U_{est\_average}$ (W.m^{-2}.K^{-1})
6	0.4	49	27	501	930	855	1095	843	714	1080	48	931	844
		46	26	500	931	825	1049	844	688	1035			
	1.1	54	24	500	683	615	767	667	530	760	54	678	663
		54	26	502	674	606	758	659	529	751			
	1.8	15	7	29	695	597	787	541	389	673	15	699	544
		15	7	31	703	601	795	546	391	685			
	2.6	10	2	22	439	375	529	342	173	460	10	451	342
		10	2	26	463	397	561	361	177	494			

Table G7 - Results obtained for the CCFS turned 0° into each other ($\lambda_{average}$, $\alpha_{average}$ and U_{est} for the 2-D PH model).

u_L (mm/s)	u_G (m/s)	λ (W.m^{-1}.K^{-1})	λ_min (W.m^{-1}.K^{-1})	λ_max (W.m^{-1}.K^{-1})	α (W.m^{-2}.K^{-1})	α_min (W.m^{-2}.K^{-1})	α_max (W.m^{-2}.K^{-1})	U_{est} (W.m^{-2}.K^{-1})	U_{est}_min (W.m^{-2}.K^{-1})	U_{est}_max (W.m^{-2}.K^{-1})	$\lambda_{average}$ (W.m^{-1}.K^{-1})	$\alpha_{average}$ (W.m^{-2}.K^{-1})	$U_{est\_average}$ (W.m^{-2}.K^{-1})
25	0.4	23	13	37	999	877	1131	786	617	950	23	987	786
		24	14	40	976	858	1114	776	620	949			
	1.1	21	13	33	928	820	1052	725	588	877	22	904	725
		23	13	37	879	779	997	724	567	853			
	1.8	22	12	38	855	741	987	687	535	849	20	860	680
		19	11	33	865	747	1003	674	524	843			
	2.6	24	10	38	794	670	932	636	472	808	24	794	634
		24	10	38	793	669	931	633	472	807			
18	0.4	22	14	32	1009	903	1113	782	644	914	22	1009	782
	1.1	21	13	31	949	855	1047	782	606	865	21	945	733
		21	13	31	940	846	1038	733	601	858			
	1.8	21	11	35	883	775	1003	696	538	851	21	877	695
		21	11	35	871	771	987	695	536	839			
	2.6	20	12	46	705	617	801	594	467	722	20	703	593
		20	12	46	700	614	798	592	465	720			

Table G7 - Results obtained for the CCFS turned 0° into each other ($\lambda_{average}$, $\alpha_{average}$ and U_{est} for the 2-D PH model) – cont.

u_L (mm/s)	u_G (m/s)	λ ($W.m^{-1}.K^{-1}$)	λ_min ($W.m^{-1}.K^{-1}$)	λ_max ($W.m^{-1}.K^{-1}$)	α ($W.m^{-2}.K^{-1}$)	α_min ($W.m^{-2}.K^{-1}$)	α_max ($W.m^{-2}.K^{-1}$)	U_{est} ($W.m^{-2}.K^{-1}$)	U_{est}_min ($W.m^{-2}.K^{-1}$)	U_{est}_max ($W.m^{-2}.K^{-1}$)	$\lambda_{average}$ ($W.m^{-1}.K^{-1}$)	$\alpha_{average}$ ($W.m^{-2}.K^{-1}$)	U_{est}_average ($W.m^{-2}.K^{-1}$)
12	0.4	21	11	31	972	874	1050	753	584	867	20	974	742
		18	10	30	976	868	1100	731	563	895			
	1.1	18	10	28	868	778	944	667	523	780	18	873	670
		18	10	28	878	782	950	674	525	784			
	1.8	17	9	25	827	735	905	632	487	738	18	814	631
		18	10	28	802	710	904	630	492	752			
	2.6	11	5	21	650	558	754	471	329	616	11	636	472
		12	4	20	623	541	705	473	293	578			
6	0.4	15	7	29	960	804	1142	680	468	916	15	960	680
	1.1	14	6	24	752	646	878	565	386	715	14	752	565
	1.8	11	5	17	618	542	700	463	323	557	12	613	461
		12	6	18	607	535	687	460	344	555			
	2.6	8	2	14	448	384	504	330	175	411	8	451	332
		8	2	14	455	391	513	333	176	417			

Table G8 – Comparison between the values obtained with the simplified and the 2-D PH model for the CCFS packings with a big gap turned 90° into each other.

		2-D model		Simplified 2-D model			
u_L (mm/s)	u_G (m/s)	$\lambda_{average}$ ($W.m^{-1}.K^{-1}$)	$\alpha_{average}$ ($W.m^{-2}.K^{-1}$)	$\lambda_{average}$ ($W.m^{-1}.K^{-1}$)	$\alpha_{average}$ ($W.m^{-2}.K^{-1}$)	$\Delta\lambda$ (%)	$\Delta\alpha$ (%)
25	0.4	83	981	178	1193	54	18
	1.1	72	945	547	1153	87	18
	1.8	83	916	256	1162	68	21
	2.6	34	814	91	1247	62	35
18	0.4	74	1028	239	1115	69	8
	1.1	63	994	121	1106	48	10
	1.8	48	959	110	1135	57	16
	2.6	27	834	126	1053	79	21
12	0.4	70	920	69	949	-2	3
	1.1	60	776	154	993	61	22
	1.8	44	851	122	1080	64	21
	2.6	16	758	68	849	77	11
6	0.4	48	931	11	810	-339	-15
	1.1	54	678	19	825	-181	18
	1.8	15	699	28	779	46	10
	2.6	10	451	31	679	68	34

Table G9 – Comparison between the values obtained with the simplified and the 2-D PH model for the CCFS packings with a big gap turned 0° into each other.

		2-D model		Simplified 2-D model			
u_L (mm/s)	u_G (m/s)	$\lambda_{average}$ ($W.m^{-1}.K^{-1}$)	$\alpha_{average}$ ($W.m^{-2}.K^{-1}$)	$\lambda_{average}$ ($W.m^{-1}.K^{-1}$)	$\alpha_{average}$ ($W.m^{-2}.K^{-1}$)	$\Delta\lambda$ (%)	$\Delta\alpha$ (%)
25	0.4	23	987	17	1415	-40	30
	1.1	22	904	17	1240	-28	27
	1.8	20	860	16	1314	-31	35
	2.6	24	794	17	1276	-40	38
18	0.4	22	1009	16	1246	-37	19
	1.1	21	945	15	1136	-41	17
	1.8	21	877	12	1104	-69	21
	2.6	20	703	17	1068	-16	34
12	0.4	20	974	14	1012	-42	4
	1.1	18	873	12	978	-54	11
	1.8	18	814	11	972	-58	16
	2.6	11	636	9	860	-24	26
6	0.4	15	960	6	977	-138	2
	1.1	14	752	7	810	-89	7
	1.8	12	613	9	655	-35	6
	2.6	8	451	6	830	-31	46

Appendix H

Table H1 – Comparison between the results obtained in MatLab and Athena programs for the $\lambda_{e,r}$ and α_w parameters - $\Delta\lambda = (\lambda_{MatLab} - \lambda_{Athena})/\lambda_{MatLab} * 100\%$ and $\Delta\alpha_w = (\alpha_{w\_MatLab} - \alpha_{w\_Athena})/\alpha_{w\_\lambda MatLab} * 100\%$).

		MATLAB									ATHENA					
u_L (mm/s)	u_G (m/s)	λ ($W.m^{-1}.K^{-1}$)	λ_{min}	λ_{max}	α ($W.m^{-2}.K^{-1}$)	α_{min}	α_{max}	U_{est} ($W.m^{-2}.K^{-1}$)	U_{est_min}	U_{est_max}	λ ($W.m^{-1}.K^{-1}$)	+- λ	α ($W.m^{-2}.K^{-1}$)	+- α	$\Delta\lambda$	$\Delta\alpha$
6	0.4	20	18	22	500	498	502	433	425	439	16	2	437	18	19	13
	1.5	250	248	252	470	468	472	465	463	467	121	97	461	16	52	2
14	1.6	153	151	155	897	895	899	865	863	868	124	53	832	27	20	7
	2.5	241	239	243	819	817	821	802	800	804	89	34	841	34	63	-3
15	0.9	101	99	103	858	856	860	815	812	817	70	25	973	53	31	-13
18	0.9	121	119	123	969	967	971	923	920	925	65	30	867	41	47	11
	1.5	198	196	200	1012	1010	1014	981	978	983	142	50	923	23	29	9
	2.4	97	95	99	957	955	959	902	899	904	91	23	932	29	7	3
	2.1	141	139	143	1008	1006	1010	965	962	967	116	31	930	24	18	8
	2.5	90	88	92	993	991	995	929	926	932	83	23	940	35	8	5
21	2.4	120	118	122	1002	1000	1004	953	950	955	100	26	989	32	17	1
	1.5	326	324	328	1080	1078	1082	1058	1056	1060	157	61	965	28	52	11
	2.5	103	101	105	1060	1058	1062	996	993	999	90	20	1036	32	12	2
22	0.4	70	68	72	1079	1077	1081	984	980	988	58	7	977	26	16	9
	1.0	218	216	220	1027	1025	1029	998	995	1000	110	30	947	28	49	8
25	1.0	193	191	195	1194	1192	1196	1149	1147	1152	135	43	1056	34	30	12
	1.6	225	223	227	1186	1184	1188	1148	1146	1150	209	106	1045	34	7	12
	2.0	271	269	273	1073	1071	1075	1047	1045	1049	149	59	1053	38	45	2
	2.3	223	221	225	1181	1179	1183	1143	1141	1145	111	30	1053	35	50	11
	2.6	260	258	262	1073	1071	1075	1046	1044	1048	101	23	1096	36	61	-2